Absorption and Metabolism of Fatty Acid: Inverse Problems and Uncertainty Studies

By

Yang Hai

A thesis submitted in partial fulfilment of the requirements of

The University of Greenwich

For the Degree of Doctor of Philosophy

Department of Mathematical Sciences

School of Computing and Mathematical Sciences

University of Greenwich

Park Row, London SE10 9LS

2015

Declaration

I clarify that this work has not been accepted in substance for any degree, and is not concurrently being submitted for any degree other than that of Doctor of Philosophy being studied at the University of Greenwich. I also declare that this work is the result of my own investigation except where otherwise identified by references and that I have not plagiarised the work of others.

Student:

Yang Hai

Supervisor:

Professor Choi-Hong Lai

Second Supervisor:

Professor Koulis Pericleous

Third Supervisor:

Dr Erwin George

Acknowledgements

I would like to give my special thanks to my supervisor Professor Choi-Hong Lai for his advice and assistance during my studies at University of Greenwich. He opened a gate and led me into a new world of computational biology. Without his support, I would not finish the dissertation.

I would like to thank Professor Koulis Pericleous and Dr Erwin George for their concern and guidance at various stages of the research process. I would like to thank Francisco-Javier Granados-Ortiz, Shih-Hau Tan, Serife Arif, Xiaoqin Hu, Carmen Su in no particular order, for their kind and invaluable help during this PhD study.

I would like to express my love and gratitude to my family, for their understanding and endless love, through the duration of my study.

Finally, I would like to thank my girlfriend, Panpan Gao, for her constant understanding, care and support.

ABSTRACT

Fatty acid is the main substance in food diet and constitutes the major energy source. The absorption and metabolism of fatty acids provide the energy supply for biological activities in the human body. Mathematical models may be used to describe the absorption and metabolism processes of fatty acids in different organs in the human body.

One of the main challenges in computational biology is to build a suitable macro-scale mathematical model for fatty acids concentrations in the blood stream. In this thesis, several models in the literature are modified by considering the transport in the absorption process and the metabolism in the blood of substances. An absorption delay is included in an interactive system of insulin-glucose-fatty acids model in Chapter 3. Data from existing literature was used in determining parameters, such as transfer rate, related to these models using inverse problem technique.

A significant process in the triglyceride absorption is the hydrolysis reaction which releases fatty acids molecules for human activities. Modelling the hydrolysis process is difficult due to the complex reaction in the digestive system. In this study a general form of compartment model is presented and one specific example is provided through the use of a “regulator” built into the compartment model. A multi-objective optimisation problem is resulted from this study and various parameters solved along with a set of in vitro data as demonstrated in Chapter 4.

In the absorption process, the substance needs to be transported through absorptive epithelial cells into the blood vessel. The diffusion and reaction at the cellular level have uncertainties unknown to the biologists. In this thesis, the transport of fatty acids in the absorptive epithelial cell is modelled by a reaction-diffusion system at the cellular model in Chapter 5 and the missing information on the membrane of the epithelial cell is treated as uncertainty in the model. The Monte Carlo method is used to study these uncertainties.

Numerical experiments demonstrated the use of three models, with suitable parameters, may describe the absorption and metabolism of fatty acids in different organs in the human body.

CONTENTS

List of Figures

List of Tables

Nomenclature

C_{int} : Nutrients concentration in the blood

C_s : Drug concentration in the stomach

C_i : Drug concentration in the intestine

C_{pl} : Absorbed drug concentration in the plasma

k_i : Intestinal transit rate for drug

k_{el} : Elimination rate of drug in the plasma

C_G : Glucose concentration

C_I : Insulin concentration

G_{pro}: Glucose production

G_{uti}: Glucose utilization

I_{pro}: Insulin production in the blood

I_{cle}: Insulin clearance in the blood

C_{liv}: Nutrients concentration in the liver

C_A : Concentration of N_2O_5

C_B : Concentration of NO_2

C_C : Concentration of O_2

C_X : Concentration of insulin in remote compartment

C_{TG} : Concentration of triglyceride

C_{DG} : Concentration of diglyceride

C_{MG} : Concentration of monoglyceride

C_{GLY}: Concentration of glycerol

C_{FA}: Concentration of fatty acids

Chapter 1 INTRODUCTION

The absorption and metabolism processes are important biological processes. The relevant physiology can be found in related research [3, 126, 162]. There is also much experimental work [44, 119, 204] in the validation of the physiology. It is well known that experimental biology is overwhelmed with data. Quantitative methods provide suitable techniques to deal with data. Some early quantitative work can be found in [11, 27, 89]. The data-based method is widely available for quantitative analysis of population dynamics and related subjects [144]. Data analysis in molecular biology allows statistical and graphical description of the molecular movement and chemical reactions [205].

Apart from the above quantitative methods of handling data, biologists and mathematicians also wish to model biological phenomena by means of computational simulation. Many mathematical models have been developed for different problems. For example, the diffusion process may be used to understand the movement of red cells in the blood [176]. The simple epidemic model as presented in [14] can be used to describe susceptible population that are to be infected imminently, and some continuum models can be used for the understanding of tumour growth [15, 88]. Experimental data may be used to determine parameters of such mathematical model. Data fitting via the inverse problem [66, 188, 189] is one technique that may be adopted by

biologists and mathematicians in constructing models. Such combined use of mathematical methods, data and models is usually referred to as computational biology [73, 79, 201]. Significant advances in computational biology have taken place due to the development of robust numerical methods [29, 111, 153, 184], computational equipment [42, 45, 83], capability of handling data [80, 92, 177], understanding of data-analytical methods and theoretical knowledge of biological systems.

This thesis limits the study to the absorption and metabolism processes. In this chapter, the basic equations related to the absorption and metabolism of three different types of nutrients are discussed. A brief discussion is also given of the related numerical methods and software. An outline of the methodology to be employed, and the objectives and layout of this thesis are presented.

1.1. The Absorption Process

The absorption process involves assimilating substances into cells or across the tissues along relevant regions of an organ. In the digestive system, various substances are absorbed by the human tissue through different enzymes and pathways. The study of the absorption process brings significant influence and development in various branches of biological research. The absorption of proteins and carbohydrates provides an understanding of how tissue and organ functions are maintained [54, 96]. Such knowledge is widely applied in the food production industry [168]. The study of absorption of drugs/medicine into the bloodstream is a related subject and considered as part of pharmacokinetics [196]. On the other hand, the absorption of lipids is closely related to the study of diabetes [114], heart diseases [90], and food supplements [140], amongst others.

1.1.1. Absorption of protein and carbohydrate

Protein is a nutrient necessary for all human activities and plays a significant role in body growth and maintenance. The absorption of protein can be divided into two phases [20]. The first phase takes place in the stomach where an enzyme called pepsin is secreted from the cell lining along the tissue wall. Pepsin can be used to degrade protein molecules into smaller amino acids or peptide molecules. The second phase takes place in the small intestine where the breakdown of protein molecules continues leading to the transport of amino acids through the epithelial cells. These amino acids have dimension small enough to be able to penetrate through the internal surface of the small intestine. From this point afterwards, they enter the bloodstream through capillaries.

A carbohydrate is a biological molecule obtained by combining carbon, hydrogen and oxygen atoms. Carbohydrate performs numerous roles in living tissues. There are three main types of carbohydrates: starches, sugars and dietary fibre. Starches and sugars are regarded as energy-yielding carbohydrate molecules because they can be digested completely and can provide the organ with 4 calories of energy per gram of concentration once they are absorbed [147]. In contrast, fibre cannot be fully digested due to the lack of enzymes to breakdown its bigger molecules, and is usually eliminated through excretion. Note that the digestible carbohydrates are starches and sugars which are broken down into the simplest molecule by the enzymes released from the small intestine. These digested starches and sugars are ready to be absorbed once they begin to move along the lumen in the small intestine. If the carbohydrates are not fully absorbed, they can be eliminated from the body. In addition, the lactose, a type of sugar, may also be excreted if there is not enough demand from the human body or due to a lack of enzyme to digest it.

There are several models developed to interpret the rate of food digestion through glucose absorption [105, 136]. Let $C_{int}(t)$ be the glucose concentration in the blood, the kinetics for the glucose absorption can be described as

$$\frac{dC_{int}(t)}{dt} = rate\ of\ glucose\ uptake - rate\ of\ glucose\ absorbed \quad (1.1)$$

This equation is used to describe the glucose kinetics in the small intestine as discussed in [9, 10, 35]. Equation (1.1) provides an essential balance description of the glucose concentration change with respect to time due to the uptake of a meal containing glucose subtracting the absorbed glucose.

There are several extensions in recent years to the above model in Equation (1.1) through modification of the resulting ordinary differential equation (ODE) [134, 141, 157] describing concentrations of certain substances. However, some nutrients depend on the transport of flows in regions like the stomach and the small intestine [69]. Such models cannot describe the absorption of lipids or fatty acids due to the complexity of fatty acids transport in the small intestine [81]. Much research has focused on the compartment model for glucose instead of fatty acids absorption due to its complexity [105, 136, 199]. A proper mathematical description is needed by combining the experience of models for protein absorption and the feature of lipid absorption.

1.1.2. The absorption of drug

Unlike the study of the digestive system for absorption of daily food, the research on absorption of drugs is for medical use, where the profiles of drugs may be changed accordingly by adjusting relevant factors that are involved in the absorption process.

The drug absorption mainly takes place in stomach and small intestine [6, 17]. The acidity (pH) environment is important for drug absorption. The pH value in the stomach can increase from about 1.5 to 7 when food is eaten. After 10 minutes, the pH value drops to 5, and continuously decreases to 3 after 3 hours from the time the food was ingested. The transport of food into the small intestine can also lead to a drop of the pH value in the jejunum, typically from 6.1 to 4.5 about 1 to 2 hours after the food intake. Other parts of the small intestine and the large intestine do not show a dramatic change of pH value after the meal, due to the transfer time of food

particles from one compartment to the other in the intestine. Therefore it can be deduced that the maximal absorption of drug molecules is in the jejunum over a period of 3- 5 hours, in the pH values range from 4.5 – 7 [5].

Besides the pH values in the small intestine, there are various other factors that allow pharmacokinetic models to control the drug effects. The rate of tablet dissolution relies on the surface area of the solid and the diffusion of molecule [52]. The bioactivity of a drug may inhibit the function of proteins in the tissue, and the effect of drug is closely related to whether the enzyme exists in the tissue or organ.

As part of the pharmacokinetic study, the human drug oral absorption kinetics is usually described by a system of ODEs [13]. Under fasting condition, the gastric emptying and intestinal transiting of drugs can be approximately described by first-order kinetics [49]. A typical drug absorption model relies on the concept of compartments [156]. In the macroscopic model, a coarse partitioning of the digestive system leads to three compartments, namely the stomach, the small intestine and the blood stream, as depicted in Figure 1.1. Note that the arrows are pointing in one direction without a reverse arrow due to the direction of substance transport.

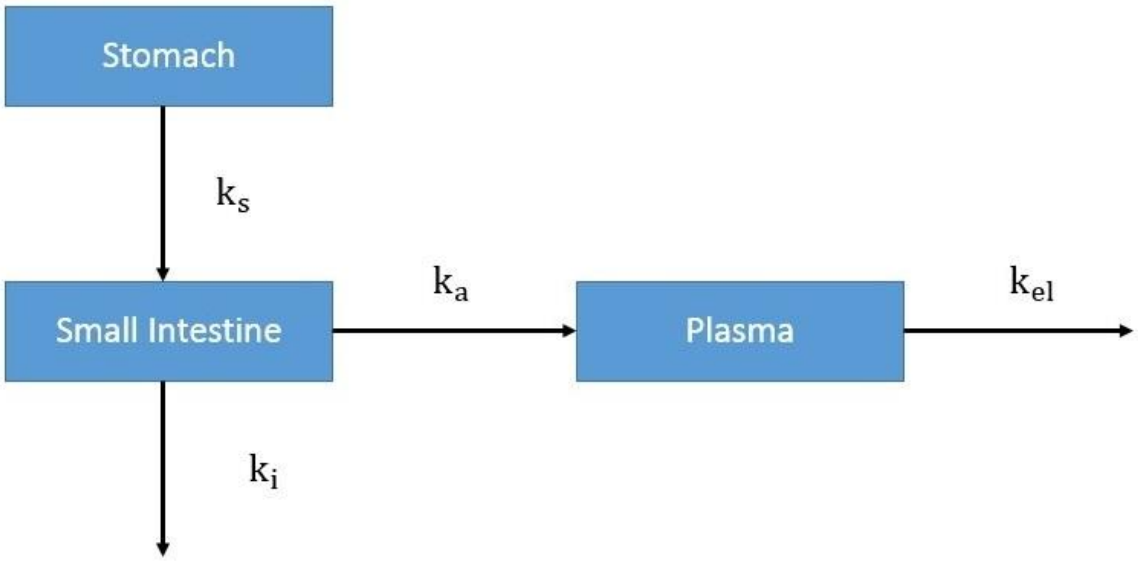

Figure 1.1 The schematic view of drug absorption

Let C_s, C_i and C_{pl} represent the amounts of drug in the stomach, intestine and the amount absorbed as reflected in the plasma, respectively. Here k_s, k_i, k_a and k_{el} are first-order transport rate of gastric emptying, intestinal transit, absorption, and elimination from plasma, respectively. To describe the drug transport in a model system, the technique of physiologically based pharmacokinetic (PBPK) modelling method can be applied in an ODE system. The first PBPK model was developed in 1996 [72], and now is widely used in drug transport research. In the PBPK model, the multi-compartment system is built, with compartments representing organs or tissue and may have interconnections corresponding to blood or lymph flows. The drug transport into a tissue is rate-limited by either perfusion or permeability. Under this limitation, the rate of entry to tissue for the quantity of drug is simply equal to the transport rate times the concentration of drug in the incoming compartment. The concept of the compartment in the PBPK model represents a unique substance concentration in different organs, and the same application can be found in [156]. The transit rate in the adjacent compartments can be defined as a constant. In this case represented in Figure 1.1, the flow transport rate is defined as k_s, k_i, k_a and k_{el} and the model can be built as follows:

$$\begin{cases} \frac{dC_s}{dt} = -k_s C_s \\ \frac{dC_i}{dt} = k_s C_s - (k_i + k_a) C_i \\ \frac{dC_{pl}}{dt} = k_a C_i - k_e \quad C_{pl} \end{cases} \tag{1.2}$$

The compartment model as described in Equation (1.2) provides a macroscopic view on the concentration of substrates. Note that such model has not taken into account metabolism and other organs connected to the plasma compartment.

1.1.3. The absorption of lipids

Lipids are organic compounds including fats, waxes, monoglycerides, diglycerides, triglycerides amongst others. The molecules of a lipid can be used for energy storage and signalling transport inside the tissue. They are also acting as one of the components of the membrane structure. The digestion of lipids mainly concerns the absorption of triglyceride, which is a unit of fat with a structure of three fatty acids linked to a glycerol molecule [164]. The key point in the digestion and absorption of fat is the solubility of a substance. The solubility of lipids is relatively poor in the aqueous environment of the digestive tract, but the digestive enzyme lipase is water-soluble. As a result, lipase can only work at the surface of fat globules as the triglyceride molecules are transported in the form of an emulsion, which is a mixture of more than one liquid. The word "emulsion" comes from the Latin word for "milk", as milk is an emulsion of fat and water, amongst other components. In an emulsion, the enzyme liquid is dispersed in the triglycerides. This emulsion contains both a dispersed and a continuous phase with an "interface" boundary between the two phases. In the emulsion form, the triglycerides can come into contact with the lipase enzyme that results in a hydrolysis process during which molecules of water are split into hydrogen cations and hydroxide anions. For triglyceride, the lipase enzyme acts at the ester bond in its structure, hydrolysing the bond and "releasing" the fatty acids. The relatively small fatty acids molecules can pass through the epithelial cells in the small intestine. In this way, units of fat can be absorbed and enter the blood vessels [43]. The hydrolysis process follows a similar compartment model as described above. Chapter 4 provides an example to illustrate the idea.

In the entire absorption system, the transport rate in the small intestine is highly affected by the metabolic process after the substance enters the blood vessel [41]. For example consider the liver, a significant organ in the body that has a wide range of functions, including enzyme synthesis, production of biochemical and various metabolism processes. Most triglycerides enter the liver after being absorbed from the small intestine and transported in the capillaries. In the blood vessel, the triglyceride can release fatty acids by metabolism process which is presented in the next section. It is therefore necessary to link the details of metabolism to the absorption model in this research. In this thesis an attempt is made to link some of the details pertaining to metabolism with the absorption compartment model in Chapter 3.

1.1.4. The releasing process for fatty acids in absorption

A triglyceride (TAG or TG) is an ester derived from glycerol and three fatty acids. As the main constituent in vegetable oil and animal fat, the triglyceride functions in the body as a source of energy [164]. Usually triglycerides are stored in adipose tissue or fat cells. The fat cells can release triglyceride molecules for the energy use in the human body, but the triglyceride cannot be used directly in the absorption process. The triglyceride has to release fatty acids which contain energy for the human activity. Also the triglyceride itself converts to diglyceride, monoglyceride or glycerol. The structure of triglyceride is shown in the Figure 1.2.

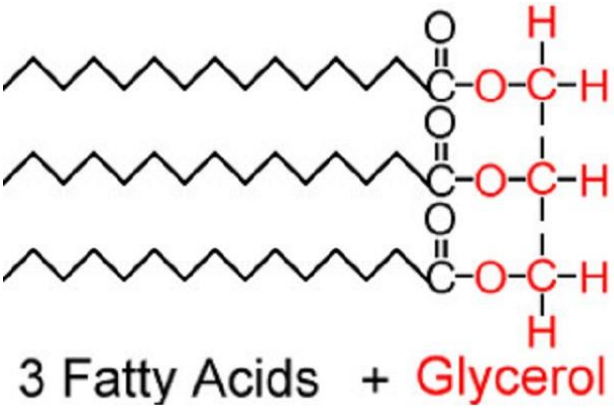

Figure 1.2 The structure of triglyceride

In the structure of triglyceride, the molecule is divided into two parts: glycerol molecule and three molecules of fatty acids. In the hydrolysis process, the ester bonds between glycerol and fatty acids are disconnected due to the reaction of lipase enzyme. In this way the fatty acids can be released in the absorption process. The triglyceride becomes diglyceride which contains two fatty acids molecules and glycerol, or monoglyceride which contains one molecule of fatty acid and glycerol. This process is known as hydrolysis.

In this study, the mathematical model is built regarding to the absorption of fatty acids. In Chapter 3 the dynamics of fatty acids in the blood vessel is considered in the absorption and metabolism system in human body. The ODE model considers the rate of change of free fatty acids concentration in the venous and arterial blood sample. In Chapter 4 a set of in vitro data is

considered. The hydrolysis reaction of triglyceride is controlled in the experiment by biologists. An ODE system is built regarding to the concentration of triglyceride, diglyceride, monoglyceride and fatty acids in the reaction. In Chapter 5 a PDE model is built considering the lipid transport in the absorptive cell. In the absorptive cell, the fatty acids and monoglyceride can enter the cell and form the triglyceride, then triglyceride moves into the blood vessel and releases the free fatty acids. This PDE model can be built by considering the fatty acids dynamics in Chapter 3, and the reaction inside the cell is similar to the reaction in the hydrolysis model in Chapter 4. In this way, the absorption of fatty acids can be represented by means of qualitative method.

1.1.5. Linkage between models and data

The mathematical model described in Equation (1.2) involves physical parameters known as absorption rates. These parameters may be constants or time dependent and may be determined by means of computational method [100]. Recently models for intestinal permeability or absorption [97, 109, 202] have shown a rapid development. The use of experimental data in determining these physical properties through the use of inverse problems is still an uncommon routine process amongst biologists, not mentioning non-linear models and many generic stochastic optimisation methods involved in the process of inverse problems.

In this thesis, the computational framework for inverse problems and the relevant optimisation methods as described in Chapter 2 is to be built and explored for the absorption and metabolism process of fatty acids. With these understandings of absorption process, mathematical models can be proposed using experimental data describing the lipid digestion. Using this framework, the absorption details can be quantitatively represented and the rate of digestion can be retrieved from the use of measurement.

1.2. The metabolism process

Metabolism refers to the chemical transformations of substances within the cells of living organs. The metabolism allows one organ to reproduce and grow, and also react to its environment. It is usually classified into two types: catabolism and anabolism. The catabolism refers to the breakdown process of big molecules inside the body. In the catabolism, the metabolism reaction can release energy for adenosine triphosphate (ATP) generation. The anabolism uses energy to form new compounds like proteins and nucleic acids. It is well known that the absorption and metabolism are closely related in the digestive system. Most substances in food need to be absorbed before the metabolism can take place in the tissue. Also many metabolism processes are necessary in order to break down the bigger molecules in the small intestine ready for the absorption process. Similar to the absorption process, the metabolism of proteins, carbohydrates and lipids have different pathways and chemical reactions [21]. In computational biology, the catabolism and anabolism processes are usually described by ODE systems.

An example of such ODE model for the metabolism of food diets is the glucose-insulin regulatory system [107, 115, 117]. The human body needs to maintain its glucose concentration level. The insulin is the main inhibitor for the glucose kinetics in blood vessels [116]. The insulin and glucose relation may be used to characterise the metabolism of the human body. Let C_G and C_I be the glucose and insulin concentration at time t. The rate of change of the concentration for glucose and insulin may be defined as

$$\begin{cases} \frac{dC_G}{dt} = G_{pro} - G_{uti} \\ \\ \frac{dC_I}{dt} = I_{pro} - I_{cle} \end{cases} \tag{1.3}$$

where G_{pro}, G_{uti} indicates the glucose production and utilization, respectively. I_{pro}, I_{cle} indicates insulin production and insulin clearance in the blood, respectively.

In this chapter, there are two types of compartment models for the absorption and metabolism process. In an absorption model such as Equation (1.2), the compartment indicates different sections of a body within which the concentration of substance is equal according to assumption. In this case, the mass transport is controlled by a flow rate and the ODE system represents the rate change of concentration of a unique substance in different compartment. In a metabolism process such as Equation (1.3), the compartments are used to describe the concentration of different substances which are involved in a chemical reaction. The rate change of concentration is proportional to the substance in the chemical reaction. More examples can be found in Chapter 3.

There are many models for the metabolism of glucose calibrated by experimental results [47, 105, 107]. In contrast, the compartment model for lipid metabolism may be more complicated due to its complexity of chemical reaction in the blood [57, 91]. In this thesis, one aim is to build a novel model of fatty acids containing the absorption process and the metabolism process.

1.3. The transport of fatty acids in cellular level

The movement of smaller compounds of nutrients in a cell is a complex process which includes certain biological mechanisms such as signalling, diffusion, chemotaxis, haptotaxis, reorientation due to the surrounding tissue fibres, cell-cell interaction, and many others [197]. There are also some mechanical considerations such as law of balance, mechanical forces, pressure, etc. [60, 133]. In the study of cellular kinetics as described in [65, 82, 145], the models are mainly for describing the cell migration through the extracellular matrix (ECM). The ECM is a collection of extracellular molecules secreted by cells, and it can be regarded as the outer environment for cell movement. These kinetic models do not provide any description inside the cell. A complete model describing the physiology inside the cell needs to be developed in order to provide better computational understanding of the process at the cellular level. This thesis attempts to provide an early study of fatty acids movement inside the epithelial cell, which forms an essential part of the lipids absorption process [8].

In this thesis, a reaction-diffusion system is built to represent the transport of lipid in the epithelial cell environment. The diffusion and the hydrolysis reaction inside the cell are considered in the intestinal epithelial cell. The study at cellular level provides a microscopic view of absorption process. The novelty of this model at the cellular level is the inclusion of a reaction term inside the cell that can be linked to the hydrolysis rate in the macroscopic kinetic model and the inverse problem as detailed in Chapter 4.

1.4. Aims and objectives of this thesis

The aim of this thesis is to extend existing compartment models by combining absorption and metabolism at the macroscopic level in order to best fit experimental data, to examine absorption at the cellular level based on a modified term in the partial differential equations (PDEs). Another aim is to explore various suitable numerical techniques in the studies related to inverse problems and data fitting. Finally, a first attempt in the understanding of effects on the outcome of absorption and metabolism due to several uncertainties which appear in the boundary conditions due to missing information and data is also included.

The main objectives of the thesis are as follows:

i. Extend the macroscopic compartment model to include the effect of metabolism for the fatty acid kinetics.

ii. Develop the concept of a regulator for the standard hydrolysis model for lipid metabolism.

iii. Propose a reaction-diffusion model for the fatty acids transport in the cellular model.

iv. Apply numerical techniques of handling in vivo and in vitro data for inverse problems.

v. Examine “Stochastic outcome” of the cellular model due to uncertain input.

1.5. Outline of the thesis

The remaining part of the thesis is organised as follows. In Chapter 2, related numerical methods and mathematical tools as applied in this research are introduced. The chapter begins with the concept of compartment model and the reaction-diffusion equations. The algorithm of inverse approach is presented in this chapter in preparation for the inverse problem to be presented in the following chapter.

In Chapter 3, a model for the fatty acids absorption and metabolism is developed to describe the fatty acids concentration data in the blood vessel. In this chapter, the existing compartment models are introduced [158]. There are modifications of these compartment models linking the fatty acids concentration to the absorption process.

Chapter 4 focuses on a significant stage of the lipid metabolism: the hydrolysis and esterification. The importance of these two processes [26] is explained and the related ODE models are built in the chapter. Modification of the model through the incorporation of Michaelis-Menten kinetics [113] is motivated in this chapter. The multi-objective optimisation problem was addressed by means of Quantum-behaved Particle Swarm Optimization (QPSO) method. A computational analysis of the weights used in the multi-objective function is provided.

Chapter 5 considers the absorption process at the cellular scale level. A partial differential equation (PDE) system is built to model the absorptive cell: the epithelium in the small intestine. A diffusion reaction system is developed indicating the movement of lipid molecules inside the cell. As the chemical reaction is the same as the esterification process described in Chapter 4, the esterification term in hydrolysis model is assumed as the reaction in the PDE model. As the membrane of epithelial cells has irregular structure and the feature is still unclear for biologists [172], the missing information and data are described as uncertainty on the boundary condition. By applying the Monte-Carlo method in the computational work, the confidence interval for lipid can be computed as the estimation of concentration of lipid inside the cell.

Finally, in Chapter 6, some conclusions are drawn which summarise the main work of the thesis and its overall direction. Various suggestions are also given for the direction of future work.

Chapter 2 Mathematical Preliminaries

This chapter gives the mathematical tools and concepts that are used in this thesis. In Section 2.1, the compartment concept and ODE for absorption and metabolism are discussed. Section 2.2 provides background of the reaction-diffusion phenomenon and the related PDEs used in the cellular model. Section 2.3 gives a brief introduction of methods in the inverse problem. Finally a brief description is given of the use of uncertainty analysis in the PDE model in an attempt to understand the effect of missing information in the absorption process.

2.1. The compartment model and ODE systems

Compartment models are often used to describe the macroscopic view of the kinetics in biological systems [194]. There are two definitions of compartment in computational biology [173, 193]. First a compartment is used to represent different substances involved in a chemical reaction. Second a compartment may refer to unique nutrients in different physical sections such as stomach or intestine in the absorption process. The compartments for part of the absorption can be indicated in the schematic view as below:

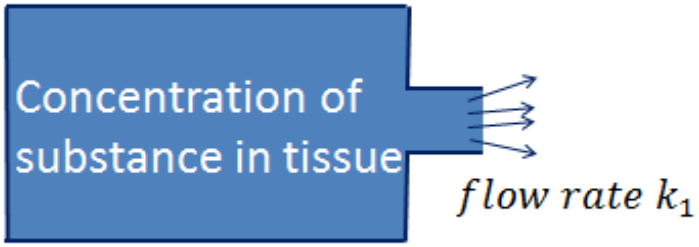

Figure 2.1 A sketch for mass balance system

Figure 2.1 indicates the mass flow for tissue in the absorption process. The absorptive organ such as stomach or small intestine can be considered as a mass balance system in the mathematical model. The substance in the compartment may have an outflow out of the system, and the nutrient in the compartment is also involved in other process such as metabolism in the small intestine. By assuming the volume of the compartment as V, the concentration of nutrient as C, the area of the interface of compartment as A. The mass balance equation can be written as below:

$$V\frac{dC}{dt} = -k_1AC + S_1 \tag{2.1}$$

where the k_1 is transfer rates from the compartment to the outer environment

In the model of Equation (2.1), a compartment system is built based on the physiologically based modelling. The term S_1 can be assumed as other chemical reactions in the digestion system. In the ODE model the different volume can be accounted for the physiologically based pharmacokinetic modelling (PBPK) [74]. In this study, the concentration of substance in the digestion system is considered in the mathematical model, and the values of parameter k_1 in Equation (2.1) are identified by inverse approach in this study by coupling with experimental data. The source term S_1 is assumed according to other chemical reactions in the metabolism process.

For the chemical reaction in the digestion process, the concentration of one nutrient in actual organs is described in the form of compartment. The model development process begins with defining the targets tissues in which the transport exists. Then the physiological parameters are defined representing the flow direction and rate. In this system, the time-dependent biological processes such as absorption are described as a system of ordinary differential equations. The parameters in the model are derived from physiological principles. The absorption system in this thesis can be built following these features of physiologically based pharmacokinetic models.

Another application of the compartment model is metabolism. Consider the reaction

$$N_2O_5 \xrightarrow{k} NO_2 + O_2 \tag{2.2}$$

which takes place in a complicated metabolism process. One can use the concept of concentration as a compartment, as described before, which results to three compartments for the reaction in Equation (2.2). Compartment A indicates the compound N_2O_5. Compartment B indicates the compound NO_2, and Compartment C indicates the compound O_2. The connection between the three components is shown in Figure 2.2.

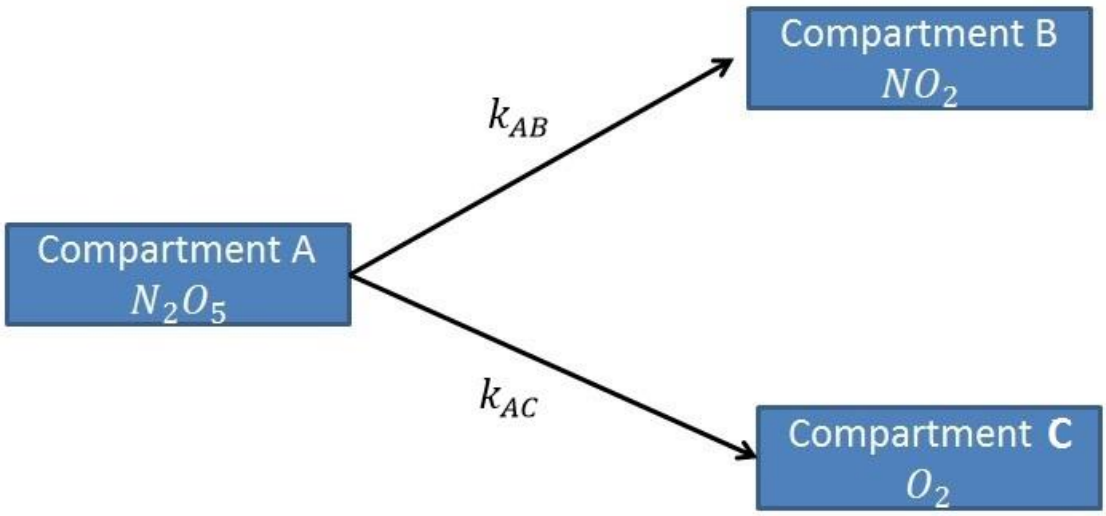

Figure 2.2 Compartments in a chemical reaction

Define C_A, C_B and C_c as the concentrations of N_2O_5, NO_2 and O_2, respectively. In the Figure 2.2, each compartment indicates different substances in a chemical reaction. There are many compartment models that describe the metabolism process which contains more than one reactants and productions [107, 143]. The kinetics for different substances related to each other as they are involved in a chemical reaction. The definition of compartment in this case is different from that in Equation (2.1) which only considers specific nutrient in different tissue. The chemical reaction may change the concentration of various nutrients in this compartment model. The kinetic equations are generally derived using law of mass action [99]. In this theory the rate of the reaction in Figure 2.2, i.e. the rate with which one molecule of N_2O_5 is transformed into NO_2 and O_2 is proportional to the amount of N_2O_5. The ODE system can be built as below:

$$\frac{dC_A}{dt} = -(k_{AB} + k_{AC})C_A \tag{2.3}$$

$$\frac{dC_B}{dt} = k_{AB}C_A \tag{2.4}$$

$$\frac{dC_C}{dt} = k_{AC}C_A \tag{2.5}$$

where the reaction rate is given by k_{AB} and k_{AC}.

As the metabolism and absorption are closely related in the human digestive system, both processes are considered simultaneously in the model building. The nutrients in the food such as lipids are transported into blood compartment by absorption, and then these substances can have a metabolism reaction in the blood vessel. In this way the compartments may have different meaning in the model development. In the absorption part, one compartment indicates the transit place in different organs. In the blood vessel part, compartment can represent the different substances, some are absorbed from absorption stage and other compartments indicate the nutrients existing in the blood vessel such as enzymes or insulin.

More complicated examples exist of using several ODEs and a generalisation of model in Equations (2.3) to (2.5). They can be written as a linear ODE system

$$\frac{d\boldsymbol{C}}{dt} = \boldsymbol{AC} \tag{2.6}$$

Where $\boldsymbol{C} = (C_1, C_2, \dots, C_N)^T$, $\boldsymbol{A}$ is a matrix, and N is the number of compartments. Initial condition such as $\boldsymbol{C}(0) = (C_1(0),\ C_2(0), \dots, C_N(0))^T$ is required in order to have a well-posed problem. Typically the eigenvalues and eigenvectors are required. For example, if A has n distinct eigenvalues, the differential equation has the following general solution:

$$\boldsymbol{C}(t) = c_1 e^{\lambda_1 t}\boldsymbol{u_1} + c_2 e^{\lambda_2 t}\boldsymbol{u_2} + \cdots c_n e^{\lambda_n t}\boldsymbol{u_n}$$

The parameters $\lambda_1, \lambda_2 \dots \lambda_n$ are the eigenvalues of matrix A, and $\boldsymbol{u_1}, \boldsymbol{u_2} \dots \boldsymbol{u_n}$ are the eigenvectors, $c_1, c_2 \dots c_n$ are constants. From the analytical solution form Equation (2.6) it can be seen that the eigenvalues and eigenvectors are key in obtaining the exact solution in such differential equations. Analytical techniques such as finding the eigenvalues of $\boldsymbol{A}$ exist for solving Equation (2.6) [104, 203].

In this thesis, numerical techniques are considered. There are typical numerical integration methods include Euler's method, Runge-Kutta methods [31], etc. On the other hand, the mathematical software Matlab has a range of differential equation solvers for initial value problems. There are some examples for these solvers such as ode34, ode113, ode15s. The work in Chapter 3 relies on a 4^{th} order Runge-Kutta method written in Matlab.

2.2. The reaction-diffusion equation

The reaction-diffusion systems are mathematical models describing the distribution of substances under the influence of two factors: local chemical reactions and diffusion which leads to the spread out of substances in space.

The reaction-diffusion systems are initially used to describe the substance reaction in chemistry [4, 53]. It can also represent the dynamics of population in biology [178], especially for the tumour growth [63]. In this study, the reaction-diffusion is used to model the transport in the epithelial cell. In the absorption process, digested food is able to pass into the blood vessels in the wall of the small intestine through the process of diffusion.

The absorption of fatty acids includes complex processes in the epithelial cell. The movement of molecule in the cellular level can be studied from just diffusion in the epithelial cell initially. One can start the analysis from the simple example of glucose diffusion at cellular level. The glucose absorption at the cellular level refers to transport from the lumen of the small intestine as shown in Figure 2.3. The layer of membrane between blood vessel and epithelial cells is called basolateral membrane and the opposite side is apical membrane. The glucose can enter the epithelial cell with the help of protein transporters [136], which provide a gradient for inflow into epithelial cells. In the basolateral membrane, the glucose has a flow out of the cell to the blood vessel.

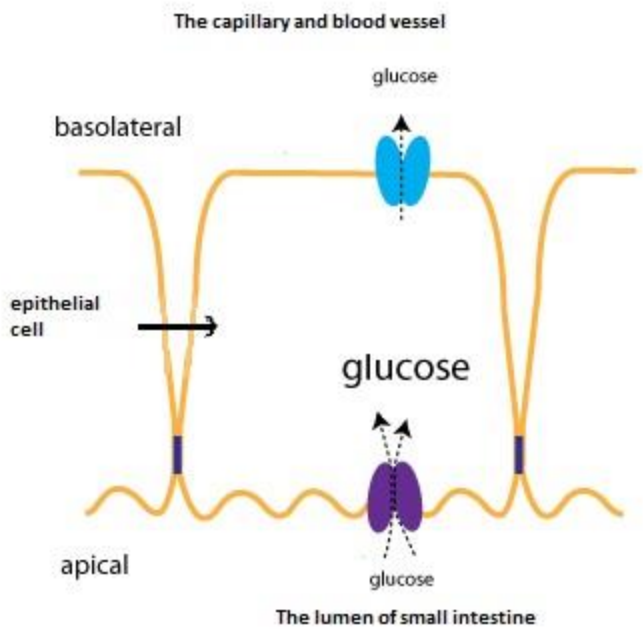

Figure 2.3 The transport of glucose through epithelial cell.

In modelling the epithelial cell as shown in Figure 2.3, the domain can be assumed in one dimension as the flow into and out of the cell in one direction. The domain can be taken by considering the rough shape of epithelial cell [137]. The flow in the membrane of a cell requires a gradient of the concentration to be imposed on the boundary condition as shown in Figure 2.4.

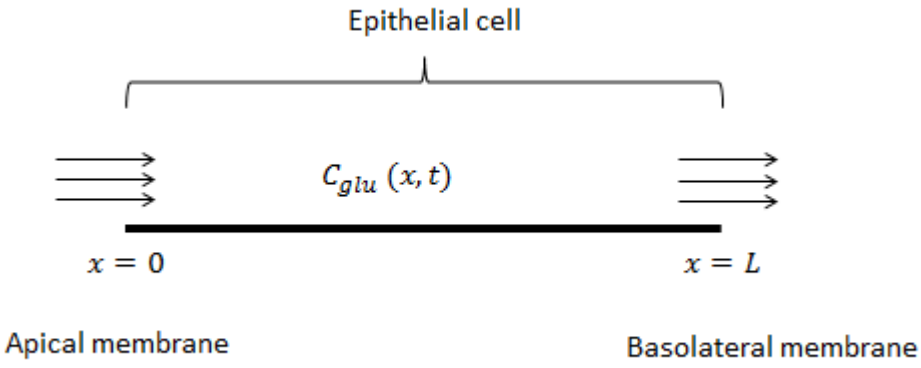

Figure 2.4 The domain for the cellular model of glucose transport

The length of an epithelial cell is set as L. The flow of glucose molecules into the cell is from the apical membrane which is along the boundary at $x = 0$, and out of the cell from the basolateral membrane, which is the boundary at $x = L$. A standard mathematical model used to describe the concentration changes with respect to time is the diffusion equation [4]. The equation is given as:

$$\frac{\partial C_{glu}}{\partial t} = D \frac{\partial^2 C_{glu}}{\partial x^2} \tag{2.7}$$

However this equation does not provide a full interpretation of the actual chemical reaction within the epithelial cell. In order to provide an insight into the possible process of chemical reactions, a reaction term is to be encapsulated into the PDE in order to describe the possible missing movement of molecules inside the cell. The equation for transport to be investigated in this thesis can now be written as below:

$$\frac{\partial C_{glu}}{\partial t} = D \frac{\partial^2 C_{glu}}{\partial x^2} + S(C_{glu}, x, t) \tag{2.8}$$

The boundary condition and initial condition are defined by considering the dynamics of concentration along the membrane of the cell, as shown below:

$$\frac{\partial C_{glu}(x=0,t)}{\partial x} = f_1(C_{glu}, t) \tag{2.9}$$

$$\frac{\partial C_{glu}(x=L,t)}{\partial x} = f_2(C_{glu}, t) \tag{2.10}$$

$$C_{glu}(x, 0) = C_0(x) \tag{2.11}$$

$C_{glu}(x, t)$ is a state variable that indicates concentration of glucose at position x at time t. D is the diffusion coefficient. In the boundary condition, $C_{glu}(x = 0, t)$ and $C_{glu}(x = L, t)$ describe the concentration of glucose along $x = 0$ and $x = L$ in Figure 2.4.

In the case of glucose transport at the cellular level, there is no chemical reaction inside the cell [85]. The source term can be set as non-reaction equation in the model ($S(C_{glu}, x, t) = 0$). The existence and uniqueness of solution in such reaction-diffusion equation can be found in [36].

The reaction term in Equation (2.8) may differ in different areas of computational biology. Examples of reaction terms from population dynamics of certain species include Fisher's equation and Newell-Whitehead-Segel equation can be found in [64, 76]. The reaction-diffusion equations are also widely used in the cancer invasion [71]. In this thesis a reaction diffusion model is built for fatty acids transport at cellular level based on the physiological knowledge.

2.3. Inverse problems for absorption and metabolism

Problems described in Section 2.1 and 2.2 are known as direct problems. These are problems with a given equation supplemented with suitable initial and boundary conditions. Very often rates of transport in Equation (2.1) to (2.11) are unknown parameters. In order to build the model using experimental data, the concept of inverse problem is needed. In contrast to the direct problem in which the cause is known and consequences need to be calculated, the inverse problem has the consequence being known and the causes such as parameters in the model are computed. These unknown parameters can be inversely determined by combining experimental data and differential equations. The process of computing unknown parameters with data and the model is known as solving an inverse problem.

In an inverse problem, the unknown parameters in the model may be represented in the vector form $\boldsymbol{P} = (p_1, p_2 \dots p_n)^T$, where n is the number of parameters. Consider the model for absorption, such as Equation (2.6), which is rewritten as

$$\frac{d\boldsymbol{C}(t;\boldsymbol{P})}{dt} = \boldsymbol{A}(\boldsymbol{P})\boldsymbol{C}(t;\boldsymbol{P}) \tag{2.12}$$

where $\boldsymbol{C}(t;\boldsymbol{P})$ is the concentration of substances in the absorption process. $\boldsymbol{A}(\boldsymbol{P})$ is a matrix which depends on the parameters. The aim of solving an inverse problem is to find an optimal parameter vector $\boldsymbol{P}$ such that

$$min_{\boldsymbol{P}}\, \Psi[\boldsymbol{P}] \tag{2.13}$$

where

$$\Psi[\boldsymbol{P}] = \left\| \boldsymbol{C}(t;\boldsymbol{P}) - \tilde{\boldsymbol{C}} \right\|^2 \tag{2.14}$$

Here $\tilde{\mathbf{C}}$ is the measurement such as experimental data for the absorption. $\boldsymbol{C}(t;\boldsymbol{P})$ is the solution of the inverse problem using the parameter vector in the above optimisation problem.

In this thesis, the methods for the inverse approach are mainly used to construct absorption and metabolism processes for fatty acids. The methods such as multi-objective optimisation are widely applied in the inverse determination of the parameter in biological models. The challenges in the application of inverse problem in computational biology include the uncertainty in the data and the under description of physiology in the mathematical model [59]. All these problems need to be solved by suitable inverse approach method and the appropriate assumptions in the model.

There are several gradient-based deterministic methods used in the inverse approach [56, 151]. Two of them which are considered to be the fundamental techniques for the gradient method are steepest descent method (SDM) and the conjugate gradient method (CGM).

As one of the simplest gradient based method, the aim of SDM is to find the local minimum of objective function $\Psi[\boldsymbol{P}]$ and the respective parameter $\boldsymbol{P}$ is the output of solving the inverse problem. To minimise Equation (2.14), define $\nabla\Psi$ as the gradient of a differentiable objective function within a given region. The SDM assumes that the decrease of $\nabla\Psi$ would be fastest by direction of $-\nabla\Psi$.

Let $\boldsymbol{P}^k$ represent the k^{th} iterative approximation of the minimisation problem, the iterative equation of the SDM can be defined as

$$\boldsymbol{P}^{k+1} = \boldsymbol{P}^k - \beta^k \nabla\Psi\,(\boldsymbol{P}^k) \tag{2.15}$$

where k is the iteration number, $\nabla\Psi\ (\boldsymbol{P}^k)$ defined as the gradient of the Equation (2.14), β^k is the step size of the update formula. The iteration terminates when $\|\nabla\Psi(\boldsymbol{P}^k)\| < \varepsilon$.

The details of the SDM can be shown as following:

Given $\boldsymbol{P}^0$

Initialize:$k = 0, \boldsymbol{G}^0 = \nabla\Psi(\boldsymbol{P}^0), \boldsymbol{D}^0 = -\boldsymbol{G}^0$;

Do while ($\|\boldsymbol{G}^k\| > \varepsilon$)

Define the step size: β^k

Obtain the new point: $\boldsymbol{P}^{k+1} = \boldsymbol{P}^k + \beta^k \boldsymbol{D}^k$;

Calculate the gradient: $\boldsymbol{G}^{k+1} = \nabla\Psi(\boldsymbol{P}^{k+1})$;

Identify the direction of search: $\boldsymbol{D}^{k+1} = -\boldsymbol{G}^{k+1}$;

$k = k + 1$;

End

In the SDM method, the step size β^k is changing in each loop. It is clear that in order to find the point where $\Psi(\boldsymbol{P}^k)$ is a minimum, the directional derivative at that point should be zero, i.e.

$$\frac{d}{d\beta^k}\left(\Psi(\boldsymbol{P}^{k+1})\right) = \nabla\Psi(\boldsymbol{P}^{k+1})^T \frac{d}{d\beta^k}(\boldsymbol{P}^{k+1}) = -\nabla\Psi(\boldsymbol{P}^{k+1})^T \nabla\Psi(\boldsymbol{P}^k) = 0$$

Therefore the β^k must be selected so that the $\nabla\Psi(\boldsymbol{P}^k)$ and $\nabla\Psi(\boldsymbol{P}^{k+1})$ are orthogonal. The computation of $\nabla\Psi(\boldsymbol{P}^k)$ can be easy if the analytical solution of $\nabla\Psi$ is given. If the problem is

nonlinear, it may require some computational technique such as the finite difference method. The SDM is easy to apply as each loop does not require large computational work. It is also stable in searching the minimum point if it exists [159]. For problems which are badly scaled such as some non-differentiable functions, SDM relies heavily on the choice of the starting point. On the other hand, SDM is suggested for solving problem when one has certain knowledge of where the minimum is. Note that there are limitations in applying SDM to ill-posed problems. As a result CGM may be used as an alternative.

The CGM is another gradient-based method that widely used in the optimisation. In contrast to SDM, the CGM does not give the direction of search beforehand in the algorithm. [142].

The CGM is given as below:

Initialize:$k = 0, \boldsymbol{G}^0 = \nabla\Psi\ (\boldsymbol{P}^0)\ , \boldsymbol{D}^0 = -\boldsymbol{G}^0$;

Do while ($\|\boldsymbol{G}^k\| > \varepsilon$)

Define the step size: β^k

Obtain the new point: $\boldsymbol{P}^{k+1} = \boldsymbol{P}^k + \beta^k \boldsymbol{D}^k$;

Calculate the gradient: $\boldsymbol{G}^{k+1} = \nabla\Psi(\boldsymbol{P}^{k+1})$;

Calculate the conjugate coefficient: $\gamma^k = \frac{(\boldsymbol{G}^{k+1})^T \boldsymbol{G}^{k+1}}{(\boldsymbol{G}^k)^T \boldsymbol{G}^k}$;

Identify the direction of search: $\boldsymbol{D}^{k+1} = -\boldsymbol{G}^{k+1} + \gamma^k \boldsymbol{D}^k$;

$k = k + 1$;

End

The SDM only needs to compute step size β^k in each loop, but CGM needs to consider conjugate coefficient γ^k which is more computationally expensive in practise as it needs to store vector in each loop in the algorithm, but the SDM may need many iterations to compute a local minimum with a required accuracy [56]. Both gradient-based methods have a better performance for linear system as the gradient can be accurately estimated. For the nonlinear or multi-objective optimisation problem, stochastic methods may be considered to find the optimal parameters.

In addition to gradient type of methods, stochastic methods are increasingly being used in optimisation [22, 97]. The main idea of using a stochastic strategy is to include a wider class of objective functions that are not continuous or differentiable. In this chapter, two classic stochastic methods are discussed: the genetic algorithms (GA) and particle swarm optimisation (PSO).

The GA was originally proposed by Holland [84]. The optimal parameter search begins with a random population in the search domain and continues for generations. The objective function in Equation (2.13) is defined as fitness which is calculated in the algorithm. The GA is presented as below:

Choose the initial population of individuals;

Evaluate the fitness of each individual in the population;

Do While(stopping criterion is not satisfied)

Select the best-fit individuals for reproduction;

Breed new individuals through crossover and mutation operations to give birth to offspring;

Evaluate the individual fitness (objective function) of new individuals;

Replace the individual fitness (objective function) according to the above evaluation

Replace least-fit population with new individuals;

End

In the GA method, the fitness function is the objective function defined in the inverse problem. The fitness function represents the difference between simulation results and the measurements. In the replacing stage in GA method, the individuals with better performance in fitness functions are selected and the search can go closer to the optimal solution. Searching for the optimal solution with a large population of individuals often requires very expensive fitness function simulation; therefore how to define a fitness function is also important for the computational efficiency.

The PSO was developed by Eberhart and Kennedy in 1995 [55]. The idea was inspired by social behaviour of bird flocking. The method involves a set of population particles such that each particle can be seen as a potential solution of the optimisation problem. The fitness function of each particle is evaluated in the algorithm. The key factor in PSO is the estimation of the velocity for particle i at k th estimation $(\boldsymbol{V}_i(k))$ which is computed by combining the best particle location with minimum fitness function and global best optimal particle obtained from previous iteration. The updated position for the next iteration can be computed as

$$\boldsymbol{X}_i(k+1) = \boldsymbol{X}_i(k) + \boldsymbol{V}_i(k) \tag{2.16}$$

The PSO method is shown in the following algorithm:

Define the personal best position for particle i is denoted as $\boldsymbol{P}_i$ which is the optimal objective function in each loop. The global best position of all particles is denoted as $\boldsymbol{P}_g$ indicating the best solution in all previous search.

Initialize the position $\boldsymbol{X}_i$, $\boldsymbol{P}_i$, $\boldsymbol{P}_g$and velocities of population.

Do while ($k < k_{max}$)

For each particle $i = 1,2 \ldots, M$

Evaluate the fitness function $f\left(\boldsymbol{X}_i(k)\right)$ according to Equation (2.16)

If $f\left(\boldsymbol{X}_i(k)\right) < f(\boldsymbol{P}_i(k))$ then

$\boldsymbol{P}_i(k) = \boldsymbol{X}_i(k)$;

If $f\left(\boldsymbol{P}_i(k)\right) < f(\boldsymbol{P}_g(k))$

$\boldsymbol{P}_g(k) = \boldsymbol{P}_i(k)$;

End for

For each particle $i = 1,2 \ldots, M$

Update the Velocity $\boldsymbol{V}_i(k)$;

Update the position $\boldsymbol{X}_i(k+1)$ by Equation (2.16);

End for

End do

The process of updating the velocity controls the performance of the PSO method. Consider a PSO system with M particles $\boldsymbol{X} = \{X_1, X_2, \dots X_M\}$ and every particle is regarded as a volume-less body in the D-dimensional space $\mathrm{X_i} \in \Omega \subseteq \Re^{\mathrm{D}}$. Define the D-dimensional position and velocity for particle i at time k as $\boldsymbol{X}_i(k) = (X_{i,1}(k), \dots, X_{i,D}(k))$ and $\boldsymbol{V}_i(k) = \left(V_{i,1}(k), \dots, X_{i,D}(k)\right)$. The optimisation problem is defined as

$$\min_X f(X)$$

The personal best position for particle i is denoted as $\boldsymbol{P}_i(k) = (P_{i,1}(k), \dots, P_{i,D}(k))$ and can be considered as the best previous position. The global best position of all particles is denoted as $\boldsymbol{P}_g(k) = (P_{g,1}(k), \dots, P_{g,D}(k))$, $g\epsilon\{1,2 \dots M\}$. The personal best position can be defined as

$$\boldsymbol{P}_i(k) = \begin{cases} X_i(k) & if\ f\left(X_i(k)\right) < f(P_i(k-1)) \\ P_i(k-1) & if\ f\left(X_i(k)\right) \geq f(P_i(k-1)) \end{cases}$$

The global best position of the swarm is solved by

$$g = arg \min_{1 \leq i \leq M} (f(\boldsymbol{P}_i(k)))$$

Then the velocity of a particle is updated by the equation

$$V_{i,j}(k+1) = V_{i,j}(k) + c_1 r_1 \left(P_{i,j}(k) - X_{i,j}(k)\right) + c_2 r_2 (P_{g,j}(k) - X_{i,j}(k))$$

where $i = 1,2, \dots M. j = 1,2 \dots D$. For the optimisation problem in this thesis, the dimension D represents the number of parameters that need to be optimised in the inverse approach. c_1 and c_2 are constants known as acceleration coefficients. c_1 indicates the maximum step size towards the personal best position, and c_2 indicates the maximum step size towards the global best position. r_1 and r_2 are random numbers distributed uniformly in $(0,1)$.

The PSO method has been widely used for problems for which it is difficult to compute their gradients and is suitable for large parameter space and candidate solutions. Several variants of

the classical PSO method can be found in the literature [40, 110, 180, 181]. As an example, the Quantum- Behaved Particle Swarm Optimisation is discussed here.

The Quantum-Behaved Particle Swarm Optimisation is a modified version of PSO. It is motivated from quantum mechanics and dynamical analysis of PSO [40]. As a relatively new version of PSO, the QPSO algorithm used a strategy which depends on a quantum delta potential well model to sample around the previous best points [69, 180]. In quantum physics, the state of a particle can be depicted by its wave function $\varphi(x,t)$. Then in a QPSO system, the hypothesis is made that each particle is in a quantum state and is formulated by its wave function instead of the position and velocity which are in PSO. In a QPSO system personal best solution $\boldsymbol{P}_i(k)$ and global best position $\boldsymbol{P}_g(k)$ are also needed in the computation and the update of the particle's position is controlled by the following equation:

$$\boldsymbol{X}_i(k) = \boldsymbol{p}_i(k) + 0.5\boldsymbol{L}_i(k)\, ln\left(\frac{1}{u_i(k)}\right) \tag{2.17}$$

where $u_i(k)$ is a random number uniformly distributed in (0,1); $P_i(k)$ is the local attractor and defined as

$$\boldsymbol{p}_i(k) = \varphi_i(k)\boldsymbol{P}_i(k) + (1 - \varphi_i(k))\boldsymbol{P}_g(k) \tag{2.18}$$

where $\varphi_i(k)$ is a random number uniformly distributed in (0,1).

In Equation (2.17), the $L_i(k)$is computed by

$$\boldsymbol{L}_i(k) = 2\beta|\boldsymbol{P}_i(k) - \boldsymbol{X}_i(k)|$$

Then the algorithm is implemented in the following procedures.

The personal best position for particle i is denoted as $\boldsymbol{P}_i(k) = (P_{i,1}(k), \dots, P_{i,D}(k))$ and can be considered as the best previous position. The global best position of all particles is denoted as $\boldsymbol{P}_g(k) = (P_{g,1}(k), \dots, P_{g,D}(k))$, $g\epsilon\{1,2 \dots M\}$

Let $\boldsymbol{P}_k = \{\boldsymbol{P}_i(k); i = 1,2 \dots \dots M\}$ be a set of approximate parameter vectors approximating $\boldsymbol{P}$. Each member of the set $\boldsymbol{P}_k$ depends on the personal best position,$\boldsymbol{P}_i(k)$, of the ith approximate parameter vector and the global best position, $\boldsymbol{P}_g(k)$, of all approximate parameter vectors. The update of $\boldsymbol{P}_i(k)$ follows the QPSO method as described in [188] leading to a new set of approximate parameter vectors denoted as $\boldsymbol{X}_k = \{\boldsymbol{X}_i(k); i = 1,2 \dots \dots M\}$. The general steps of the algorithm are shown below.

Initialize the population of $\boldsymbol{X}_0$ and the personal best population $\boldsymbol{P}_i(k)$;

Do while $k < k_{max}$

For each particle $i = 1,2 \dots M$

Evaluate the fitness $\varphi\big(\boldsymbol{X}_i(k)\big)$

If $\varphi\big(\boldsymbol{X}_i(k)\big) < \varphi\big(\boldsymbol{P}_i(k)\big)$ then

$\boldsymbol{P}_i(k) = \boldsymbol{X}_i(k)$

If $\varphi\big(\boldsymbol{P}_i(k)\big) < \varphi\big(\boldsymbol{X}_i(k)\big)$ then

, $\boldsymbol{P}_g(k) = \boldsymbol{X}_i(k)$

End

Compute the mean best position;

For each particle $i = 1,2 \ldots M$

Use the mean best position to compute $\boldsymbol{P}_i(k)$ and then $\boldsymbol{X}_i(k)$ according to Equation (2.17) and (2.18)

End

End do

Compared to the gradient-based methods, the QPSO has its advantages on the computation time and convergence. For the SDM, it is suggested that [159] the method is appropriate when one has some knowledge about the interval where the minimum located. The SDM is generally considered to be a poor choice for an optimisation and it may be used in conjunction with other optimizing methods to obtain a better convergence result. As an improvement of SDM, the CGM has a regulation process inside every loop of the algorithm. As a conclusion, the gradient-based method has fast convergence, while the inherent difficulties with the gradient-based methods are the dependence on the initial guess. The other disadvantage for gradient-based methods is the demand for complicated gradient computation, especially for the non-linear problem.

The stochastic method such as GA and PSO gives a different type for searching the optimal result. In a genetic algorithm, the concept of candidate solutions is introduced. The iterative process of selection of the best solution in the candidate solutions leads the optimisation process towards a better solution. However, GA does not scale well with the increase of complexity of the problem. This means the optimisation problem must be tractable to evolutionary search and be broken down into the simplest representation to fit the mutation and operator inside the GA. For specific optimization problems, other optimization algorithms may be more efficient than GA in terms of speed of convergence. An alternative method is PSO. The PSO algorithm is a computational method that iteratively improves candidate parameters with measurement in the inverse approach. The PSO method allows fewer assumptions about the problem when compared to gradient-based methods and it does not need the gradient of the problem be optimized. As a

development for PSO method, the QPSO considers the quantum mechanism of the particles in the iterative method. The update equation for each generation of particles is given in Equation (2.17). According to the global convergence criterion in [195], one can conclude that the QPSO method is a global convergent algorithm whereas the original PSO is not. Also the QPSO does not need to compute velocity vector which is compulsory in the PSO method. The experimental results also indicates that for many well-known benchmark functions the QPSO has a better convergence when compared to PSO method [188 ,189].

In this thesis, the QPSO is used in the inverse problem in Chapter 3 and Chapter 4. $\boldsymbol{P}_k$ in the algorithm represents the unknown parameters in the ODE system.

2.4. The uncertainty study and Monte Carlo method

There are two sources of uncertainties in absorption and metabolism process. First the incomplete model used in the absorption and metabolism. For example the activity of enzymes related to the function of villi [171] is not described in the model [155]. Second the errors introduced into the experimental data during nutrients administration [61].

In this thesis, the uncertainty of the movement of molecules along the membranes of epithelial cells is discussed. As shown in Figure 2.3, the membrane of intestinal epithelial cells which is linked to intestinal lumen in apical side has a finger-like projection called villi [37]. Many enzymes in form of nutrients lie on the surface of villi [171], and the activities of enzymes attached to the villi vary in terms of individuals [122]. Due to this unclear information in biological experiment, the uncertainty is assumed in the cellular model. In the reaction-diffusion equations for epithelial cells, the uncertainty of molecule movement on the villi membrane takes place at the boundary condition of PDEs at $x = 0$, which is defined as Neumann boundary condition in this thesis:

$$\frac{\partial C(0,t)}{\partial x} = p_1 C(0,t) + \epsilon C(0,t) \tag{2.19}$$

where p_1 is the first-order kinetic parameter in this equation and $C(0,t)$ is the substance concentration such as lipids or fatty acids on the boundary. The $\epsilon C(0,t)$ handles the uncertainties in the boundary condition.

Probability Density function

In a random experiment, one needs to assign a probability to each measurable subset of the possible outcomes of the randomness in the simulation. When considering the probability distribution for the random samples, the difference between discrete and continuous random variables should be distinguished. In a discrete distribution, the possibility to each possible value is defined. For a continuous case, probabilities can be nonzero only if they refer to intervals. Most often, the equation used to describe a continuous probability distribution is called a probability density function. The randomness of ϵ in Equation (2.19) often follows a probability density function in the uncertainty analysis [102]. In statistics, the probability density function (PDF) is a function that describes the relative likelihood of a random variable to take on a given value. Consider an example of uniform distribution: random variable X is in an interval with minimum a and maximum b, and X is equally probable to be any number in interval (a, b), then the PDF of X's distribution is:

$$f(x) = \begin{cases} \frac{1}{b-a} & for\ a \le x \le b \\ 0 & for\ x < a\ or\ x > b \end{cases} \tag{2.20}$$

where $f(x)$ indicates the probability density at a particular value of x. The integration of Equation (2.20) equals to one, indicating the probability of all possible values for X is one.

Expected Value

For any probability density distribution, the expected value $E(Y)$ is defined as

$$E(Y) = \int_{-\infty}^{+\infty} xf(x)\,dx$$

The above definition is defined as the expect value for a continuous random variables with the identified distribution. The sample of data set is usually used in the uncertainty analysis. In this study, the sampling distribution is to describe the randomness in the uncertainty analysis. A sample is a set of observable random variables $X_1, X_2 \dots X_N$, The number N is called the sample size [148]. Then the sample of variables can be written as

$$\boldsymbol{Y} = (X_1, X_2 \dots X_N) \tag{2.21}$$

The sample of $\boldsymbol{Y}$ is called identically distributed if every X_i has the same probability distribution [148]. Note that in a sample, the X_i need not be independent or identically distributed. For a sample with finite population, the population mean can be used to calculate the expect value of the sample. In probability theory, the law of large numbers is usually applied in the expected value analysis. According to this theorem, the average of the result obtained as the number of trials tends to infinity tends to the expected value. For example, one has N is the sample size in $\boldsymbol{Y}$. If N is an extremely large number, the average values of $X_1, X_2 \dots X_N$ is defined as expected values or mean of such PDF. The expected value of sample of Y is represented as $E(\boldsymbol{Y})$, which means:

$$E(\boldsymbol{Y}) = \frac{X_1 + X_2 + \cdots X_N}{N} \tag{2.22}$$

where N is the sample size.

The law of large number is significant in the application as it considers a long-term result for the mean of some random events. It is assumed in the law that the average of the results obtained from a large size of sample should be closer to the expected value, and it trends to become closer if the sample size is larger.

Variance

The variance of sampling probability distribution is defined as:

$$Var(\boldsymbol{Y}) = E([\boldsymbol{Y} - \mu]^2) \tag{2.23}$$

where μ is the mean values of samples $\boldsymbol{Y}$. From Equation (2.23) it can be seen that variance measures how far a set of numbers is from the average number. In the uncertainty analysis, the mean and variance of samples can be calculated to measure the uncertainty in computational work and more details are represented in Chapter 5.

The randomness for uncertainty may have various probability density distributions. One example provided in this thesis is the normal distribution. The normal (or Gaussian) distribution is a common continuous probability distribution and often used in the natural and social sciences to represent real-valued random variables whose distribution are not known [7, 137]. The probability density of the normal distribution is:

$$f(x|\mu_n, \sigma_n) = \frac{1}{\sigma_n\sqrt{2\pi}} e^{-\frac{(x-\mu_n)^2}{2\sigma_n^2}} \tag{2.24}$$

Here μ_n is the mean of distribution and σ_n^2 is the variance. The notation of normal distribution in Equation (2.24) is written as $\mathcal{N}(\mu_n\ , \sigma_n^2)$.

Monte Carlo method

With the PDF of random variables in Equation (2.19), the parameter uncertainty can be defined with appropriate probability distribution. The uncertainty analysis can be processed by means of Monte Carlo method. The Monte Carlo method is an algorithm that provides repeating random sampling to generate simulation results. To be specific, the samples are generated by repeating random sampling with a normal distribution in this study, which means:

$$\boldsymbol{Y}_1 = (\ \epsilon_1, \epsilon_2 \ldots\ \epsilon_N) \tag{2.25}$$

Each ϵ is a random number with normal distribution. $\boldsymbol{Y}_1$ is the samples with all possible random variables in this simulation. N is the sample size which means the number of repeating sampling. With $\boldsymbol{Y}_1$ obtained in Equation (2.25), there are N possible values for ϵ in boundary condition of the model in Equation (2.19). The Monte Carlo method requires for N simulations of model to obtain N numerical results in reaction diffusion models. The numerical results can reflect the uncertainty in the boundary condition. A schematic view can be seen as below:

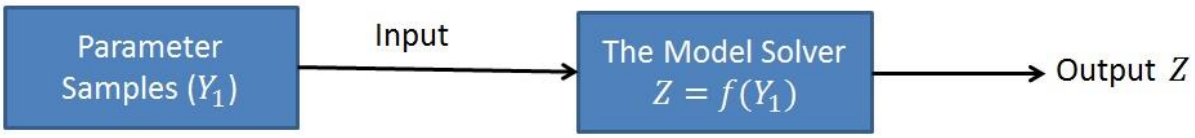

Figure 2.5 Sketch of the Monte-Carlo method for the uncertainty of parameter in the model.

In this thesis, the output $\boldsymbol{Z}$ indicates the sample of substance concentration in the reaction-diffusion model. The sample size of $\boldsymbol{Z}$ is same as the size of $\boldsymbol{Y}_1$. The features of $\boldsymbol{Z}$ is affected by the uncertainty in sample $\boldsymbol{Y}_1$. In this thesis the normal distribution samples are used which is the standard way in many biological applications [7]. More details are discussed in Chapter 5.

2.5. Summary

In this section, related mathematical tools used in this thesis are presented. Section 2.1 provides a discussion of compartment models and their application in the absorption and metabolism processes. A typical compartment model describing the absorption and metabolism is usually written in the form of ODE. Section 2.2 provides a discussion of the reaction-diffusion system which can be used as cellular model for substance movement in the epithelial cells of small intestine. Next the inverse approach applied in this thesis is discussed in Section 2.3. Finally in Section 2.4, the uncertainty analysis in PDE model is explained as well as the Monte Carlo method.

Chapter 3 A modified model for the fatty acids absorption and metabolism

Chapter 1 explains the concept of a compartment and its application in medical biology. Typically a compartment may be used to represent the concentration of fatty acids in the absorption process, or may be used to represent different chemical compounds. In this chapter, a compartment model is applied to the absorption and metabolism process of fatty acids.

The fatty acid concentration in the plasma usually shows a large fluctuation in a short period of time in response to various human activities [68]. The key factor in the concentration regulation is the inhibition of hormone-sensitive lipase by insulin [62]. After the hydrolysis of chylomicron-triglyceride (TAG) by lipid protein in adipose tissue, there seems to be regulation of the change of the fatty acids concentration due to esterification by adipocytes and release into plasma as free fatty acids [130]. Note that fatty acids may or may not take effect along the pathway of esterification [163], and both hydrolysis and esterification are affected by the metabolism process in the blood.

Several compartment-based metabolism models describing fatty acid kinetics exist in the literature [13, 24, 124, 138]. The model provided by Srinicasan et al [174] built a four compartment model describing the concentration of glucose, fatty acids and insulin in different physical sites. Boston [25] presented a two compartment model in 2004 to describe fatty acids and glucose kinetics for an individual cow and speculated that such model might be useful for modelling fatty acid kinetics in humans. A modified version of Boston's model was developed by adding insulin compartment following a range of experimental protocol [12, 119]. Some other models [43, 101] have been built for glucose and insulin compartments in human body and may be used to determine dose-response curves. Much of the work in the literature paid attention to the stability of the ODEs and the interaction between different chemicals.

As far as metabolism is concerned, much of the research concentrated on the chemical reactions within blood vessels. The compartment models as described above are used to model such chemical activities without taking account of the absorption process before the substance enters blood vessel. Both metabolism and absorption are physiologically and computationally complex. Therefore fully coupling them would lead to a very difficult computational problem. In this chapter, the main concern is to consider two tasks. Firstly, a linear time-dependent compartment model for absorption is built to describe the mass flow transit in different compartments. Experimental data is used to identify mass transfer rate of fatty acids using an inverse problem approach. Secondly a novel non-linear compartment model is introduced to compute the absorption and the metabolism processes of fatty acids.

3.1. The inverse problem for multi-compartment absorption model

Food is digested in the stomach forming a thick fluid known as chyme which enters the duodenum where mixing with enzymes takes place. This mixed fluid passes along the small intestine releasing fatty acids on the way. Here absorption of fatty acids will take place by 'diffusing' through small intestine wall full of epithelial cells and reaching blood capillaries in

the end. A multi-compartment model may be built such that each compartment represents part of the digestive system. Concentration of substances in each compartment may be modelled through suitable means of transfer from one compartment to another.

Note that there is a time lag between fatty acids appearing in the plasma and the intake of food supplement. This elapsed time represents the time required for (i) transfer of food from oesophagus to the stomach and eventually into the intestine for absorption, (ii) food dissolution in the delivery system, (iii) the action of some inhibition reactions, (iv) delay of enzyme activation and (v) molecule transfer through the absorbing site tissues. Due to these reasons the appearance of free fatty acids in the plasma is delayed and this situation is known as the absorption delay [139].

Hence it is important to develop a model, which governs concentration of fatty acids in the absorption phase, without requiring excessive knowledge of the underlying digestion process. In order to achieve this, a transit compartment absorption model [161] before the plasma compartment may meet this requirement.

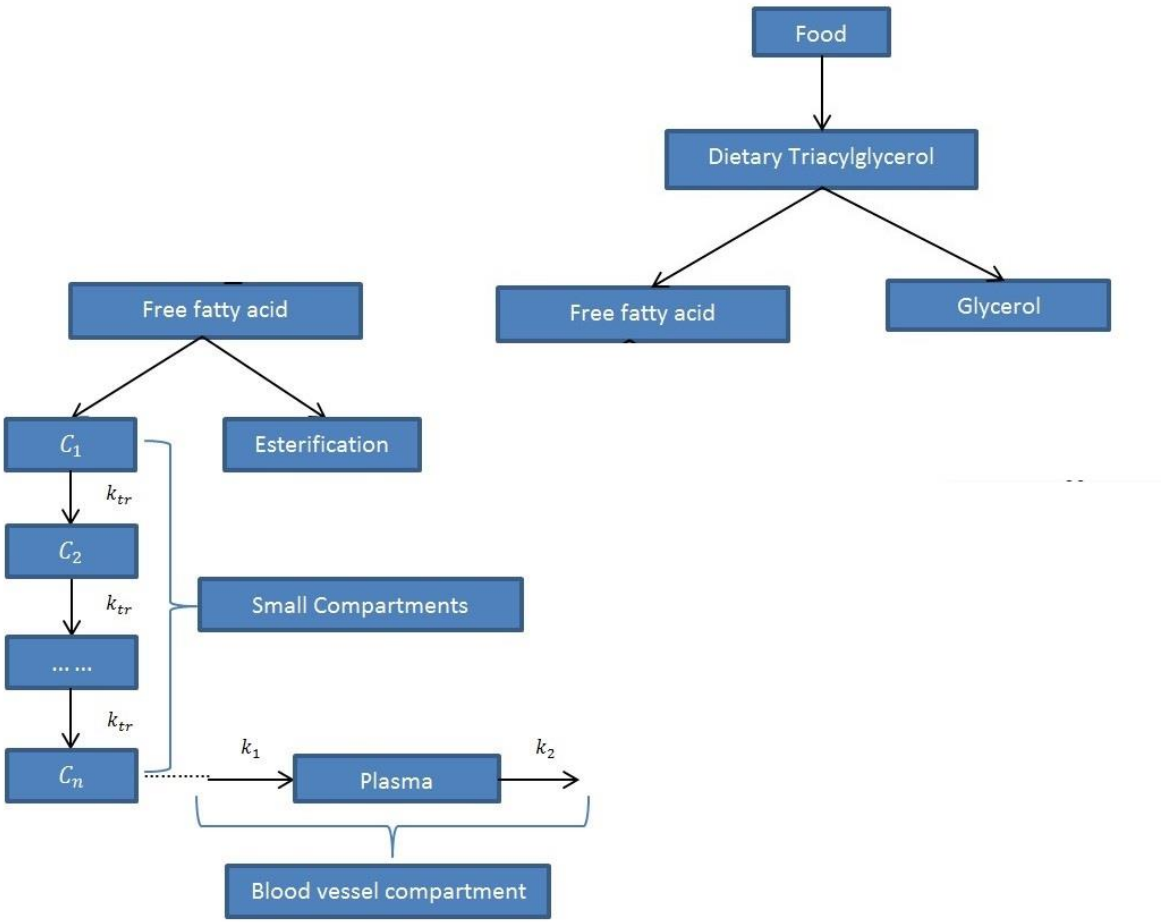

Figure 3.1 Schematic view of the fatty acid flowing through the chain of transit compartments

Figure 3.1 depicts a simple compartment system containing several transit compartments after considering the physiological remarks discussed above. Fatty acids are released from triacylglycerol and appear in the first transit compartment where the concentration of fatty acid is denoted as C_1. The food passes through different compartments and the concentrations of fatty acids in the nth compartment is denoted as C_n. The flow between these transit compartments is assumed to have the same rate k_{tr}. The rate of change of concentration in different compartments $\frac{dC_i}{dt}, i = 1.2 \ldots . n$ can now be modelled by a system of differential equations as given by Equation (3.1).

$$\frac{dC_1}{dt} = -k_{tr}C_1$$

$$\frac{dC_2}{dt} = k_{tr}C_1 - k_{tr}C_2$$

$$\dots\ \dots\ \dots\ \dots \tag{3.1}$$

$$\frac{dC_n}{dt} = k_{tr}C_{n-1}$$

This ODE system indicates a delay for the transfer or release of the fatty acid and requires a non-zero initial condition for C_1 and zero initial condition for the rest. In this thesis, the initial condition of C_1 is related to the experimental data. The analytic solution of C_n can be obtained as

$$C_n(t) = \Gamma \frac{(k_{tr}t)^n}{n!} e^{-k_{tr}t} \qquad (n \neq 1) \tag{3.2}$$

where Γ is a constant. A typical number of transfer compartments are used in [139] was $n = 8$.The initial condition for the first compartment is denoted as C_0 which is typically from literature or experiment [179]. The value of C_0 is the same as Γ in Equation (3.2). The transfer rate in this absorption delay system is associated with the maximum absorption time [161] and can be defined as

$$k_{tr} = \frac{n+1}{T_{max}}$$

To investigate the feature of the time-dependent profile in Equation (3.2), the values of the parameters can be defined as $T_{max} = 360\ min, \Gamma = 1\ mol \cdot L^{-1} \cdot min^{-1}$, $n = 9$ .The concentration of the substances ($C_n(t)$) can be plotted as below:

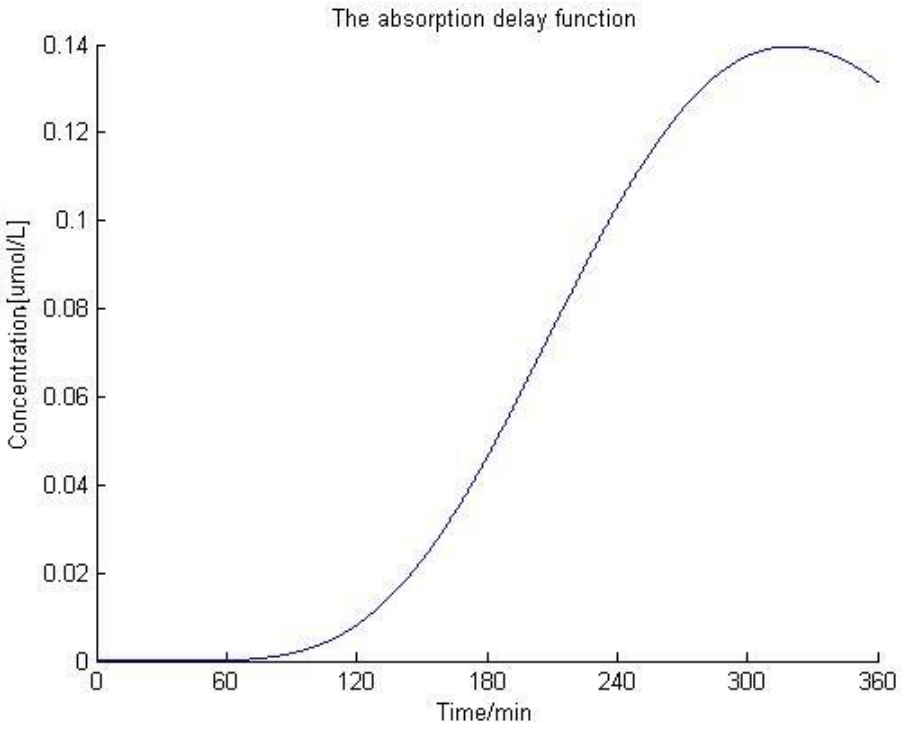

Figure 3.2 The delay function for the absorption

From above figure it is obvious that the concentration of $C_n(t)$ is very close to zero in the first 60 minutes, the increase of the concentration has a delay and started from about 70 minutes. The feature of absorption can be represented from the dynamic of $C_n(t)$ and it can provide an inflow into the plasma compartment.

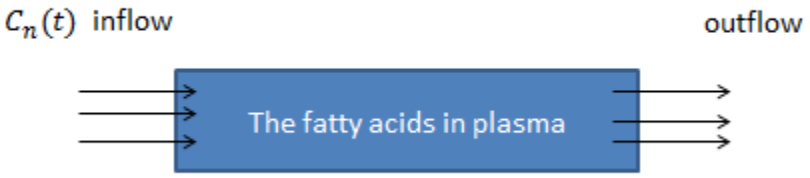

Figure 3.3 The transport into plasma compartment with absorption delay

Fatty acids are transported from the last compartment to the plasma compartment. The absorption delay function can describe the source for inflow to the plasma compartment and the absorption rate of fatty acid into plasma is denoted as k_1. The absorption delay can provide an inflow into the plasma compartment and the similar application can be found in [161]. The decrease of fatty acids is due to metabolism with the rate of change given by k_2. The analytic solution of the last small compartment can be used towards the plasma compartment and the equation governing the kinetics of fatty acids in plasma can be written as

$$\frac{dC_{pl}}{dt} = k_1 C_n - k_2 C_{pl} \tag{3.3}$$

If k_1 and k_2 are known, Equation (3.3) subject to a suitable initial condition $C_{pl}(0)$ is a direct problem. If k_1 and k_2 are unknown, the aim is to determine the two parameters k_1 and k_2 in Equation (3.3) using experimental data.

The experimental data as provided in [179] was adopted in the numerical tests below. The data involved 14 healthy female volunteers aged between 29 to 70 years old who were prevented from smoking, alcohol and unaccustomed exercise for 24 hours before the study. The meal which contains 60g fat and 13g protein was given to volunteers at 0 min and blood samples were taken from artery and venous vein at 30 minute intervals for the first two hours and 60 minute intervals in the next four hours. There are two sets of data as provided in [179]: the fatty acids concentrations in the artery and the venous blood vessel, respectively.

The aim of the inverse problem as described in Chapter 2 is to find the optimal parameter vector $\boldsymbol{P}^* = \begin{pmatrix} k_1^* \\ k_2^* \end{pmatrix}$ such that

$$\min_P \Psi(\boldsymbol{P}^*)$$

where

$$\Psi(\boldsymbol{P}) = \left\| C_{pl}(t; \boldsymbol{P}) - \tilde{C} \right\|^2$$

Here $\tilde{C}$ is the experimental data in [179]. $C_{pl}(t;\boldsymbol{P})$ is the numerical solution of the direct problem evaluated at $\boldsymbol{P}$. The problem in Equation (3.3) is a linear differential equation and there are only two unknown parameters in the inverse problem. The gradient-based method is appropriate as it suits linear problems and gives a quick approach in the inverse problem [142]. The conjugate gradient method is used to solve the minimisation problem which involves updating the approximate solution $\boldsymbol{P}^k = \begin{pmatrix} k_1 \\ k_2 \end{pmatrix}$ where the superscript k is the iteration number in the conjugate gradient method. The norm of the gradient of least square error function $\|\nabla\Psi(\boldsymbol{P}^k)\|$ is computed in the conjugate gradient method. A direct problem is governed by Equation (3.3) with $\boldsymbol{P}^k$. The direct problem is solved by means of a 4th-order Runge-Kutta method. When $\boldsymbol{P}^k$ converges to $\boldsymbol{P}^*$ the concentration $C_{pl}(t;\boldsymbol{P}^*)$ in veins and in arteries are computed and plotted along with the experimental data in Figures 3.4 and 3.5, respectively.

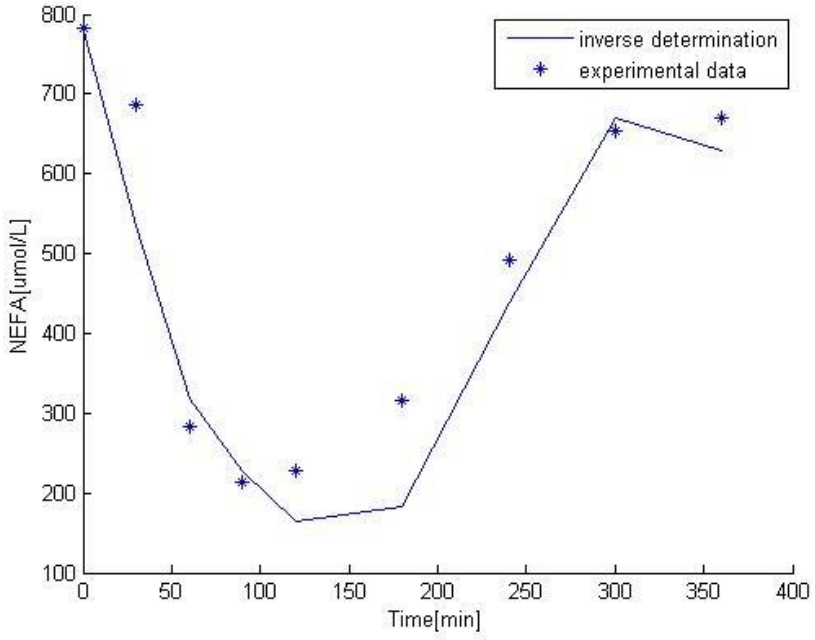

Figure 3.4 The concentration of fatty acids in veins.

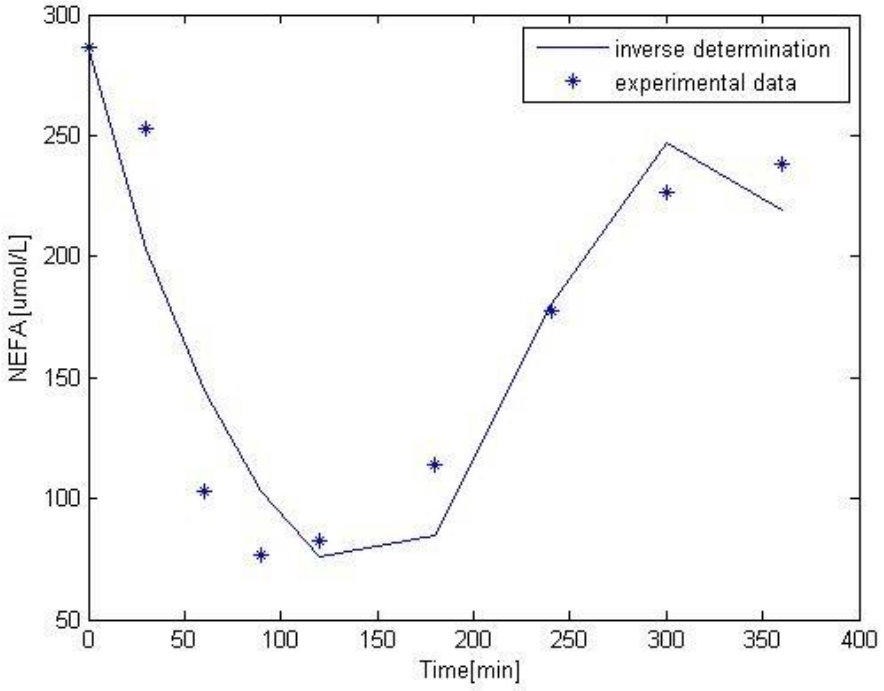

Figure 3.5 The concentration of fatty acids in arteries.

It can be found that the non-esterified fatty acids (NEFA) concentration has a dramatically decrease initially and then gradually increase according to the experimental data. The fatty acids have a smaller concentration in arteries than in veins due to the metabolism in the transportation through tissues in the biological experiment [179]. At convergence the values of $\|\nabla\Psi(\boldsymbol{P}^k)\|$ are 9.9×10^{-11} and 9.6×10^{-11} respectively, and $\boldsymbol{P}^*$ can be seen as the optimized parameter for this model.

Note that the number of small compartments may affect the value of gradient of error function $\nabla\Psi(\boldsymbol{P}^k)$. A comparison is made with the numerical tests for concentration of fatty acids in veins with different compartment number n as exist in Table 3.1. To evaluate the error between the simulation result and the measurement for fatty acids arterial blood vessel, define that :

$$\delta = \frac{\left\| \boldsymbol{C}(\boldsymbol{P}^k) - \widetilde{\boldsymbol{C}} \right\|^2}{\left\| \widetilde{C} \right\|^2}$$

where $\boldsymbol{C}(\boldsymbol{P}^k)$ is the computational simulation with optimal parameters, $\widetilde{\boldsymbol{C}}$ is the experimental data for fatty acids concentration in the arterial blood. It is seen from numerical result that n may affect the numerical results in the inverse approach.

n	$k_1(min^{-1})$	$k_2(min^{-1})$	δ
8	0.0032	0.0018	12.53%
10	0.0034	0.0017	12.82%
12	0.0041	0.0114	13.89%

Table 3.1 The numerical tests with different compartment number

A comparison between the estimated concentration and the experimental data is made in the above results. It is seen from the table that with different theoretical compartment assumptions, the parameters have a slight difference in the inverse approach. Also the approach accuracy is affected by this theoretical number. Therefore it can be summarised that there are two factors which affect the accuracy of the above absorption compartment model. First the value of n in the model, representing the number of compartments has to be finite integer which may affect the accuracy of the inverse approach. Second the absorption delay does not include any metabolism process in the blood vessels. This is due to incompleteness of the model as discussed earlier. A modification is considered in the section below.

3.2. The interactive system of insulin-glucose-fatty acid model

The absorption model in Section 3.1 describes the transfer of fatty acids in the absorption compartment, but the metabolism reaction in the last plasma compartment is neglected in Equation (3.3). In this section, a metabolism process involving insulin-glucose-fatty acids regulation is taken to an example.

The metabolism of fatty acids in the blood is controlled by the glucose-insulin system in the human body [149]. The insulin is a strong inhibitor for hydrolysis of TAG [67] and the glucose can provide energy coupled with fatty acids [149]. There are many studies about this metabolism system [1, 150, 166] and a general existing model for glucose-insulin-fatty acids system is presented in the next section.

3.2.1. Existing models for glucose-insulin-fatty acids system

To investigate the glucose-insulin system, one of the most developed models is the model proposed by Bergman [16]. There are three compartments representing plasma insulin, remote insulin and plasma glucose concentrations. According to the assumption, plasma insulin enters a "remote compartment" where it becomes active in accelerating glucose disappearance into the periphery and liver, and inhibiting the glucose production. Over the years, researches in an attempt to link the glucose-insulin system with the dynamics of fatty acids have taken place [150, 166]. There are several researchers who considered how the insulin inhibits glucose-fatty acid regulation [23, 187]. In 2008, Roy [157] built a multi-compartment model containing the concentration of insulin, glucose and free fatty acid. There are six compartments defined in Roy's model including glucose, fatty acids, insulin and three remote compartments for these substances. A schematic view of Roy's model is shown in Figure 3.6.

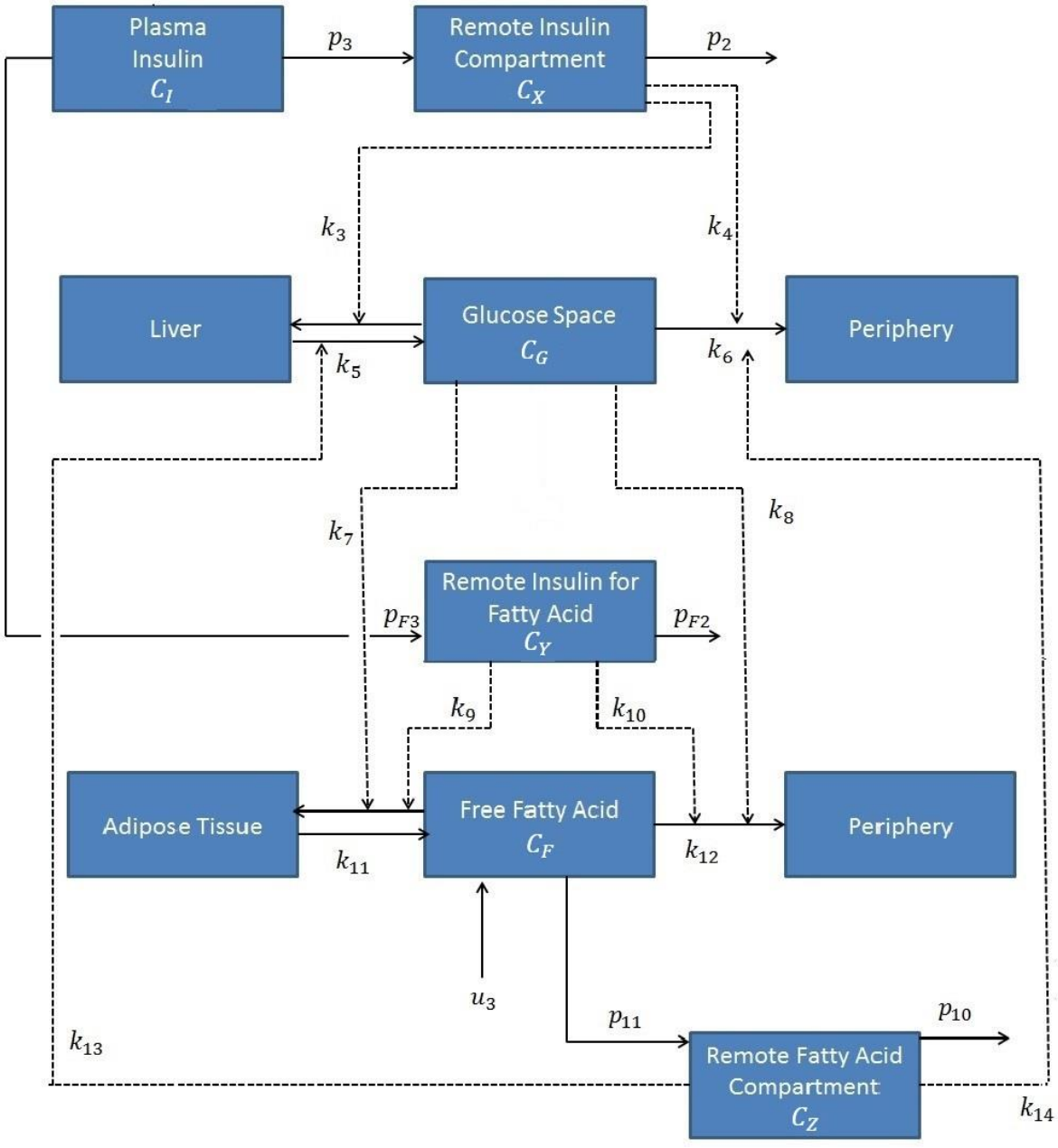

Figure 3.6 The schematic view of existing model of insulin, glucose and fatty acids.

It is assumed in section 2 that these reactions can be considered as a mass balance equation, the volume of each compartment indicates the concentration of one substance in the tissue and the chemical reactions are added to the mass balance system in the Figure 3.6. The volume is assumed to be equal in each compartment in [157]. Let C_I and C_X be the concentrations of insulin in plasma and the remote compartment for insulin respectively. By applying the law of mass action, two ODEs for these compartments can be written as below:

$$\frac{dC_I}{dt} = -nC_I \tag{3.4}$$

$$\frac{dC_X}{dt} = -p_2C_X + p_3(C_I - I_b) \tag{3.5}$$

In Equation (3.4), the decrease of insulin is due to the transport into remote compartment C_X and C_Y, therefore it has $n = p_3 + p_{F3}$. Here I_b is the basal plasma insulin concentration which is usually taken as a constant in the equation. The basal concentration used in a biological sense refers to a minimal level that is necessary for health or life [206]. The constant rate n indicates the clearance of the insulin in plasma. The parameters p_2 and p_3 control the appearance and disappearance respectively in the remote insulin compartment C_X.

In Figure 3.6, C_G , C_Y , C_F and C_Z indicates the concentration of glucose, remote insulin compartment, fatty acids concentration, and remote fatty acids compartment, respectively. In the assumption of this model, the concentration of glucose is inhibited by the remote compartment instead of the insulin itself, and the fatty acid is involved in the glucose dynamic change. The equation for glucose C_G is described as below:

$$\frac{dC_G}{dt} = -p_1C_G - p_4C_XC_G + p_6C_GC_Z \tag{3.6}$$

Here $\mathrm{p_1} = \mathrm{k_5} + \mathrm{k_6}, p_4 = \mathrm{k_3} + \mathrm{k_4}$ and $p_6 = \mathrm{k_{13}} + \mathrm{k_{14}}$ in the model in Figure 3.6. The flow rate from glucose compartment to periphery and liver is represented by p_1. The inhibition influence of insulin is governed by parameter p_4 and the influence from remote fatty acids compartment is governed by p_6.

For fatty acid, the remote insulin dynamics regulates the hydrolysis of TAG, and then inhibits the free fatty acid in the blood. The remote compartment for insulin is described as:

$$\frac{dC_Y}{dt} = -p_{F2}C_Y + p_{F3}(C_I - I_b) \tag{3.7}$$

The parameter p_{F2} represent the decrease of the concentration in this compartment, and the insulin in plasma can enter this remote compartment at the rate of p_{F3}. The I_b indicates the basal insulin concentration.

The fatty acid concentration in plasma is affected by substances in the blood. The adipose tissue can release fatty acid from its storage, and the absorption and transport in body also provide a source term $u_3(t)$ for fatty acid compartment. The circulatory system connects to the periphery environment. This indicates some metabolism process and chemical reaction to release energy for the balance of human biological system would take place. The rate of change of fatty acid concentration change is governed by the equation:

$$\frac{dC_F}{dt} = -p_7C_F - p_8C_YC_F + p_9(C_G)C_FC_G + p_7F_b + u_3(t) \tag{3.8}$$

In this equation, F_b represents the basal fatty acid concentration and $p_8 = \mathrm{k}_9 + \mathrm{k}_{10}$. The fatty acids release from lipid is controlled by $p_9(G)$, and it is assumed to be a function of glucose concentration and defined as:

$$p_9(C_G) = ae^{-bC_G} \tag{3.9}$$

Here a and b are constants. In Equation (3.8), the rate at which fatty acids is taken by external compartment is assumed to be p_7 and the consumption in fatty acid compartment has a rate of p_8.

This model also includes a remote compartment for fatty acids which can affect the glucose uptake in the liver and peripheral tissues. The dynamics is governed by the equation:

$$\frac{dC_Z}{dt} = -k_2C_Z + k_1(C_F - F_b) \tag{3.10}$$

where $k_2 = k_{13} + k_{14} + p_{10}$ and $k_1 = p_{11}$ It can be seen that the parameter transformation in the equation can be summarised as:

p_1	$k_5 + k_6$
p_4	$k_3 + k_4$
p_6	$k_{13} + k_{14}$
p_7	$k_{11} + k_{12}$
p_8	$k_9 + k_{10}$
p_9	$k_7 + k_8$

Table 3.2 The parameter transformation

The parameters in the ODEs were determined by numerical and experimental tests as shown in [157]. The values are given in Table 3.3.

Parameter	Value
p_1	$6.8 * 10^{-2}\ min^{-1}$
p_2	$3.7 * 10^{-2}\ min^{-1}$
p_3	$1.2 * 10^{-5}\ min^{-1}$
p_4	$1\ umol^{-1}L\ min^{-1}$
p_5	$0\ min^{-1}$
p_6	$6.1 * 10^{-5} umol^{-1}L\ min^{-1}$
p_7	$3 * 10^{-2} min^{-1}$
p_8	$4.5\ umol^{-1}L\ min^{-1}$
$\boldsymbol{a}$	$2.1 * 10^{-4}\ umol^{-1} min^{-1}$
B	$5.5 * 10^{-3}\ umol^{-1}$
k_1	$2 * 10^{-2}\ min^{-1}$
k_2	$3 * 10^{-2}\ min^{-1}$

p_{F2}	$1.7 * 10^{-1}\ min^{-1}$
p_{F3}	$1 * 10^{-5}\ min^{-1}$

Table 3.3 Parameter of the model in [157]

The kinetic model described in this section relates to the metabolism process in blood. However, this model does not include the absorption of fatty acids into plasma. This is an important contribution to the fatty acid concentration in plasma [179] and cannot be ignored from the metabolism process. The mass transfer $u_3(t)$ into fatty acids compartment may be assumed in Equation (3.8), but this cannot provide details of absorption of fatty acids. To improve this limitation of the model, some modifications are made in the following section.

3.2.2. The modification of the model

In Section 3.2.1, the metabolism process is modelled without describing the absorption of fatty acids in the blood vessel, which can be modified by considering an absorption process. It is described in Section 3.1 that the absorption process for fatty acids can be described by a transit compartment model in Equation (3.1). By adding these transit compartments into the fatty acids compartments in Section 3.2.1, the modified model can be represented in a schematic view as below:

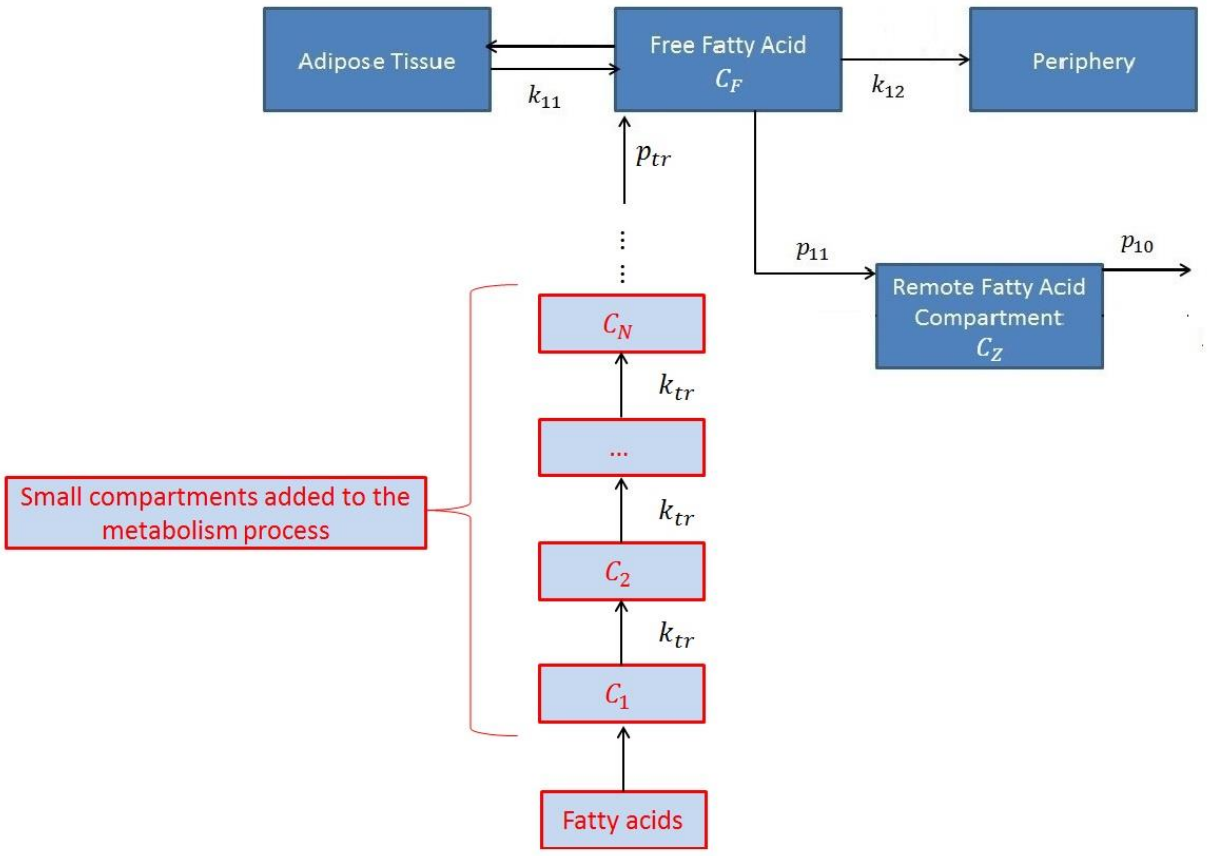

Figure 3.7 Schematic view of small compartments added to the metabolism process.

The compartments C_Z, C_F represent the fatty acids remote fatty acids compartment and the fatty acids in plasma, which is same as the compartment defined in Section 3.2.1. The small compartments represent the absorption process which has been defined in Section 3.1. In Figure 3.7, the mass transfer term into C_F has been replaced by a set of transit compartments that describe the fatty acids transport in the absorption process. Therefore the system represented in Figure 3.6 can be summarised as below:

$$\frac{dC_I}{dt} = -nC_I \tag{3.11}$$

$$\frac{dC_X}{dt} = -p_2C_X + p_3(C_I - I_b) \tag{3.12}$$

$$\frac{dC_G}{dt} = -p_1C_G - p_4C_XC_G + p_6C_GC_Z \tag{3.13}$$

$$\frac{dC_Y}{dt} = -p_{F2}C_Y + p_{F3}(C_I - I_b) \tag{3.14}$$

$$\frac{dC_Z}{dt} = -k_2C_Z + k_1(C_F - F_b) \tag{3.15}$$

$$\frac{dC_F}{dt} = -p_7C_F - p_8C_YC_F + p_9(C_G)C_FC_G + p_7F_b + u_3(t) \tag{3.16}$$

As the analytical solution for C_N is calculated in Equation 3.2. The source term to fatty acids compartment $u_3(t)$ in Equation (3.16) can be modified and defined as:

$$u_3(t) = p_{tr}\Gamma\frac{(k_{tr}t)^n}{n!}e^{-k_{tr}t} \tag{3.17}$$

In the assumption of absorption delay model in [161], the k_{tr} can be assumed according to the mean transit time. If the experiment duration last for 360 minutes in the lab, the k_{tr} can be defined as below:

$$k_{tr} = \frac{n+1}{360} \tag{3.18}$$

In the next section, the data used in Section 3.1 can be used for the inverse problem to determine the unknown parameters p_{tr} and n in Equation (3.17). By assuming $n = 3, p_{tr} = 1, \Gamma = 100$ before the approach, the feature of concentration change for $u_3(t)$ can be seen as below:

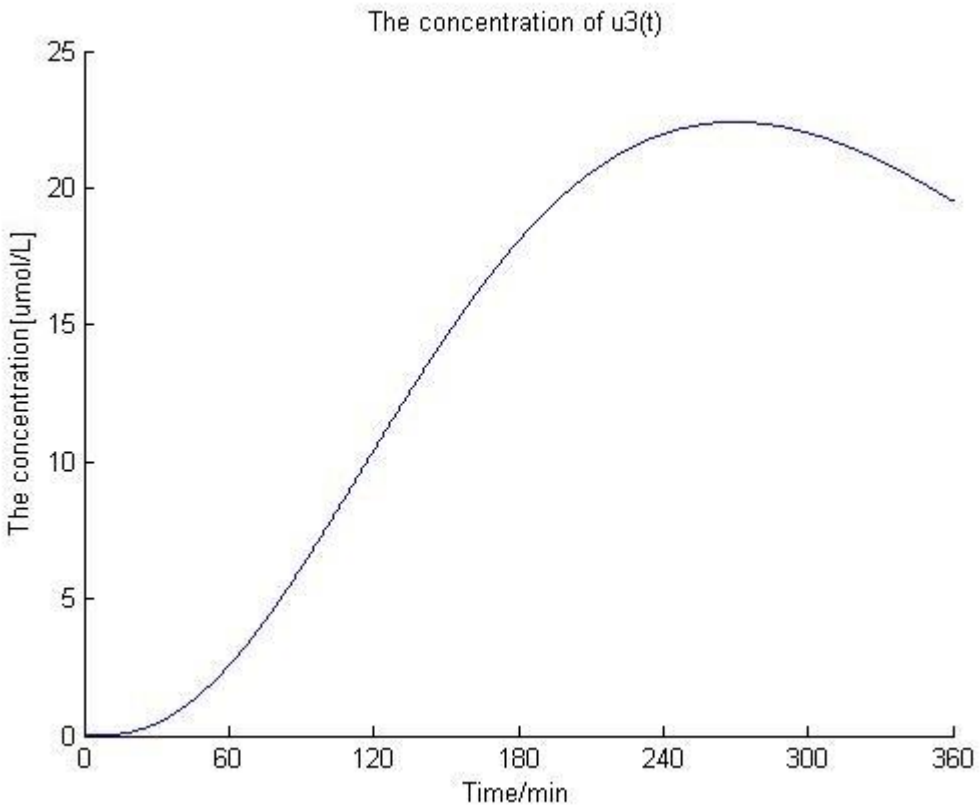

Figure 3.8 The profile of $u_3(t)$

From the above figure the profile of $u_3(t)$ can represent the absorption delay phenomenon for the metabolism system in the blood. The rate increases slowly at first and rises dramatically two hours after the absorption starts. This absorption delay feature explains the decrease of fatty acids initially in the experimental data. It means the metabolism controls the dynamic change for fatty acids before the absorption rate reaches a relatively high level in the blood vessel. In contrast to the linear model presented in Section 3.1, the modified model can describe detailed transport and reaction in absorption and metabolism process for fatty acids. The approximations of the two models involved in the inverse problem are compared in Section 3.3.

3.2.3. The inverse problem for the modified model

According to the condition in Fielding's experiment [179], the data is measured for the fatty acids concentration in plasma. Then the numerical simulation of fatty acids compartment C_F in

the modified model can be used for approximating the measurement in the experiment. The initial condition used in the ODE may be taken from those of the experimental condition.

The initial condition for the model can be defined easily for some compartments that are closely related to the data pool, but some theoretical remote compartments that are assumed in the model need to be assumed based on a specific case of the measurement. In Fielding's [179] experiment, the glucose is not measured in the data, therefore the initial condition is defined as in Roy's [157] numerical simulation. As the initial condition for insulin is given in the experiment, and the measurement of fatty acids is obtained from lab, the initial condition for insulin and fatty acids are defined in terms of experimental data. For the remote compartment for insulin, glucose and fatty acids, the absorption delay can leads to a zero initial condition according to the assumption in the mathematical model.

In this way, the initial conditions of the model adapted from [157, 179] are defined as below:

$$C_G(0) = 370\ umol/L \tag{3.19}$$

$$C_Y(0) = 0\ umol/L \tag{3.20}$$

$$C_F(0) = 765.73\ umol/L \tag{3.21}$$

$$C_Z(0) = 0\ umol/L \tag{3.22}$$

$$C_I(0) = 9.29\ umol/L \tag{3.23}$$

$$C_X(0) = 0\ umol/L \tag{3.24}$$

As the balanced concentration of inhibitor, the insulin basal concentration is defined in the same way as the initial condition in the experiment. This means:

$$I_b = I(0) = 9.29\ umol/L \tag{3.25}$$

For the basal concentration for fatty acids compartment F_b in Equation (3.15), the value of F_b represents a balanced concentration of fatty acids in steady states for human body, which is not given in the experimental data. Also the basal fatty acids concentration has a big difference for

individuals [135]. In this computational exercise, different values of F_b(0, 25, 50, 75, 100) are used in the inverse approach to determine the unknown parameters.

In the inverse problem, the experimental data is the same as the measurement in Section 3.1 in [179]. The objective function has been defined in Chapter 2. As the fatty acids concentration is modelled in an interactive system in Equation (3.16), the gradient of this non-linear system is difficult to simulate and computationally expensive in the inverse approach. Therefore some stochastic methods such as QPSO method can be applied to obtain the unknown parameters in the model.

In the QPSO method, the initialisation of the first generation of parameter vectors is defined in a specific interval. For a given number of iterations in the update process, this interval gives the lower and upper boundaries of the search-space. The smaller length of this search-space leads to a higher accuracy of the optimisation as the computational work can focus on a smaller interval for candidate solutions and then become more efficient. In this study a wide range for parameter initialisation ($p_{tr} \in [0, 100]$ and $n \in [0, 100]$) is test at first to give a rough guess for a smaller search-space. With these simulation tests in QPSO method, the updated best position for parameters is found to be located in a smaller interval (($p_{tr} \in [0, 1]$ and $n \in [0, 6]$)). As parameters converge quickly to this small interval even with a large search-space, the new initialisation choice can be set in the QPSO method with a smaller interval to ensure the computation work can be efficiently applied in the inverse approach.

The mathematical model is described in Equation (3.11) to (3.16), and QPSO method is applied in Matlab code. The direct problem is solved by 4^{th} order of Runge-Kutta method. The numerical result is shown as follows:

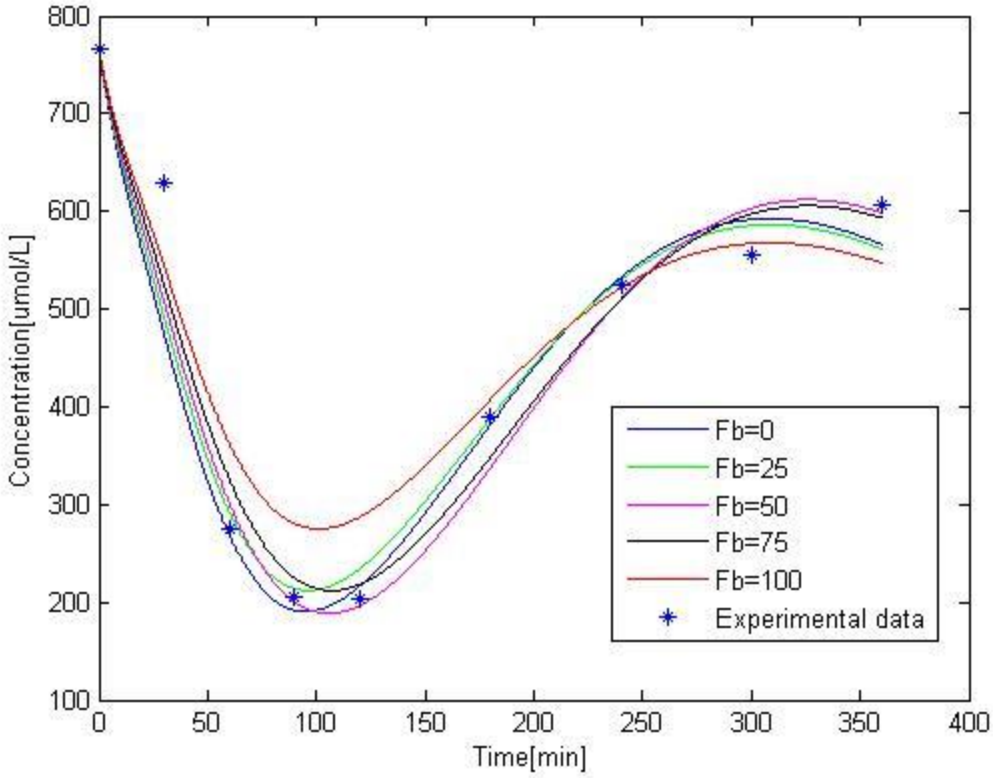

Figure 3.9 The concentration of fatty acid

In Figure 3.9 the star points describe the experimental data as the measurement and the curves represent the numerical simulations of fatty acids compartment with different basal concentration in the model. When the basal concentration is assumed range from 0 to 75, the simulation can fit the measurement well. When $F_b = 100$, the computation simulation (red curve) does not present the dynamics accurately, especially when t=100 min. It can be deduced that the basal concentration of fatty acids affected the minimum of the fatty acid concentration in this reaction, and large basal concentration is not suitable for Fielding's [179] experiment.

To investigate the influence of basal fatty acids concentration in the inverse approach, the different F_b are tested in Figure 3.9. As another benchmark, the objective function with different basal concentrations represented the result of optimisation process. Let P_{err} be the percentage of approximation error in the measurement

$$P_{err} = \sum_{i=1}^{N} \frac{1}{N} \left| \frac{\boldsymbol{C}_i(t;\boldsymbol{P}) - \widetilde{\boldsymbol{C}}_i}{\widetilde{\boldsymbol{C}}_i} \right| \tag{3.26}$$

The $C_i(t;\boldsymbol{P})$ indicates the computational simulation with optimal parameters and $\widetilde{C}_i$ is the measurement. N is the number of experimental data and P_{err} represnts how far the numerical result is from the data. The smaller P_{err} indicates a better approximation of inverse approach. The optimal parameter and the value of P_{err} are listed as below

F_b	p_{tr}	n	P_{err}
0	0.749439657613942	3	0.062388209529882
25	0.707162516177295	3	0.067633061863528
50	0.811871818488958	4	0.068404417619363
75	0.763152632905667	4	0.082551075001087
100	0.580381436588291	3	0.154027123429660

Table 3.4 The unknown parameter and the error function in the inverse approach.

From the table above, it is obvious that when $F_b = 100$, the p_{tr} has the smallest value and the objective gives the worst result among all the simulations. This indicates that if the basal concentration of fatty acids exceeds a specified benchmark, the appearance rate from the source

term would become slow and it can affect the accuracy of inverse approach. As a comparison, when F_b are given values which are less than 100, the flow rate from source term range from 0.7 to 0.9 and the P_{err} is less than 10%, indicating an acceptable inverse determination for biologists.

In the optimisation process, the initialisation of parameters is carefully chosen in the QPSO method to ensure the efficiency of the computational work. In a wide range of search-space, the optimisation solution usually converges to a small interval, which means a small perturbations in parameters cannot leads to a large fluctuation for error function with the QPSO method.

3.3. The comparison of two models for fatty acids concentration

In this chapter, the same experimental data has been used in two different models: First one is the linear absorption model presented in Section 3.1. Second one is the modified model by combining absorption and metabolism process and presented in Section 3.2. The approximations of these two models can be compared by computing the P_{err} defined in Equation (3.26).

Let $P_{err-lin}$ be the percentage of approximation error in linear absorption model in Section 3.1, and $P_{err-mod}$ be the percentage of error in nonlinear model in Section 3.2. The basal concentration of fatty acids F_b in the nonlinear model is chosen as 25. It can be seen that:

$P_{err-lin}$	$P_{err-mod}$
0.143475627820439	0.067633061863528

Table 3.5 The comparison of error functions of two models.

It can be seen from table 3.5 that the modified non-linear model has smaller error percentage in the measurement, which indicates a better approximation for fatty acids in the inverse problem. The second model in Section 3.2 describes both the absorption and metabolism process for fatty acids and the metabolism of fatty acids is involved in an insulin-glucose regulation system. This novel model can provide a physiological-based system for fatty acids concentration and can develop the accuracy of data fitting in the inverse problem, which has been proved in this section.

3.4. Summary

This chapter proposed a model by coupling the metabolism and absorption process for fatty acids. The existing model is extended for fatty acids concentration in the blood. The modified model provides a better data fitting performance in contrast to the linear absorption model in the inverse problem. This novel model provides a first attempt to combine an absorption delay assumption in the metabolism of fatty acids in the blood. The inverse approach gives a proper estimation of absorption rate for fatty acids.

These models in this chapter provide a macroscopic view of fatty acids concentrations in the plasma. There are more chemical reactions, such as the hydrolysis and esterification of fatty acids, involved in the absorption and metabolism process. Next chapter the attention is paid on the hydrolysis process in the fatty acids absorption. The experience of compartment model can be used for the model building in the next chapter.

Chapter 4 A mathematical model for the hydrolysis of triglyceride

As introduced in Chapter 1 fatty acids have to be released through hydrolysis from triglyceride (TAG) molecules before it can be absorbed. There were many studies related to this essential reaction in biology [33, 39, 146]. On the other hand, there were many mathematical models [78, 103, 131] describing hydrolysis which are usually linear. There were many other theoretical models where parameters have not been calibrated through experiments. Much work was related to the stability of the solution of the models. In this chapter there are three main discussions: First a general form of the hydrolysis model is adopted to describe the dynamics of lipids and fatty acids in the hydrolysis process incorporating possible model error or unknown reaction by introducing a regulator into the ODE system. Second a specific regulator example for an olive oil emulsion is determined through experimental data and is examined. Finally the resulting inverse problem is solved using QPSO technique.

4.1. The stepwise hydrolysis process

The hydrolysis, or lipolysis, refers to the process of releasing fatty acids from TAG. There are several substances involved in the hydrolysis, including TAG, monoglyceride(MG), diaglyceride(DG), glycerol and fatty acids(FA). The hydrolysis of ester bonds in TAG is the principal phase in the intestinal absorption of TAG. In the hydrolysis phase, the reaction is controlled by lipase enzyme, and the pancreatic lipase can act on the ester bonds in TAG and lead to the formation of DG or MG [112]. In the first phase, the TAG converts to DG and releases one fatty acid. In the second phase, the DG converts to MG and releases one fatty acid. All these reactions lead to a stepwise process. The reverse reaction of hydrolysis, which is known as esterification, may take place at the same time in the human body. The free fatty acids may attach to the ester bonds of DG or MG to form the TAG molecules. During these processes, the optimal pH and the position of ester bonds may lead to different hydrolysis or esterification rate as these factors may affect the activity of enzyme [32].

In the hydrolysis process, TAG is stepwise converted into DG, MG and glycerol accompanied with the liberation of a fatty acid at each step. To build a compartment model indicating these reactions, define the compartment TAG, DG, MG, glycerol and fatty acids with concentration C_{TG}, C_{DG}, C_{MG}, C_{GLY} and C_{FA}, respectively. Figure 4.1 depicts a compartment system containing several compartments that represent the concentration of substances based on the physiological remarks as mentioned above.

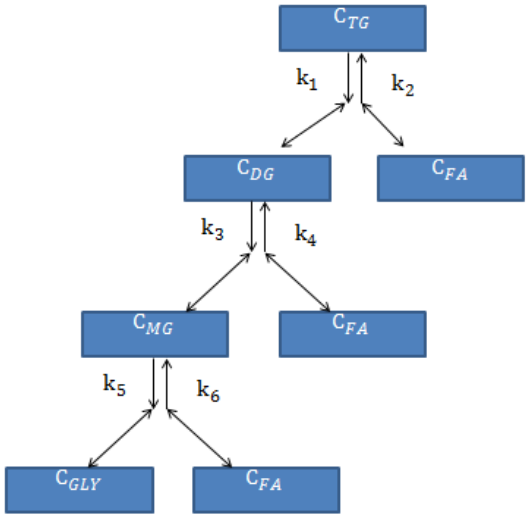

Figure 4.1 Schematic view of the triglyceride hydrolysis through the compartment

The hydrolysis leads to the breakdown of TAG to release fatty acids molecules. The rates of this reaction for each step are assumed to be k_1, k_3 and k_5. Meanwhile, the TAG is formed by combining DG or MG with fatty acids, which is known as the process of esterification. Esterification and hydrolysis are, in essence, reversals of one another, and the reverse reaction rate is assumed to be k_2, k_4 and k_6 as presented in Figure 4.1 .

Some mathematical models have been analysed for the hydrolysis considering the enzyme reaction [94, 170, 183]. The model in [38] presented a three compartment model including glycerol, fatty acids and TAG. The hydrolysis process is simply assumed as one step. This model is extended in [123] where the hydrolysis has two steps and the model has four compartments including fatty acids, TAG, DG and MG. The recent developed model in [200] provides a six compartment model by adding glycerol and water molecule in the hydrolysis process. All these models assumed the hydrolysis rate k_1, k_3 and k_5 as constant in the hydrolysis process. Typically these models are ODE system which can be summarised as below:

$$\frac{dC_{TG}}{dt} = -k_1 C_{TG} + k_2 C_{DG} C_{FA} \tag{4.1}$$

$$\frac{dC_{DG}}{dt} = k_1 C_{TG} - k_2 C_{DG} C_{FA} - k_3 C_{DG} + k_4 C_{MG} C_{FA} \tag{4.2}$$

$$\frac{dC_{MG}}{dt} = k_3 C_{DG} - k_4 C_{MG} C_{FA} - k_5 C_{MG} + k_6 C_{GLY} C_{FA} \quad (4.3)$$

$$\frac{dC_{GLY}}{dt} = k_5 C_{MG} - k_6 C_{GLY} C_{FA} \quad (4.4)$$

$$\frac{dC_{FA}}{dt} = k_1 C_{TG} - k_2 C_{DG} C_{FA} + k_3 C_{DG} - k_4 C_{MG} C_{FA} + k_5 C_{MG} - k_6 C_{GLY} C_{FA} \quad (4.5)$$

In this ODE system, $\frac{dC_{TG}}{dt}$, $\frac{dC_{DG}}{dt}$, $\frac{dC_{MG}}{dt}$, $\frac{dC_{GLY}}{dt}$ and $\frac{dC_{FA}}{dt}$ represent the rates of concentration change of TAG, DG, MG, glycerol and fatty acids. In these mathematical models, the reverse reaction such as esterification of DG or MG is neglected in the model. The reaction terms and the number of equations in these ODE models have big difference due to various experimental conditions. In the next section, a general form of hydrolysis model is proposed by combining all substances involved in the TAG hydrolysis. Unknown terms described as regulators are added to the ODE system. These regulators can be adjusted for missing reaction in the hydrolysis process.

4.2. A general form of the hydrolysis model

To consider a general form for the hydrolysis process, the missing information in the ODE model needs to be adjusted. There are many enzymatic reactions in the hydrolysis that directly or indirectly affect the reaction rate to form fatty acids. For example, the fatty acids molecules are attached to the lipid molecules with ester bonds in the molecule structure. The enzyme needs to react on the ester bonds to release fatty acids molecules. Also the enzyme itself needs to be active before becoming involved in the hydrolysis reaction. Therefore defining some regulators in the ODE model may be necessary to describe the missing information.

In order to take account of the effects due to (i) activation of main enzymes and their eventual action on the triglycerides, (ii) the optimal pH and temperature that provide the environment for the reaction, (iii) the action of some inhibition reactions, (iv) design of the experiment and (v) the individual difference in the blood sample if it is in vivo test, unknown regulator terms are included in the model in Equations (4.6) to (4.10).

$$\frac{dC_{TG}}{dt} = -k_1 C_{TG} + k_2 C_{DG} C_{FA} + \sigma_1(C_{TG}, C_{DG}, C_{MG}, C_{GLY}, C_{FA}, t) \quad (4.6)$$

$$\frac{dC_{DG}}{dt} = k_1 C_{TG} - k_2 C_{DG} C_{FA} - k_3 C_{DG} + k_4 C_{MG} C_{FA} + \sigma_2(C_{TG}, C_{DG}, C_{MG}, C_{GLY}, C_{FA}, t) \quad (4.7)$$

$$\frac{dC_{MG}}{dt} = k_3 C_{DG} - k_4 C_{MG} C_{FA} - k_5 C_{MG} + k_6 C_{GLY} C_{FA} + \sigma_3(C_{TG}, C_{DG}, C_{MG}, C_{GLY}, C_{FA}, t) \quad (4.8)$$

$$\frac{dC_{GLY}}{dt} = k_5 C_{MG} - k_6 C_{GLY} C_{FA} + \sigma_4(C_{TG}, C_{DG}, C_{MG}, C_{GLY}, C_{FA}, t) \quad (4.9)$$

$$\frac{dC_{FA}}{dt} = k_1 C_{TG} - k_2 C_{DG} C_{FA} + k_3 C_{DG} - k_4 C_{MG} C_{FA} + k_5 C_{MG} - k_6 C_{GLY} C_{FA} + \sigma_5(C_{TG}, C_{DG}, C_{MG}, C_{GLY}, C_{FA}, t) \quad (4.10)$$

σ_i refer to unknown regulators for each compartment . As each substance affects each other directly or indirectly, σ_i depends on all the substances and time.

This model now contains all substances involved in hydrolysis. The regulator terms σ_i take account of the effects due to possible missing reactions and data measurement. In the next section, an application of this model is carried out with a set of in vitro data. The hydrolysis model is modified to include an enzymatic reaction.

4.3. A modification based on the enzymatic reaction

As a regulator in the model σ may be used to represents the enzymatic reaction in the hydrolysis process. To illustrate the function of an enzyme, an enzymatic kinetic, first proposed in [121] and known as Michaelis-Menten kinetics, can be described in a basic enzymatic reaction as below:

$$S + E \underset{k_{-1}}{\overset{k_1}{\rightleftarrows}} SE \xrightarrow{k_2} P + E \quad (4.11)$$

Here k_1 , k_{-1}, k_2 are constants. The reaction says that one molecule of substance S combines with one molecule of enzyme E to form one molecule of complex SE, which eventually produces one molecule of product P and one molecule of E.

The concentration of above substances can be defined as C_S, C_E, C_{SE} and C_P, respectively. By applying the law of mass action, and ODE system can be built as below:

$$\frac{dC_S}{dt} = -k_1 C_E C_S + k_{-1} C_{SE} \tag{4.12}$$

$$\frac{dC_E}{dt} = -k_1 C_E C_S + (k_{-1} + k_2) C_{SE} \tag{4.13}$$

$$\frac{dC_{SE}}{dt} = k_1 C_{SE} C_S - (k_{-1} + k_2) C_{SE} \tag{4.14}$$

$$\frac{dC_P}{dt} = k_2 C_{SE} \tag{4.15}$$

subject to the initial conditions

$$C_S(0) = s_0, C_E(0) = e_0, C_{SE}(0) = 0, C_P(0) = 0 \tag{4.16}$$

Adding Equation (4.13) and Equation (4.14) leads to

$$\frac{dC_E}{dt} + \frac{dC_{SE}}{dt} = 0 \rightarrow C_E(t) + C_{SE}(t) = e_0$$

Using the above relation, the system of ODE reduces to only two, involving C_S and C_{SE}, namely

$$\frac{dC_S}{dt} = -k_1 e_0 C_S + (k_1 C_S + k_{-1}) C_{SE} \tag{4.17}$$

$$\frac{dC_{SE}}{dt} = k_1 e_0 C_S - (k_1 C_S + k_{-1} + k_2) C_{SE} \tag{4.18}$$

with

$$C_S(0) = s_0, C_{SE}(0) = 0 \tag{4.19}$$

Under the assumption in [121], the enzyme concentration is much less than the substance concentration, the complex concentration remains stable in a short reaction time as all enzyme

molecules have been involved in the reaction. This is known as Michaelis–Menten equilibrium and the rate change of C_{SE} equals to 0, which indicates:

$$k_1 e_0 C_S - (k_1 C_S + k_{-1} + k_2) C_{SE} = 0 \tag{4.20}$$

It can be obtained that

$$C_{SE} = \frac{k_1 e_0 C_S}{k_1 C_S + k_{-1} + k_2} \tag{4.21}$$

Substitute Equation (4.21) into Equation (4.15)

$$\frac{dC_P}{dt} = \frac{P_1 C_S}{P_2 C_S + \mathrm{P}_3} \tag{4.22}$$

where $P_1 = k_2 k_1 e_0$, $P_2 = k_1$, $P_3 = k_{-1} + k_2$, which are all constants in the Equation (4.22). The Michaelis-Menten kinetic provides the dynamic for reaction production with enzyme involved in it. It represents the function of enzyme and has been applied to many biological models [50, 95, 169] including the hydrolysis models [19, 46]. In this section, the Michaelis-Menten kinetics can be used as regulator terms in the general forms of hydrolysis model as the feature of enzyme can be appropriately described in the ODE system.

An in-house set of in vitro experimental data provided by Institute of Food Research (IFR) was used to provide a numerical approximation of the modified model. The experiment involved an olive oil emulsion (about 5mg/ml) stabilised with sodium caseinate (2 mg/ml) which was digested in individual tubes with porcine lipase(0-180 minutes). The emulsion is a mixture of two or more lipids and the caseinate is a complex for a family of proteins which are commonly found in milk. The porcine lipase is the enzyme that activates the hydrolysis process in the lab.

The experimental data is shown as below:

Time/min	Fatty acid [mg/L]	TAG[mg/L]	DG[mg/L]	MG[mg/L]
0	0.060248	3.44784	0.35599	0.011523

2.5	0.143353	2.7173	0.454372	0.022032
5	0.201921	2.63131	0.526373	0.036352
10	0.330118	2.43299	0.707849	0.045228
20	0.476237	2.38568	0.865891	0.06626
40	0.725705	1.70638	0.932213	0.130605
60	0.761048	1.42584	1.1929	0.146772
120	0.886076	0.97226	1.244026	0.153829
180	0.943472	0.79464	1.468038	0.15868

Table 4.1 The experimental data in hydrolysis process

As in the experiment, the enzyme porcine lipase lacks the ability to cleave the MG into fatty acids and glycerol. It means that the concentration of glycerol in Equation (4.6) to (4.10) can be neglected and the last equation for the glycerol can be removed along with other rate constants associated with glycerol concentration. Also the reverse reaction due to the esterification is small enough to be ignored in the mathematical model. Therefore the reaction can be simplified to a reaction shown as below:

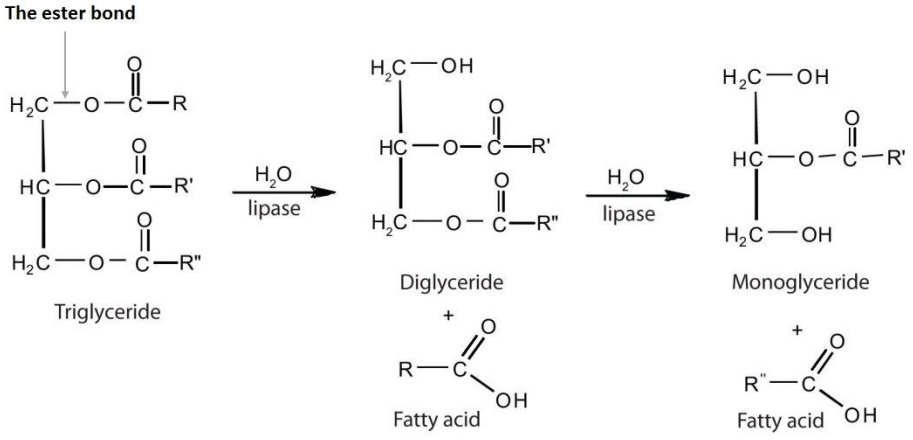

Figure 4.2 Schematic view of the hydrolysis process in the experiment

In Figure 4.2, the TAG is an ester derived from one glycerol and three fatty acids. The experiment that mentioned above only focused on the breakdown of TAG into DG, MG and fatty acids. The lipase enzyme can bind to the ester bond of TAG, which leads to the releasing of fatty acids, which indicates that the regulator terms in mathematical models can be defined in terms of enzymatic kinetic and the Michaelis–Menten kinetics can be applied. Similar application can be found in the literature [75]. The linear reaction term can lead to the hydrolysis for the triglyceride and the enzymatic reaction is handled by the regulators in the model.

Note that in the system of Michaelis–Menten kinetics [75], the assumption indicates that the parameters in the kinetic represent the reaction rates, and the value of parameter needs to be positive according to the chemical reaction. For triglyceride equation, the concentration of substances are not produced in the hydrolysis process, which cannot be explained by the Michaelis–Menten kinetics directly, therefore the values of parameters are obtained by the inverse approach instead of biological explanation .

With above modifications of the general form, the modified model is given as below:

$$\frac{\partial C_{TG}}{\partial t} = -k_1 C_{TG} + \frac{k_7 C_{TG}}{C_{TG}+k_8} \tag{4.23}$$

$$\frac{\partial C_{DG}}{\partial t} = k_1 C_{TG} - k_3 C_{DG} + \frac{k_9 C_{DG}}{C_{DG}+k_{10}} \tag{4.24}$$

$$\frac{\partial C_{MG}}{\partial t} = k_3 C_{DG} + \frac{k_{11} C_{MG}}{C_{MG}+k_{12}} \tag{4.25}$$

$$\frac{\partial C_{FA}}{\partial t} = k_1 C_{TG} + k_3 C_{DG} + \frac{k_{13} C_{FA}}{C_{FA}+k_{14}} \tag{4.26}$$

Here the aim is to determine 10 parameters $\boldsymbol{P} = \begin{pmatrix} k_1 \\ k_3 \\ k_7 \\ k_8 \\ \vdots \\ k_{14} \end{pmatrix}$ in Equation (4.23) to (4.26). The method in inverse problem is needed to obtain such information along with the experimental data.

4.4. The inverse approach

In this section, an inverse problem is solved with modified model and the experimental data in Table 4.1. The numerical method introduced in Chapter 2 is applied in this problem. As the hydrolysis process includes more than one substance in the reaction, a multi-objective optimisation problem is solved in the inverse approach and the weights of different substances are given in this optimisation. A novel way of identifying these weights is constructed by analysing the feature of chemical reaction in the lab and numerical tests of weights values. There are three tasks in this section. First the error function for the multi-objective function is built by combining all substances in the reaction. Second the optimisation is divided into two phases: optimise the TAG concentration at first and then consider the DG, MG and fatty acids concentration. Finally the prediction of reaction can be tested with the obtained parameters in the inverse problem

4.4.1. The analysis of weight in the multi-objective optimisation

The aim of the inverse problem is to find the optimal parameter vector $\boldsymbol{P}^* = \begin{pmatrix} k_1^* \\ k_3^* \\ k_7^* \\ k_8^* \\ \vdots \\ k_{14}^* \end{pmatrix}$ by solving

the minimisation problem

$$\min_{P} \Psi(\boldsymbol{P}^*)$$

The substance concentrations in Equation (4.23) to (4.26) is denoted as $C_{TG}(t;\boldsymbol{P})$ $C_{DG}(t;\boldsymbol{P}), C_{MG}(t;\boldsymbol{P})$ and $C_{FA}(t;\boldsymbol{P})$. The inverse problem technique is to construct an error function denoted by

$$\Psi(\boldsymbol{P}) = \omega_1 \left\| C_{TG}(t;\boldsymbol{P}) - \widetilde{C_{TG}}(t) \right\|^2 + \omega_2 \left\| C_{DG}(t;\boldsymbol{P}) - \widetilde{C_{DG}}(t) \right\|^2 + \omega_3 \left\| C_{MG}(t;\boldsymbol{P}) - \widetilde{C_{MG}}(t) \right\|^2 + \omega_4 \left\| C_{FA}(t;\boldsymbol{P}) - \widetilde{C_{FA}}(t) \right\|^2 \quad (4.27)$$

where $\widetilde{C_{TG}}(t)$, $\widetilde{C_{DG}}(t)$, $\widetilde{C_{MG}}(t)$, $\widetilde{C_{FA}}(t)$ are the experimental data and ω_i are the different weights for each objective in this optimization. ω_i is the weight for different objective functions of TAG, DG, MG and fatty acids. The ω_i has

$$\sum_{i=1}^{4} \omega_i = 1 \tag{4.28}$$

The aim of the inverse approach is to minimise the error function $\Psi(\boldsymbol{P})$ with multi-objective optimisation, $C(t;\boldsymbol{P})$ is the solution of the direct problem defined in Equation (4.23) to (4.26) with a given value of $\boldsymbol{P}$. As described in Chapter 2, the QPSO can be applied to find the optimal parameters for this minimisation.

According to the form of the Equation (4.27), this is a typical multi-objective optimisation problem. It can be seen in the Equation (4.28) that the value of ω_i need to be determined before applying inverse approach, but for this multi-objective analysis, there is no specific preference for the 2-norm error of four substances as the concentrations for different lipids are equally important from a biological view, therefore the different values of ω_i need to be tested in the numerical simulation.

As the chemical reaction follows the process presented in Figure 4.2, it can be seen that the TAG concentration is constantly decreasing which leads to the increase of other lipids. At the starting point of the metabolism process involved in the experiment only TAG exists. In the hydrolysis process DG, MG and fatty acids are produced. Therefore it is natural to define weights for DG, MG and fatty acids to be equal. It is defined as

$$\omega_2 = \omega_3 = \omega_4 = \omega \tag{4.29}$$

The Equation (4.28) is viewed as

$$\omega_1 + 3\omega = 1 \tag{4.30}$$

where $\omega_1 = \beta$, ω is obtained as

$$\omega = \frac{1-\beta}{3} \tag{4.31}$$

In this way the choice of weights in Equation (4.27) is reduced to β only. With different values of β, the optimal parameters can be determined with the minimum error function in Equation (4.27). With application of QPSO method introduced in Chapter 2, the parameter value with corresponding error function values are shown below with β changing from 0.1 to 0.8. In the QPSO method, the same iteration number ($k_{max} = 1000$) is used initially for different β values in this multi-objective problem for each simulation. A wide range for initialisation for all parameters are used in the QPSO algorithm, then a smaller interval for each parameter is tested based on the results from the large search-space. The gradient-based method such as SDM is then used to check if the optimal parameters from QPSO method are the optimum in the inverse approach. It is found that with a large search-space in QPSO method the parameters all converge to a smaller interval even with a random initialisation in this space, which indicates a good convergence for this system.

β	0.1	0.2	0.3	0.4
$\Psi(\boldsymbol{P})$	0.165633029	0.377122	0.250197	0.61611
k_1	0.001837363	-0.010923409	-0.01439261	0.0167888
k_3	0.2159649856	0.3893087306	0.4018080891	0.06509283
k_7	0.011859164	-0.239990524	0.053960516	4.09187E-05
k_8	-3.460806065	6.99922874	-3.989699992	-1.043699505
k_9	1.499675998	1.30885094	1.281637558	0.35804974
k_{10}	5.626514768	2.047998312	1.878148536	6.006201616
k_{11}	4.896738545	-0.933206279	6.907048929	-3.6429716
k_{12}	-2.725959385	0.1387126	-2.102293013	5.627447666
k_{13}	-2.265500013	-2.946433229	-2.235752097	-1.112701393
k_{14}	6.18484457	4.442532483	3.246452121	6.93238111

β	0.5	0.6	0.7	0.8
$\Psi(\boldsymbol{P})$	0.642513	0.644276	0.643547	0.655057
k_1	0.089621460	0.1345975472	0.134938551	0.136322390
k_3	0.5051400084	0.0363963162	0.034460981	0.041193668
k_7	0.504058488	0.946903784	1.055687723	1.061378167
k_8	4.946578491	6.077493444	6.926996344	6.89363348
k_9	-3.322153932	0.022432169	0.021945104	0.023579508
k_{10}	0.51632245	-1.102568008	-1.141036809	-1.084711158
k_{11}	-3.755308792	-2.076939237	1.127960795	-2.802246863
k_{12}	2.228855131	6.490074439	-3.843806574	6.463038662
k_{13}	-3.031248959	0.046771595	0.047143212	0.057755256
k_{14}	6.402257572	-0.783372551	-0.78328057	-0.715458489

Table 4.2 The estimated parameter values from the inverse approach

The Table 4.2 indicates the result of error function defined in Equation (4.27) and the parameters which lead to the corresponding error. It can be found that k_1 and k_3 are positive values as the TAG and DG have hydrolysis leading to the decrease of the concentration which converts to other lipids.

Note that for the parameters for the non-linear term in the ODE model, the parameters may have a negative value from Table 4.2. The Michaelis-Menten kinetic in a chemical reaction indicates that the parameter in the dynamic need to be positive to satisfy the biological background, but parameters in this model are identified according to the experimental data instead of theoretical biological model. The complex enzymatic reaction and noises in the experimental data may lead to a big difference for these parameters. Therefore the negative value for parameters is allowed in this study. From the comparison, it can be found that when β is getting large, the

approximation is losing accuracy, especially when β is more than 0.5. Figures 4.3 to 4.6 show the results of numerical estimation and the data when β is equal to 0.6, 0.7 and 0.8.

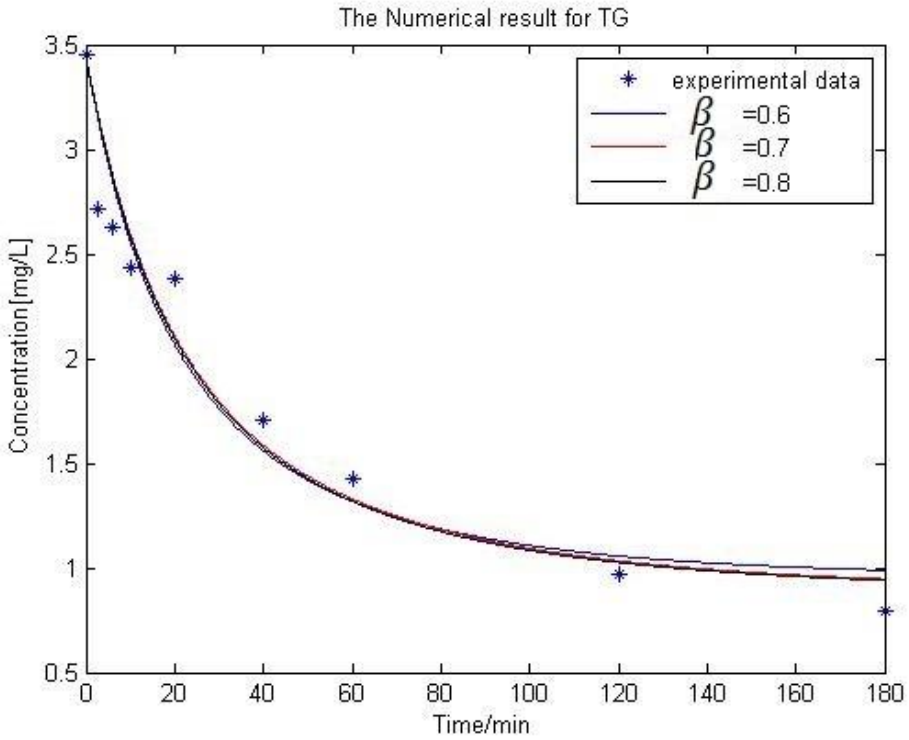

Figure 4.3 The concentration of Triglyceride with in vitro data

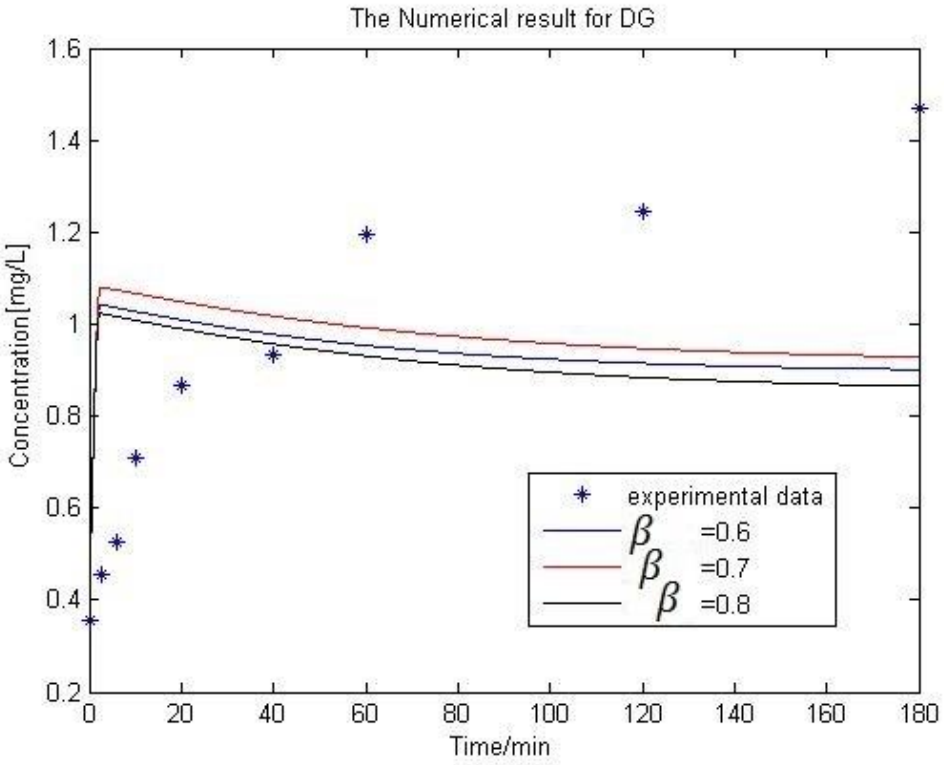

Figure 4.4 The concentration of diglyceride with in vitro data

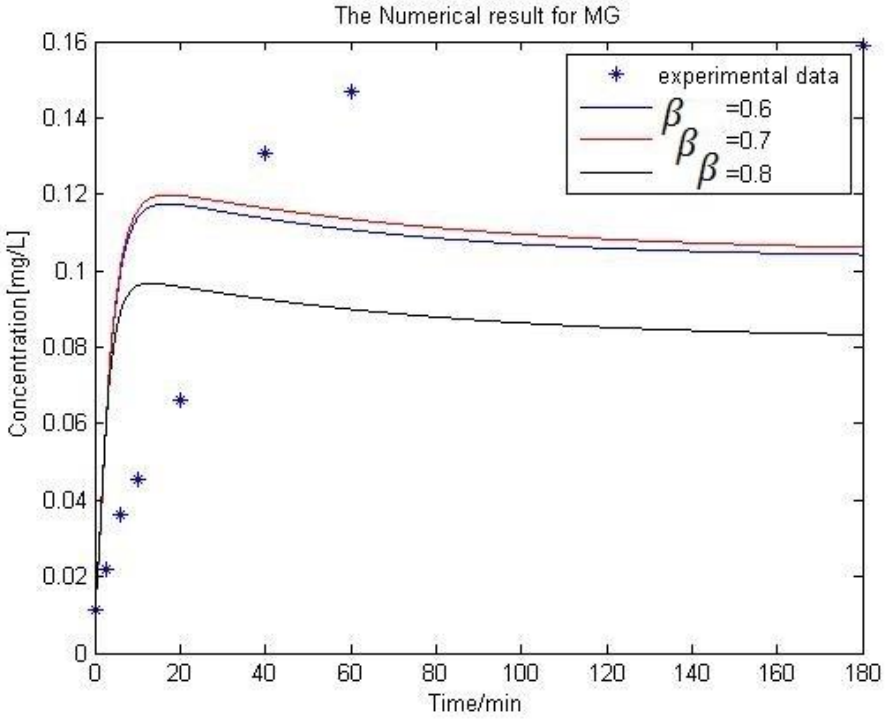

Figure 4.5 The concentration of monoglyceride with in vitro data

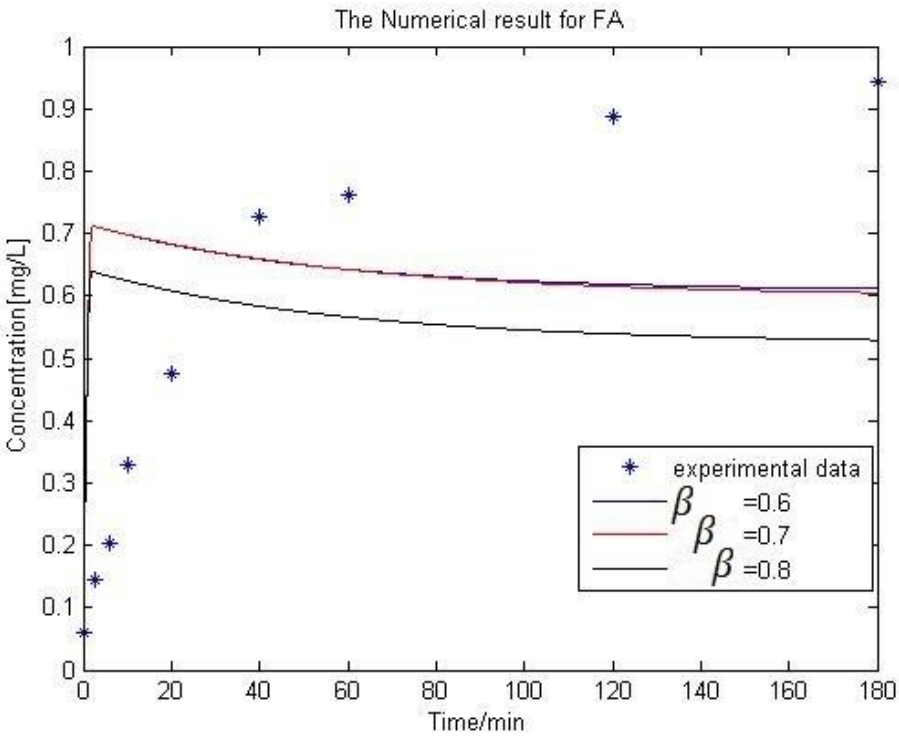

Figure 4.6 The concentration of fatty acids with in vitro data

The β is the weight of triglyceride concentration in the optimisation process and the larger weight means the more importance in the optimisation process, but it can also lead to the loss of accuracy for DG, MG and fatty acids as can be shown in Figures 4.3 to 4.6. Therefore it can be concluded that the large weight for triglyceride may have disadvantage of inaccuracy of other substances. For Figure 4.6, it can be seen that the differences among weight equal to 0.6, 0.7, and 0.8 do not have a good approximation. Therefore it is not appropriate to define a too large weight ($\beta > 0.4$) for TAG as it may affect the accuracy for the inverse approach for data of other lipids. Then next the small values of β can be analysed in Figures 4.7 to 4.10.

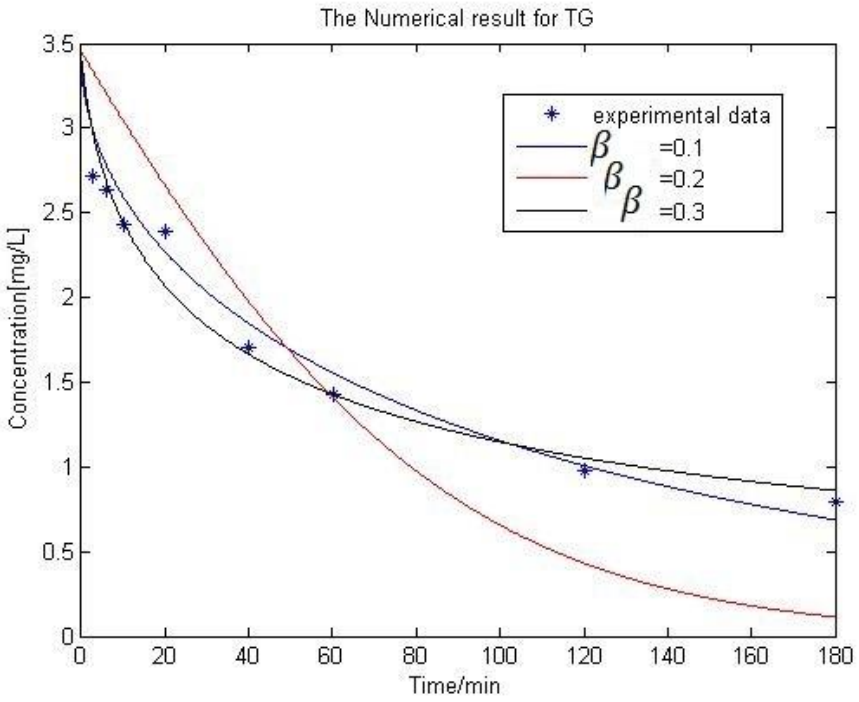

Figure 4.7 The concentration of triglyceride with small β in multi-optimisation

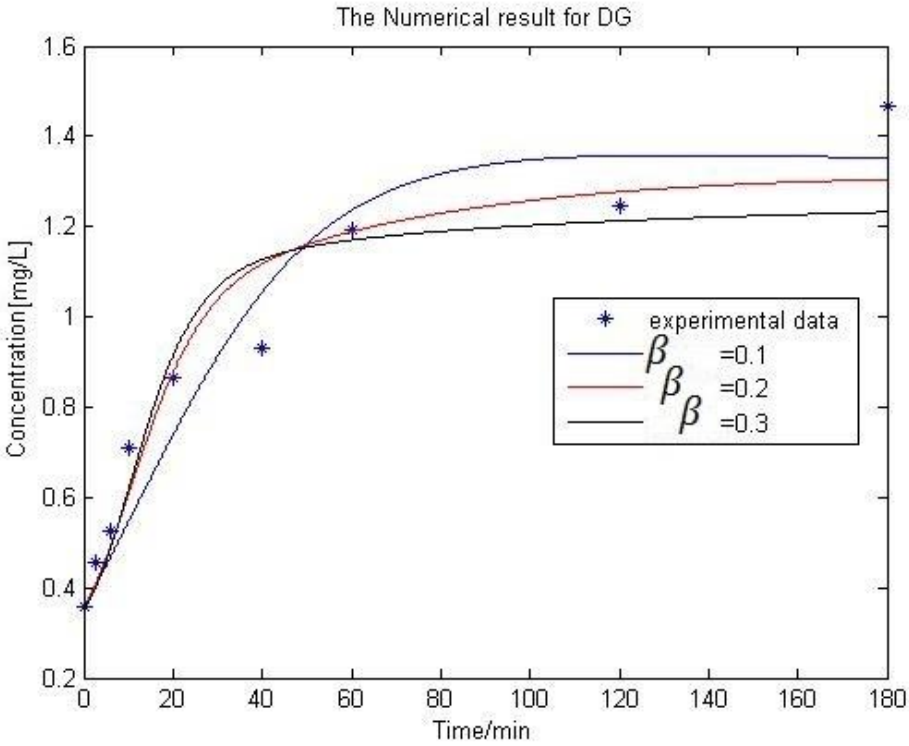

Figure 4.8 The concentration of diglyceride with small β in multi-optimisation

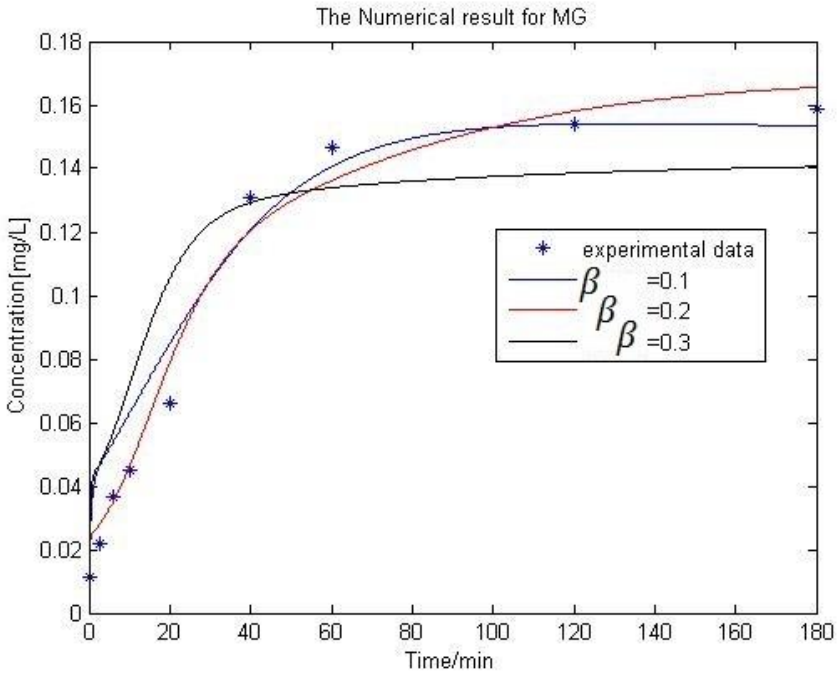

Figure 4.9 The concentration of monoglyceride with small β in multi-optimisation

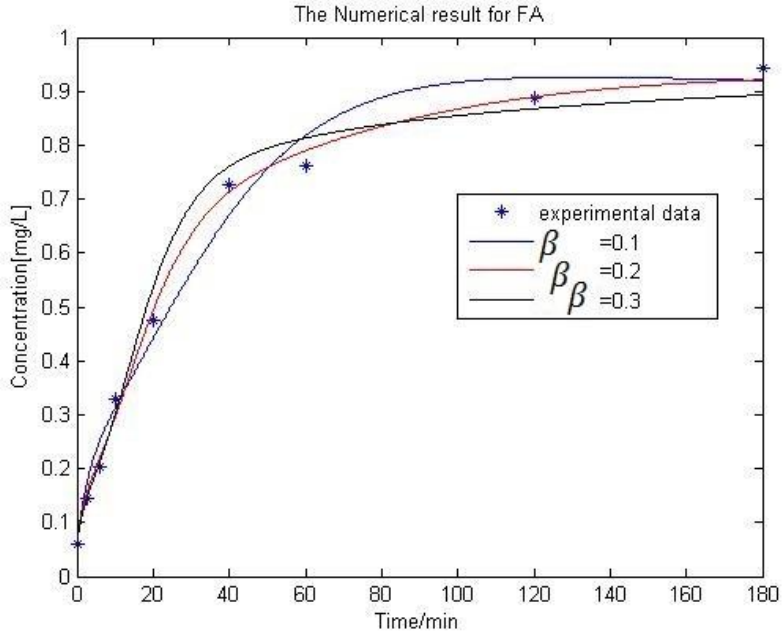

Figure 4.10 The concentration of fatty acids with small β in multi-optimisation

It can be summarised from Figures 4.7 to 4.10 that when β =0.1, the curve fitting for TAG is acceptable. In contrast to β =0.2 and 0.3, it has the smallest objective error and it can be seen as the optimal result for this multi-objective problem.

It can be seen from above figure that the different values for parameters in Table 4.2 leads to a different approximation results. However, when parameters for a specific substance's data are close with different weights in multi-objective optimisation, the data fitting all gives similar results. For example, for the numerical results for substances concentration with $\beta = 0.7$ and $\beta = 0.8$ in Figure 4.2, the errors between experimental data and numerical results are almost same, and the parameters do not have a big difference in Table 4.1. This indicates that the optimisation results can be almost equal where the parameters are close, which indicates that parameters are identifiable from the experimental data in this study. The similar conclusion can be found in related literature [129]. Even though the optimisation gives acceptable results when β is small in the above study, it may lead to a relatively large error to estimate 10 parameters simultaneously in this research. In the next part, the estimated parameters can be split into two groups. The experimental data for TAG can easily determine the optimal parameters in part of the ODE equations. Therefore fewer parameters can be optimised with experimental data to avoid the possible parameter identifiability problem.

4.4.2. The role of TAG in the inverse approach

For most cases, the weighted values for different substances can be tested by the above method, but for this special case in Equations (4.23) to (4.26), the TAG concentration is not affected by DG, MG and fatty acid density. This indicates that the parameters in Equation (4.37) can be obtained purely dependent on TAG data for this model. The inverse problem can be divided into two phases: firstly k_1, k_7, k_8 are determined to optimise the triglyceride concentration, then the other parameters can be obtained with measurement of DG, MG and fatty acid. This optimisation process fully considers the physiological reaction in the chemical reaction. The performance of this optimisation has a better data fitting result for TAG concentration in contrast to the typical

optimisation method in the above section. The details of the optimisation process are described in this section.

In the first stage, the error function φ_{TG} is defined as

$$\Psi_{TG} = \left\| C_{TG}(t; \boldsymbol{P}) - \widetilde{C_{TG}} \right\|^2$$

When we apply QPSO method in Equation (4.23) and TAG data in Table 4.1, the resulting optimal parameter is

$$\boldsymbol{P} = \begin{pmatrix} k_1 \\ k_7 \\ k_8 \end{pmatrix} = \begin{pmatrix} 0.001078630790470 \\ 0.012641123024406 \\ -3.450745861588872 \end{pmatrix}$$

With the parameter determined, the comparison between numerical result and measurement can be checked as below:

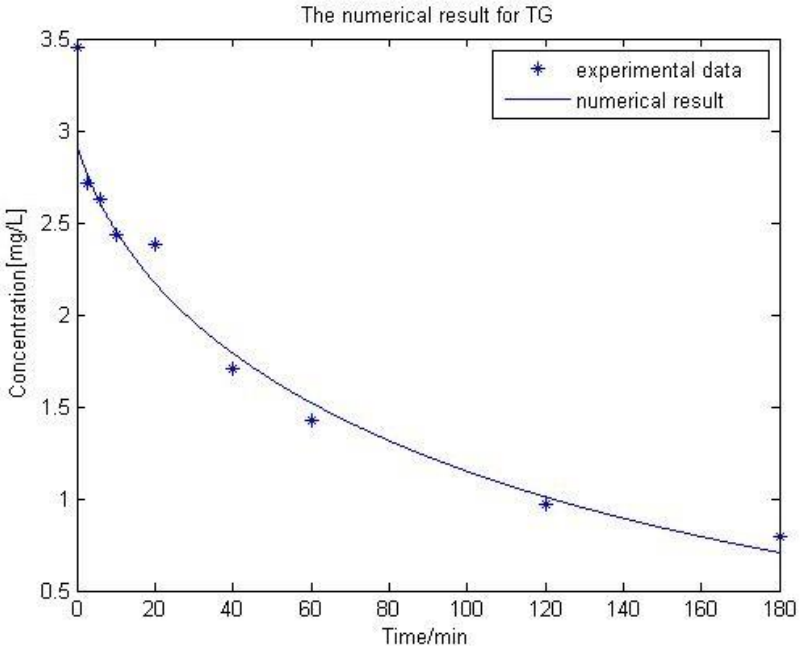

Figure 4.11 The concentration of triglyceride in single objective optimisation

The rate change of concentration of triglyceride is purely dependent on the parameter k_1, k_7, k_8, therefore it can be concluded that the result in Figure 4.11 is the same as the multi-objective optimisation in Equation (4.41) when $\beta = 1$. All the computation effort is used for the single objective regardless of the accuracy of three other substances. Therefore the comparison can be made between the result in Figure 4.11 and the result in Table 4.3.

Ψ_{TG}	Value
Numerical result in Figure 4.11	0.273552584889044
Numerical result in Table 4.3 when $\beta = 0.1$	0.442305609111378
Numerical result in Table 4.3 when $\beta = 0.2$	1.411283534099235
Numerical result in Table 4.3 when $\beta = 0.3$	0.443217130062414
Numerical result in Table 4.3 when $\beta = 0.4$	0.959798338809792
Numerical result in Table 4.3 when $\beta = 0.5$	0.682994390616921
Numerical result in Table 4.3 when $\beta = 0.6$	0.669194243328586
Numerical result in Table 4.3 when $\beta = 0.7$	0.658058116877952
Numerical result in Table 4.3 when $\beta = 0.8$	0.657638056121929

Table 4.3 The error function for Triglyceride with different weight in multi-objective optimisation

It is obvious that the accuracy for TAG has a big advantage in the single objective optimisation. Another conclusion from table 4.3 indicates that a bigger weight for triglyceride does not lead to smaller 2-norm error when comparing β more than 0.5 and equal to 0.1. This may because the error for DG and MG has affect the accuracy of TAG optimisation.

In the second phase of inverse approach, the objective function for other lipids can be defined as

$$\Psi(\boldsymbol{P}) = \epsilon_1 \left\| C_{DG}(t;\boldsymbol{P}) - \widetilde{C_{DG}}(t) \right\|^2 + \epsilon_2 \left\| C_{MG}(t;\boldsymbol{P}) - \widetilde{C_{MG}}(t) \right\|^2 + \epsilon_3 \left\| C_{FA}(t;\boldsymbol{P}) - \widetilde{C_{FA}}(t) \right\|^2 \quad (4.32)$$

As for these three substances, the DG can be seen as the starting point for the reaction. Specially, the DG can release the fatty acids and itself convert to MG. Therefore as a key substance in the lipolysis, the value of DG weight can be analysed. Then the ϵ_i can be assumed as

$$\epsilon_1 = \gamma \quad ,\epsilon_2 = \epsilon_3 = \frac{1-\gamma}{2} \tag{4.33}$$

Same as the investigation for triglyceride weight, the different value of γ is tested for the numerical approximation and the result is shown in the table

γ	0.1	0.2	0.3	0.4
$\Psi(\boldsymbol{P})$	0.193928867	0.165334	0.150912	0.13273
k_3	0.2982565586	0.141373	0.1816438	0.1357425
k_9	2.34556682	0.538391	0.890705	0.50044
k_{10}	6.551638617	2.510537	3.598836	2.389329
k_{11}	8.214225969	8.535141	-9.79047	-6.91689
k_{12}	-3.245260232	-6.60183	5.999756	5.686707
k_{13}	-3.312617434	-2.11552	-2.83532	-2.05523
k_{14}	6.595936159	9.376749	9.708228	9.430163

γ	0.5	0.6	0.7	0.8
$\Psi(\boldsymbol{P})$	0.115717	0.102553	0.082642	0.070869
k_3	0.079271	0.13908	0.08096	0.177106
k_9	0.193578	0.557188	0.20565	0.993732
k_{10}	1.13656	2.698881	1.221399	4.242805
k_{11}	6.584783	-9.63703	-6.94672	7.726727
k_{12}	-9.5509	8.001426	9.59085	-4.98429
k_{13}	0.950856	-2.19456	0.688616	2.404318
k_{14}	-9.09094	9.875942	-6.63739	-9.76059

Table 4.4 The numerical result for other parameters

It is shown that with the increase of γ the objective function is decreasing. As in the Figure 4.12 to 4.14, though the value of objective function has a better accuracy from Table 4.5, the improvement in the curve is only obvious for DG concentration, the MG and fatty acid do not have a big difference from the result. This indicates that this γ test can be a good search for optimisation of DG concentration.

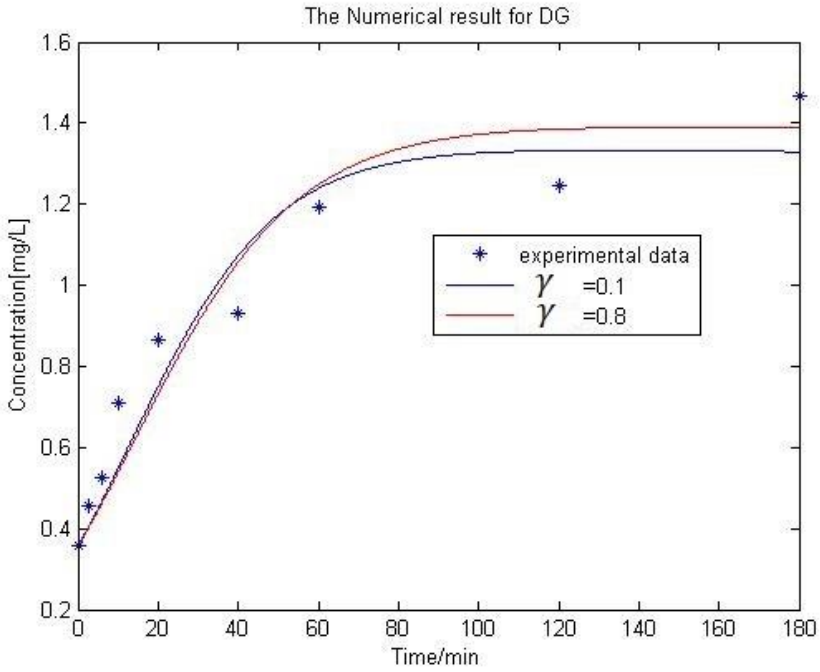

Figure 4.12 The concentration of diglyceride with $\gamma = 0.1$ and $\gamma = 0.8$ in optimisation

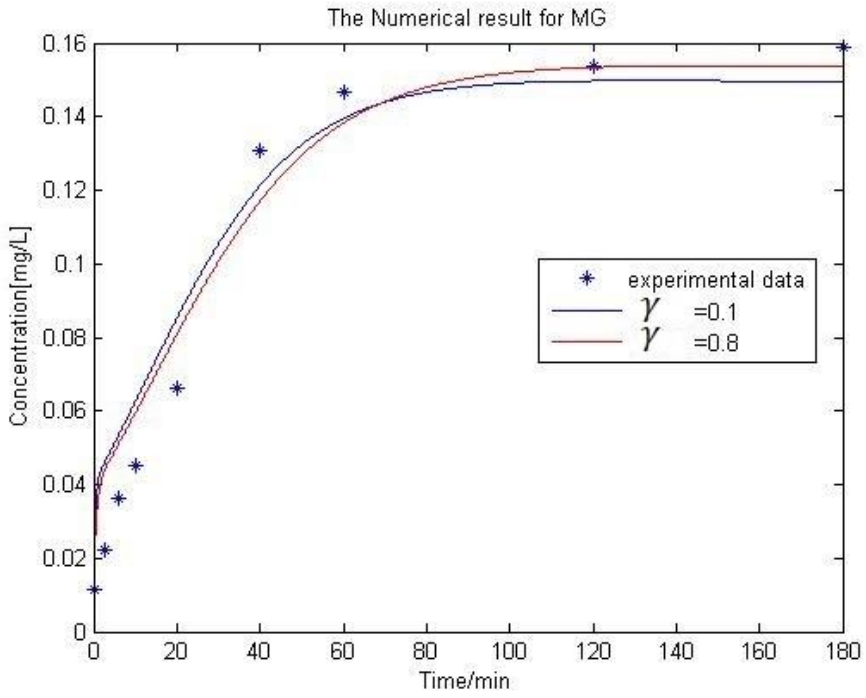

Figure 4.13 The concentration of monoglyceride with $\gamma = 0.1$ and $\gamma = 0.8$ in optimisation

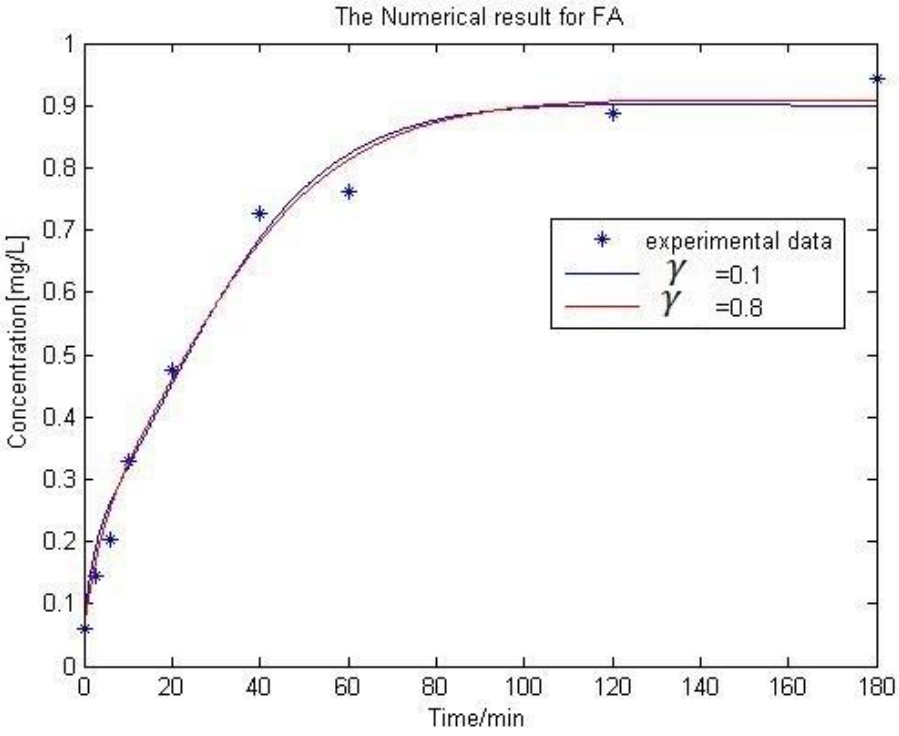

Figure 4.14 The concentration of fatty acids with $\gamma = 0.1$ and $\gamma = 0.8$ in optimisation

From the above result, the MG and fatty acid is not affected by the change of σ as much as the TAG. Define the error function for lipids as:

$$\Psi_{\mathrm{DG}} = \left\| C_{DG}(\mathrm{t}; \boldsymbol{P}) - \widetilde{C_{DG}}(\mathrm{t}) \right\|^2 \tag{4.34}$$

$$\Psi_{\mathrm{MG}} = \left\| C_{MG}(\mathrm{t}; \boldsymbol{P}) - \widetilde{C_{MG}}(\mathrm{t}) \right\|^2 \tag{4.35}$$

$$\Psi_{\mathrm{FA}} = \left\| C_{FA}(\mathrm{t}; \boldsymbol{P}) - \widetilde{C_{FA}}(\mathrm{t}) \right\|^2 \tag{4.36}$$

The table 4.6 lists the error function for different substances with different γ.

γ	0.1	0.2	0.3	0.4
Ψ_{DG}	0.305691073	0.29658	0.299094	0.293578
Ψ_{MG}	0.041990437	0.038846	0.038436	0.0388
Ψ_{FA}	0.115930756	0.096865	0.099137	0.097123

γ	0.5	0.6	0.7	0.8
Ψ_{DG}	0.27962	0.295347	0.281888	0.313971
Ψ_{MG}	0.038091	0.038788	0.035707	0.037097
Ψ_{FA}	0.107065	0.101054	0.102431	0.097947

Table 4.5 The objective function for different weights

It can be observed in the table that when γ is too small or two large ($\gamma = 0.1$ and $\gamma = 0.8$), the numerical result for Ψ_{DG} does not have a good performance ($\Psi_{DG} > 0.3$) when compared to other weight. Another conclusion can be drawn from numerical tests that the larger weight for σ does not always lead to a better accuracy for diglyceride, when compared to the Ψ_{DG} when $\gamma = 0.5$ and $\gamma = 0.6$.

In this part, the optimisation process is divided into two parts: firstly a multi-objective optimisation problem is solved by considering all the substance concentration simultaneously. Secondly the parameters are divided into two groups: The TAG concentration is considered to optimise the parameters for Equation (4.23) first. With the determined parameters k_1, k_7, k_8, the parameters for DG, MG,FA can be optimised. In this way the optimisation can have a better accuracy from the numerical results, but the disadvantage is also obvious. In the second step of the method, splitting parameters into more groups may not give a better result. For example for Equation (4.24), if the DG concentration is considered in a single-objective optimisation problem and the parameter k_1, k_3, k_9, k_{10} are optimised and determined with the experimental data for DG, the optimisation for TAG and MG may be affected as parameter k_1, k_3 also control the Equation (4.23) and (4.25). Therefore there are only two stages for the inverse approach in this numerical example for an acceptable optimisation for a computational application.

4.4.3. The prediction of reaction

As a function of mathematical model for biologists, the above system can be used to predict the dynamic of concentration with an appropriate description in the model. The optimal parameter when $\gamma = 0.5$ is chosen and the reaction time is extended to 720 minutes. The result is shown below.

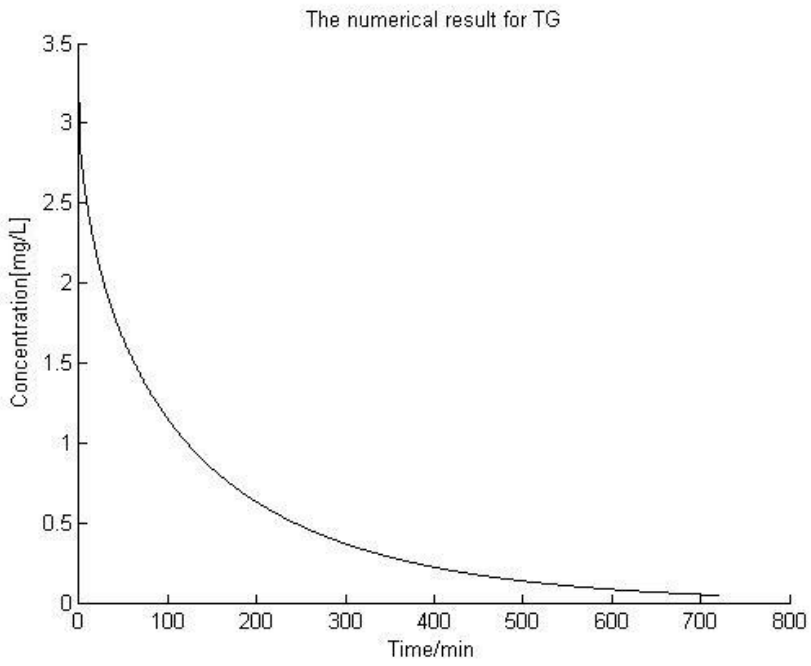

Figure 4.15 The prediction for triglyceride concentration

The hydrolysis reaction is catalysed by the lipase enzyme and the prediction of the substance concentration is affected by the activity of lipase. The function of the lipase is directly related to the concentration of triglyceride on the interface of emulsion. For this experiment, the activity of enzyme reaches a maximum when the lipase is fully contacted with the triglyceride molecules. The free fatty acids and other lipids monotonically increase along with time. The free fatty acids may form triglyceride again and make the triglyceride reach a balance of concentration. The rate of the triglyceride decrease then gradually tends to zero and all the substances have a steady state in this model.

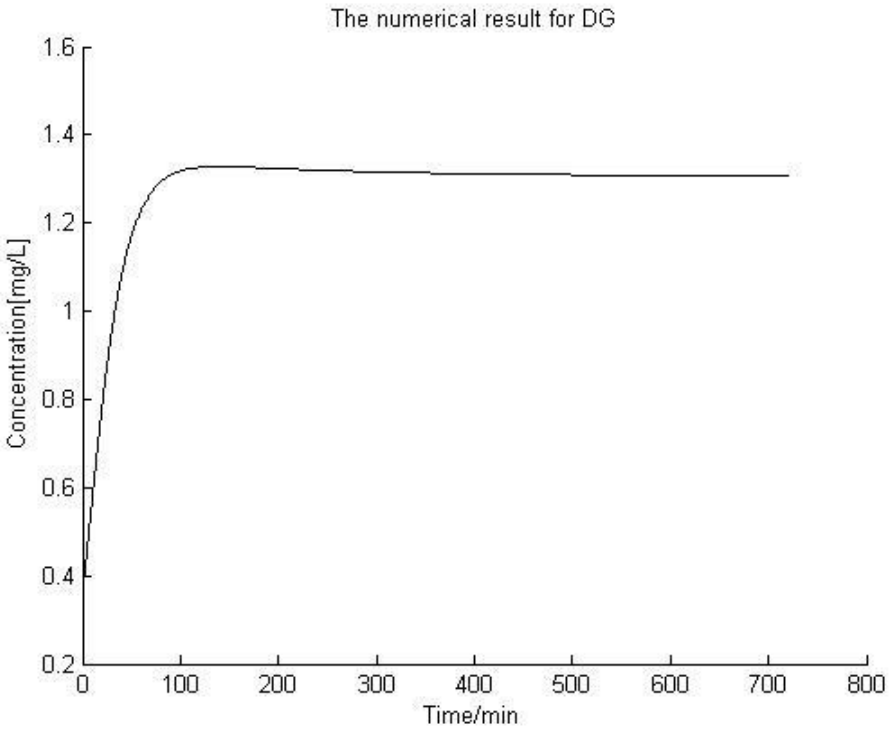

Figure 4.16 The prediction for diglyceride concentration

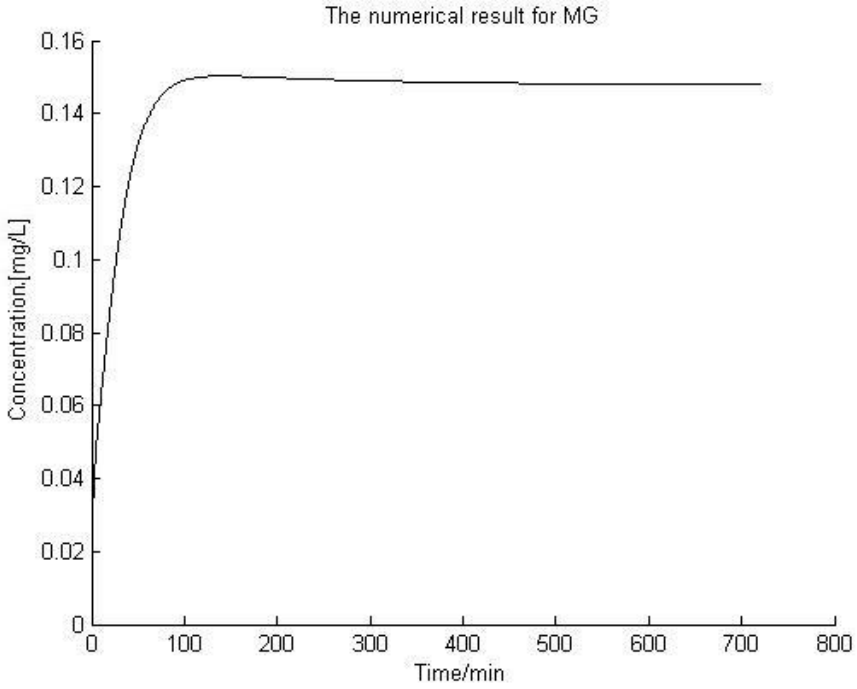

Figure 4.17 The prediction for monoglyceride concentration

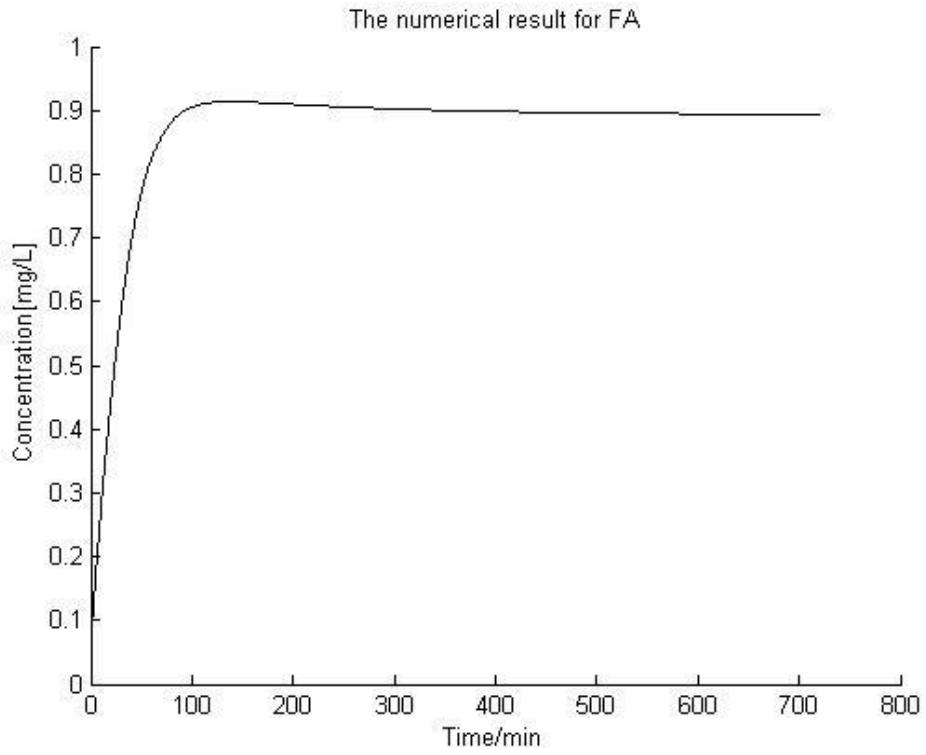

Figure 4.18 The prediction for fatty acids concentration

From Figure 4.15 the TAG concentration represents a monotonic decrease in a longer reaction period, but the tendency becomes slow and the concentration gets close to zero and remains stable. The rate change of TAG also describes the whole reaction which includes the other lipids concentration and fatty acid. The MG and DG do not have transformation from triglyceride and also remain stable after 400 minutes. The increase of fatty acids also have a small rate of change in a long reaction time. The prediction of the concentration from computational simulation can be associated to the lab condition in the experiment. As the enzyme in the reaction does not process the esterification reaction for process, the substance concentration cannot have a heavy fluctuation after the hydrolysis reaction. The prediction from the model can fit well the physiologycal features of chemical reaction in the experiment, and the inverse approach can provide an appropriate estimation for the reaction rate of hydrolysis.

4.5. **The summary**

This chapter proposes a novel model for TAG hydrolysis in the absorption process. The contribution of this hydrolysis model includes a first attempt to develop a regulator term in the compartment model to describe the possible unknown reactions in the stepwise hydrolysis process. A modification is made to the general form of the hydrolysis model to include the enzymatic reaction in the experiment. The multi-objective optimisation problem is addressed in the inverse problem by taking account of the physiology itself.

This hydrolysis model is designed for a macroscopic view of chemical reaction for lipid. In the metabolic pathway for human, the enzyme is usually stored inside the cell. Therefore a diffusion-reaction PDE model for the intestinal cell may be needed to represent the digestive system precisely. More details are presented in the next chapter.

Chapter 5 Some aspects of uncertainties in fatty acids absorption at cellular level

At the cellular level, analysis of absorption often refers back to the knowledge of cell biology. Understanding how cells work is fundamental in biological science. The research of cell biology is related to the cell proliferation [175], genetic biology [18] and cancer research [152], amongst others. In this thesis, the model developed in the cell is to be linked up with the macroscopic kinetic absorption phenomenon of TAG and fatty acids at a smaller level. By combining the MG and fatty acids through the esterification process inside the cell into the cellular transportation model, one can use it to estimate and predict lipid dynamics at the cellular level.

In this chapter, the movement of molecules in and out of the cell is studied. For the main absorption tissue, the intestinal epithelial cell is the pathway for all digested molecules before entering the metabolic system. The mathematical model describing the movement of lipids inside the epithelial cell can be used to understand the transport phenomena which are represented by a reaction diffusion system of PDEs [65, 82]. The membrane of epithelial cell, which is represented as the boundary conditions in the PDEs, has different kinds of proteins with various functions [185]. The shape of membrane is irregular and the surface of membrane differs a lot

for individuals [122]. Such information is too complicated to be included in the model and could lead to uncertainties in the boundary conditions.

5.1. The relation between cellular transport and absorption

As mentioned in Chapter 1 the transport of substances in absorption process takes place in the epithelial cells of small intestine. Epithelium, or epithelial cell, is one of the most basic cell types in animal tissue and organ. It does not contain blood vessels, but the cell can transport substance from connective tissue through basement membrane [58]. Epithelial cells cover the inner and outer linings of body cavities, such as the stomach and the urinary tract. As the barrier between the outside world's contaminants and the body, these cells replicate often to replace damaged or dead cells [167]. In this thesis, the study for epithelial cell is limited to the absorption process in the small intestine tissue and attention is paid to the TAG transport inside the intestinal epithelial cell.

The analysis of fatty acids absorption in blood vessels is modelled by means of a compartment model with a delay function in Chapter 3. The change of fatty acids concentration in such analysis is mainly due to the inhibition of insulin and the hydrolysis of TAG. The simplified ODE model as described in Chapter 3 assumes the absorption process without considering the transport of fatty acids at the cellular level. This limitation may be addressed by building a model in terms of the concentration of lipid when it goes into the blood vessel through the epithelial cells along the small intestine. A schematic view of the lipid transport pathway is shown in Figure 5.1.

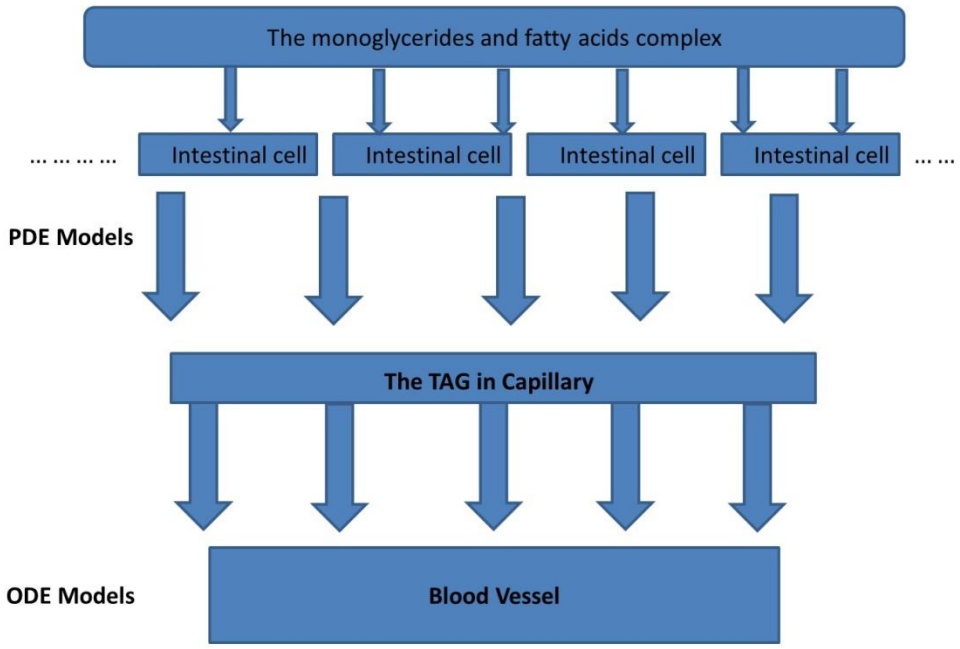

Figure 5.1 The schematic view of lipid transport

After the transport into the intestinal epithelial cell, the MG and fatty acids are released from the TAG molecule and move out of the cell [112]. A TAG molecule has to pass through some layers such as submucosa and serosa [93]. At this stage molecules can then transport through to the capillary and finally reach the blood vessel [136]. Therefore it can be concluded that the TAG is mainly controlled by the transport through epithelial cells in the small intestine. The function and structure of epithelial cell is the key factor in the mathematical model for cellular transport of TAG.

5.2. The TAG absorption in intestinal epithelial cells

TAG's transport in the blood and intestine is facilitated by the transport proteins and enzymes in the body. Microscopic studies concluded that the triglyceride particles, which range in diameters from $0.3 - 0.6\mu m$, cannot pass through apical membrane to enter the intestinal epithelial cell [165]. The TAGs are mainly digested by the lipase and become the emulsion particles (or micelles) in the small intestine lumen. In this process, the lipase activates the hydrolysis reaction

of TAG and the production of emulsion which consists of a complex of MG and fatty acids. Both the MG and fatty acids are taken up from the intestinal lumen and migrated into the epithelial cells of the small intestine. Once inside the epithelial cell, an esterification process of producing TAG happens around the Golgi part of the cell. These procedures are depicted as in Figure 5.2:

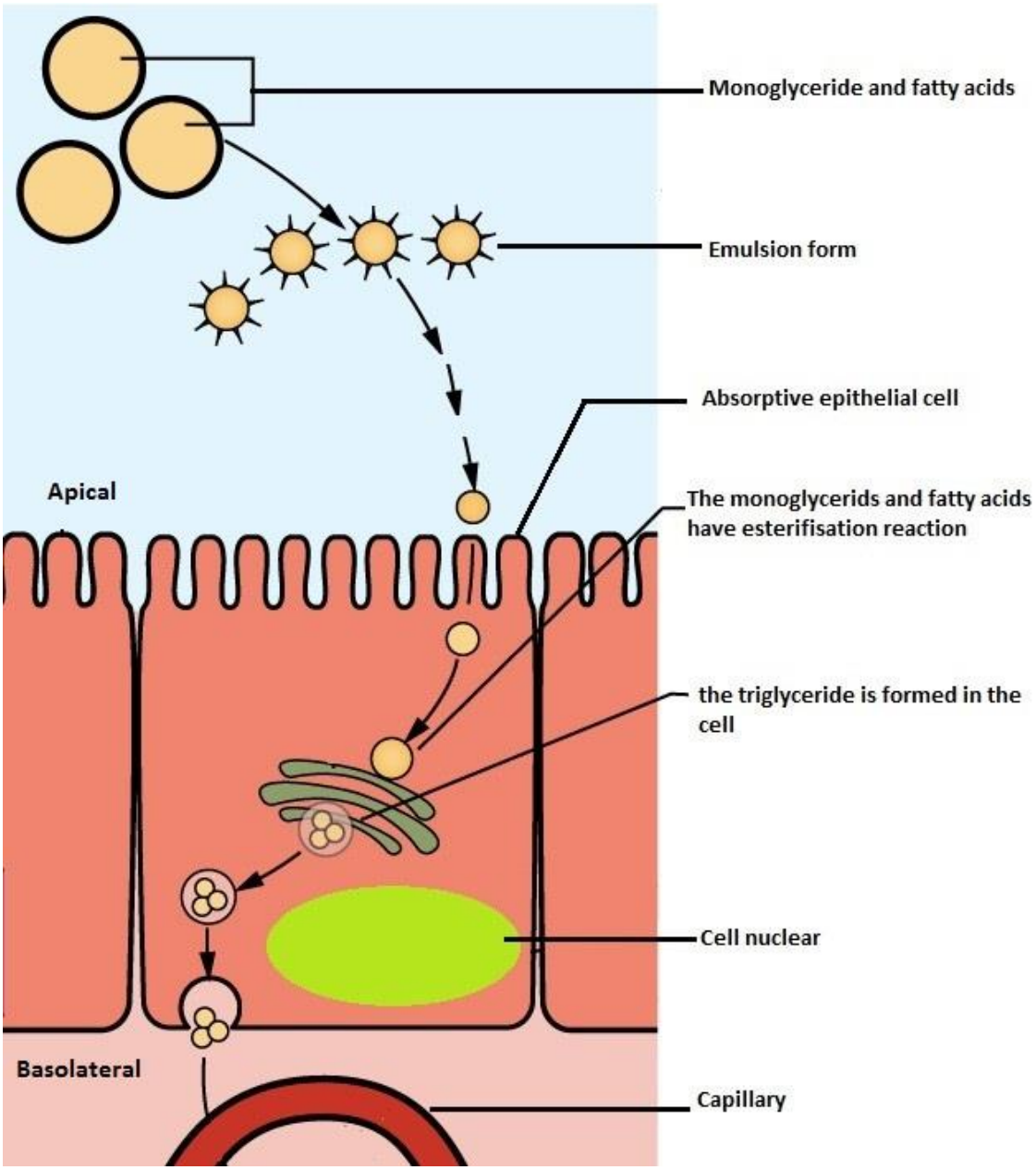

Figure 5.2 The pathway of triglyceride transport inside epithelial cell of small intestine.

After the formation of TAG in the epithelial cell, these molecules can move out of the cell by active transport [182]. The next site for TAG movement is the capillary near the outer wall of small intestine. In this way, the TAG can be transferred and circulated in the blood vessel where metabolism takes place. The adjacent epithelial cells do not have communication to each other, therefore the molecule transport inside the cell only has one direction from apical membrane to basolateral membrane, the PDE model for the diffusion inside the cell can be simplified to a one-dimension problem in this case.

Within the intestinal cells, there are many factors that may affect the rate of the movement of lipids and fatty acids in this transport process. These factors include the structure emulsion form, the binding proteins in the membrane, the functions of a cell and the activation of enzymes inside the cell. In the next section, a mathematical model is built by considering these factors in the TAG absorption.

5.3. Modelling lipid transport inside the epithelial cell

The general reaction-diffusion model for an epithelial cell is discussed in Chapter 2 and an example of glucose transport is considered in Equation (2.7). However the TAG transport inside the cell is more complicated as the hydrolysis and esterification reactions are involved [125]. Some modifications using the concept of regulator in the model need to be considered in this section.

As shown in Figure 5.2, the apical membrane of epithelial cell contains small, finger-like structures known as villi. The villi link the lumen of small intestine and the inner enviroment of epithelial cells. This complex structure of villi can be simplified to a regular domain and the membrane property is represented by the boundary condition. For substance transport inside the cell, the domain can be assumed to be one-dimensional and the transport can be represented in the figure below:

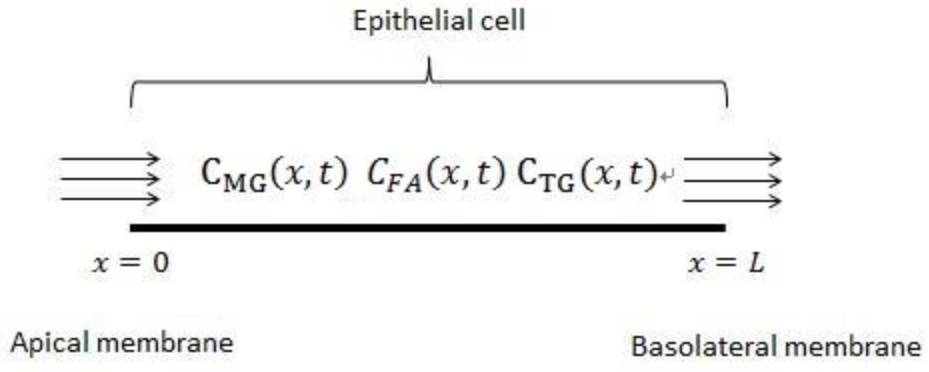

Figure 5.3 The cellular transport for lipid

As the distribution of substances inside the cell is considered. The compartmental model in Chapter 3 cannot be applied in this study. The PDE model describing diffusion and reaction of substances inside the cell is discussed in this chapter. The length of the epithelial cell is set as L. The flow of substances into the cell is from the apical membrane, which is along the left boundary at $x = 0$, and out of the cell from the basolateral membrane, which is the right boundary at $x = L$. The TAG molecules from basolateral site can enter the blood vessel and be involved in the metabolism which is presented in Chapter 3. A standard mathematical model used to describe the concentration changes with respect to time is the diffusion equation [178]. Consider the concentration $C_i(x,t)$ as one of the substances inside the cell, the equation of transport can be written as:

$$\frac{\partial C_i}{\partial t} = D\frac{\partial^2 C_i}{\partial x^2} \tag{5.1}$$

Equation (5.1) describes a diffusion model for molecular movement inside the epithelial cell. However, as revealed in Figure 5.2, the lipid molecules inside the cell undergo an esterification reaction that should also be taken into account for the transport of molecules. A source term in the PDE model is probably the best way to encapsulate the esterification reaction inside the cell.

5.3.1. The inclusion of esterification in the transport model

Define the concentration of TAG, MG and fatty acids as C_{TG}, C_{MG} and C_{FA}, respectively. Let S_{TG}, S_{MG} and S_{FA} be additional reaction terms which are also known as regulators here. The regulator may be used to provide a regulation to any missing process in physics. The PDE models can be written as below

$$\partial_t C_{TG} = D_{TG}\nabla^2 C_{TG} + S_{TG} \tag{5.2}$$

$$\partial_t C_{MG} = D_{MG}\nabla^2 C_{MG} + S_{MG} \tag{5.3}$$

$$\partial_t C_{FA} = D_{FA}\nabla^2 C_{FA} + S_{FA} \tag{5.4}$$

where D_{TG}, D_{MG} and D_{FA} are the diffusion coefficients of molecules, and S_{TG}, S_{MG} and S_{FA} are the source terms.

When substances enter the cell, one molecule of MG binds to two molecules of fatty acids to form the TAG. This is the same as the esterification process described in Chapter 4 and the reaction is given as below:

$$MG + 2\ Fatty\ Acid \overset{k_1}{\rightarrow} TAG \tag{5.5}$$

In the ODE model the compartment model can be built by applying the law of mass action. For the reaction-diffusion model in Equation (5.2) to (5.4), the regulators S_{TG} , S_{MG}, S_{FA} aim to incorporate all of the missing processes and chemical reactions inside the cell. For simplicity these source terms can be taken to present the esterification term in the ODE model. By applying the law of mass action to Equation (5.5), the reaction diffusion model in 1-D becomes:

$$\frac{\partial C_{TG}}{\partial t} = D_{\mathrm{TG}}\frac{\partial^2 C_{TG}}{\partial x^2} + k_1 C_{MG} C_{FA}^2 \tag{5.6}$$

$$\frac{\partial C_{MG}}{\partial t} = D_{MG}\frac{\partial^2 C_{MG}}{\partial x^2} - k_1 C_{MG} C_{FA}^2 \tag{5.7}$$

$$\frac{\partial C_{FA}}{\partial t} = D_{FA}\frac{\partial^2 C_{FA}}{\partial x^2} - k_1 C_{MG} C_{FA}^2 \tag{5.8}$$

where k_1 is the esterification rate of the reaction inside the cell. Here k_1 represents the rate that fatty acids binding to the ester bonds, which can be assumed to have a close value with the reaction rate for MG in the hydrolysis model in Chapter 4 ($k_1 = 0.17$). Some other parameters in the reaction-diffusion model are presented in the next section.

5.3.2. A numerical example

In the diffusion-reaction cellular model, the diffusion coefficients represent the level of mass diffusivity. There are many factors which control the diffusion of molecules, such as the temperature, pH values and reaction inside the cell [106, 198]. To represent the effect of these factors, Manitz et al. [118] built a two-dimensional multi-layer diffusion model, and some models have been used for describing unsaturated fatty acids diffusion [160]. According to the literature related to lipid diffusion [108, 190], the diffusion coefficient of lipid is around $10^{-10} cm^2/s$ to $10^{-8} cm^2/s$. The diffusion coefficients as provided in the literature are:

$$D_{\mathrm{TG}} = 36\ \mu m^2/h \tag{5.9}$$

$$D_{\mathrm{MG}} = 36 \mu m^2/h \tag{5.10}$$

$$D_{\mathrm{FA}} = 54\ \mu m^2/h \tag{5.11}$$

This set of diffusion coefficients are the same as those in [120] and are used in the current numerical example described here.

The domain is assumed to be one dimension and the length of cells determines the size of domain. In 1987, Brown [28] estimated the size of the epithelial cell of human lens (a structure

in the eye) in vivo. The study found that the epithelial cells range from 4-21 μm. Large differences exist in mean cell size between individuals. An appropriate shape of the epithelial cell is taken to consider the domain size and is defined as

$$x \in [0\,,4]$$

It is almost the size of an intestinal epithelial cell in μm scale.

The initial conditions are based on the concentrations of molecules inside a real cell. In 1998, Bas Teusink did an experiment and found that the concentration of substance was slightly less than 0.4 mM inside and was approximately 100 mM outside the cells [186]. The initial condition in this study can be assumed as a constant value 0.4 mM for MG and fatty acids and 0.6 mM per unit length for TAG concentration. Hence the initial conditions are assumed to be

$$\mathrm{C_{TG}}(\mathrm{x}, 0) = 0.4\ \mathrm{mmol/\mu m} \tag{5.12}$$

$$C_{MG}(x, 0) = 0.4\ \mathrm{mmol/\mu m} \tag{5.13}$$

$$C_{FA}(x, 0) = 0.6\ \mathrm{mmol/\mu m} \tag{5.14}$$

From Figure 5.3 it is considered that on the apical membrane of the epithelial cell ($x = 0$), the TAG cannot enter the epithelial cell, which means that the TAG has a zero-flux boundary condition along the apical membrane. This zero flux boundary condition also applies to MG and fatty acid along the $x = L$ where the substances do not have communication with exterior environment. The gradient of TAG concentration across the basolateral membrane is proportional to the concentration itself. This gives a Neumann boundary condition. The MG and FA have a transport into the epithelial cell at the apical membrane ($x = 0$). As the inflow is connected to the absorption pathway in the human digestive system, the assumption from macroscopic absorption model can be used to describe the mass flow before the epithelial cell part. The absorption delay phenomenon in Chapter 3 can be assumed for MG and FA along $x = 0$ as a theoretical time-dependent profile representing the concentration on the other side of the apical membrane. The boundary conditions used in the numerical example are summarised as below:

$\frac{\partial C_{TG}(0,t)}{\partial x} = 0$	$\frac{\partial C_{TG}(L,t)}{\partial x} = k_4 C_{TG}(L,t)$
$\frac{\partial C_{MG}(0,t)}{\partial x} = k_2 \frac{(k_{tr}t)^n}{n!} e^{-k_{tr}t}$	$\frac{\partial C_{MG}(L,t)}{\partial x} = 0$
$\frac{\partial C_{FA}(0,t)}{\partial x} = k_3 \frac{(k_{tr}t)^n}{n!} e^{-k_{tr}t}$	$\frac{\partial C_{FA}(L,t)}{\partial x} = 0$

Table 5.1 The boundary condition for reaction diffusion model

The lipids and fatty acids go in and out of the cell in the process of absorption, the membrane on both sides controls the transport rate across the membrane. In Table 5.1 the rate across the boundary for TAG is assumed to satisfy the first order dynamics in terms of substances concentration. The constant k_4 is related to the uptake ability of membrane for intestinal cells. In Nada's research [78], the uptake of fatty acid and lipid was measured at $23^{\circ}C$ and the uptake of lipids complex by cells were recorded along with time. The parameter in the boundary condition for this cellular model can be assumed to be the same as the uptake rate for epithelial cell. Hence the parameter in boundary conditions are assumed as

$$k_4 = 0.32\ \mu\text{m}^{-1} \tag{5.15}$$

The boundary condition for MG and FA on the boundary $x = 0$ is related to the delay function from macroscopic absorption process in Chapter 3. According to the application of delay function in [161], the transfer rate k_{tr} is controlled by the absorption time T and theoretical compartment number n: $k_{tr} = \frac{n+1}{T}$ $(\ min^{-1})$. The delay function describes the concentration of substances on the membrane and the transport rate along the boundary is taken from Nada's research [78] by considering the uptake rate by cell and assumed as

$$k_2 = 0.2\ mmol*\ \mu m^{-2} \tag{5.16}$$

$$k_3 = 0.4\ mmol*\ \mu m^{-2} \tag{5.17}$$

In this section, the initial and boundary conditions are described along with the assumption of other related biological coefficients in the model. The numerical tests can be seen as a

computational estimation for TAG absorption at cellular level. The delay for arriving to the small intestine lumen is faster than arriving the blood vessel compartment and the theoretical compartment number is set as $n = 2$ and the absorption time is set as $T = 10\text{min}$ $(\frac{1}{6}h)$

5.4. The numerical methods for the cellular model

For the reaction diffusion system in the study, the finite difference method is applied in the numerical simulation. Consider one of the concentration in Equation (5.2) to (5.4) written as

$$\frac{\partial C}{\partial t} = D\frac{\partial^2 C}{\partial x^2} + S \tag{5.18}$$

Here C refers to one lipid substance in the epithelial cell. Using a forward difference at time t_n and a second-order central difference for the space derivative at position x_i, the Equation becomes

$$\frac{C_i^{n+1} - C_i^n}{\Delta t} = D\frac{C_{i+1}^n - 2C_i^n + C_{i-1}^n}{\Delta x^2} + S^n \tag{5.19}$$

where Δt is the step size for time and Δx is the step size for space, and $i = 1,2,3 \ldots M$ .Then the Equation (5.19) can be written as:

$$C_i^{n+1} = HC_{i+1}^n + (1 - 2H)C_i^n + HC_{i-1}^n + \Delta t S^n \tag{5.20}$$

where

$$H = \frac{D\Delta t}{\Delta x^2}$$

The discretisation scheme of Equation (5.20) can be used for all substances in the reaction diffusion system, but may be different for the boundary conditions. For the TAG boundary condition in Table 5.1, the zero flux boundary condition at $x = 0$ ($i = 1$ in the space scheme) can be discretised as:

$$\frac{C_2^n - C_0^n}{2\Delta x} = 0 \tag{5.21}$$

Substitute Equation (5.21) to Equation (5.20) when $i = 1$, one can obtain

$$C_1^{n+1} = 2HC_2^n + (1 - 2H)C_1^n + \Delta t S^n \tag{5.22}$$

For the TAG concentration on the x = L (i = M in the space scheme), the TAG molecule has a flow out of the cell from the basolateral membrane, and the Neumann boundary condition can be discretised as :

$$\frac{C_{M+1}^n - C_{M-1}^n}{2\Delta x} = k_4 C_M^n \tag{5.23}$$

Substitute into Equation (5.20), one can obtain

$$C_M^{n+1} = 2HC_{M-1}^n + (1 - 2H + 2\Delta x k_4 H)C_M^n + \Delta t S^n \tag{5.24}$$

The boundary condition for MG and fatty acids is defined in a similar form. For the boundary condition at x = 0, the boundary condition for MG and fatty acids can be summarised as:

$$\frac{\partial C(x=0,t)}{\partial x} = f(t) \tag{5.25}$$

It can be discretised as:

$$\frac{C_2^n - C_0^n}{2\Delta x} = f(t) \tag{5.26}$$

Substitute into Equation (5.20) when i = 1, one can obtain

$$C_1^{n+1} = 2HC_2^n + (1 - 2H)C_1^n - 2\Delta x H f(t) + \Delta t S^n \tag{5.27}$$

The MG and fatty acids have a zero flux boundary condition at x = L, the discretisation is the same as the TAG concentration at x = 0, and can be defined as:

$$C_M^{n+1} = 2HC_{M-1}^n + (1 - 2H)C_M^n + \Delta t S^n \tag{5.28}$$

The convergence of finite difference method in the model

To test the convergence of the finite difference method, the algorithm can be applied with different spatial and temporal mesh sizes. In this study, the spatial interval is defined as $x \in [0,\ 4]$um and the temporal interval is defined as $t \in \left[0,\ \frac{1}{6}\right]$ hours. When the grid points for spatial is fixed as 41, which means $\Delta x = 0.1$ um, different grids point for time discretisation can be used in the simulation. The concentration of TAG in the time discretisation is taken with the grid point $g_t^i = 2^i * 10^3 + 1$ (i = 2,3 ... 8). The grid point $G_t = 2^9 * 10^3 + 1$ is assumed as the most accurate numerical result and the convergence of this method according to temporal mesh sizes can be tested by computing the 2-norm error between the simulation with g_t^i grid point in finite difference method and the simulation with G_t grid point in the finite difference method. Take TAG concentration for example, the computation can be done for

$$E_i = \left\| C_{TG}\left(with\ g_t^i\ discretisation\right) - C_{TG}(with\ G_t\ discretisation) \right\|^2$$

The numerical result can be seen in the following table.

Grid point	E_i
$2^2 * 10^3 + 1$	$1.64 * 10^{-4}$
$2^3 * 10^3 + 1$	$8.17 * 10^{-5}$
$2^4 * 10^3 + 1$	$4.06 * 10^{-5}$
$2^5 * 10^3 + 1$	$1.99 * 10^{-5}$
$2^6 * 10^3 + 1$	$9.65 * 10^{-6}$
$2^7 * 10^3 + 1$	$4.51 * 10^{-6}$
$2^8 * 10^3 + 1$	$1.93 * 10^{-6}$

Table 5.2 The 2-norm error for different temporal mesh sizes

It can be found in Table 5.2 that the error for TAG concentration is decreasing with the increasing of the grid point number, which means the numerical simulation converges to the finest mesh size. The temporal interval is defined as $t \in \left[0, \frac{1}{6}\right]$ hours .When the mesh size Δt is in $O(10^{-2})$ ($g_t = 2^2 * 10^3 + 1$) , the order of error E_i is in $O(10^{-4})$, and when the mesh size Δt is in $O(10^{-3})$ ($g_t = 2^i * 10^3 + 1, i = 3,4,5$) , the order of error E_i is in $O(10^{-5})$. To investigate the order of error of convergence in time for the numerical method, the value of ln(temporal grid points) against ln(errors) can be plotted based on the data obtained in Table 5.2. The figure can be seen as below:

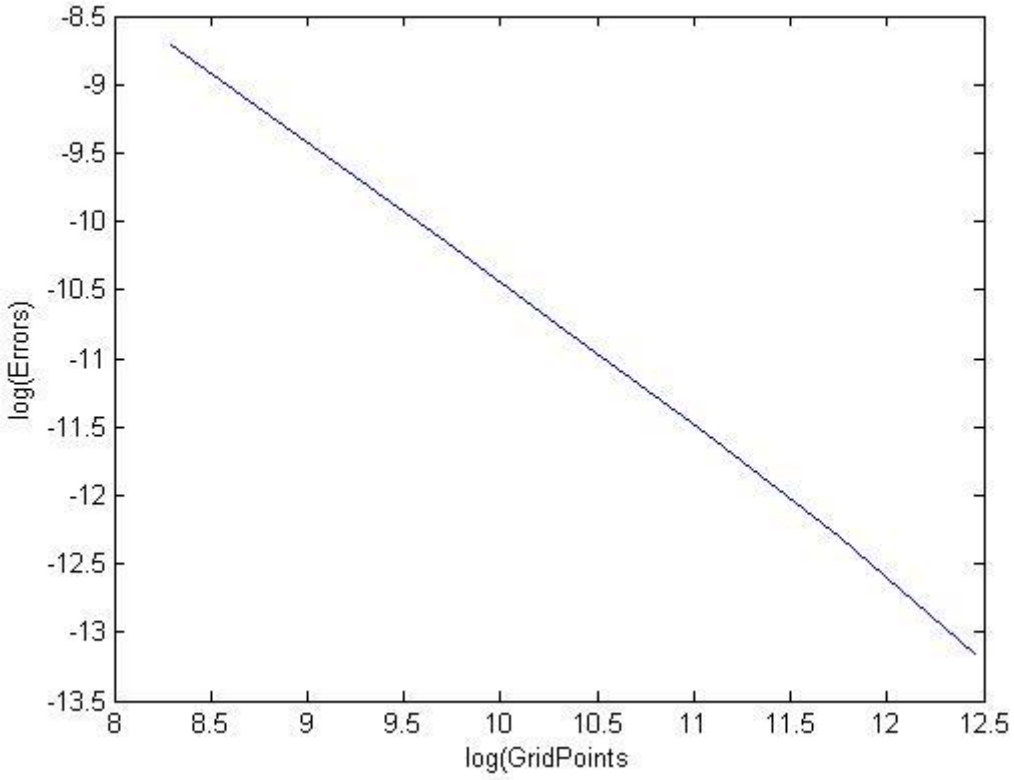

Figure 5.4 ln(temporal grid points) against ln(errors)

It is shown in Figure 5.4 that the ln(temporal grid points) against ln(errors) line is essentially linear from the numerical results. The absolute value of the slope in Figure 5.4 indicates rate of convergence of the method. By applying the polyfit function in MATLAB the absolute value of

slope is 1.06, which indicating the scheme has a first order convergence in time in this simulation test.

To evaluate the influence of step size in space, the temporal mesh size in the finite difference method can be fixed ($G_t = 2^9 * 10^3 + 1$). Different spatial grid points ($g_x^j = 2^j * 10 + 1$ ($j = 2,3 \dots 5$).) are tested in the algorithm and the comparison can be made with the finest spatial grid point ($G_x = 2^6 * 10 + 1$). As the mesh sizes are different in space for each case, one point for TAG concentration at $x = L, t = \frac{1}{6}$ can be taken and the error can be defined as

$$E_j = \left| C_{TG}(x = L)\left(with\ g_x^j\ discretisation\right) - C_{TG}(x = L)(with\ G_x\ discretisation) \right|$$

The numerical result can be seen in the following table.

Spatial Grid point	E_j
$2^2 * 10^3 + 1$	$2.44 * 10^{-6}$
$2^3 * 10^3 + 1$	$6.04 * 10^{-7}$
$2^4 * 10^3 + 1$	$1.44 * 10^{-7}$
$2^5 * 10^3 + 1$	$2.88 * 10^{-8}$

Table 5.3 The 2-norm error for different spatial mesh sizes

It is clear that with more spatial grid points in the algorithm, the smaller error can be obtained for the point $x = L\ (L = 4\ um)$. When the mesh size Δx is in $O(10^{-5})$ ($g_x = 2^2 * 10^3 + 1$), the order of error E_i is in $O(10^{-6})$, and when the mesh size Δx is in $O(10^{-6})$ ($g_t = 2^5 * 10^3 + 1$) , the order of error E_i is in $O(10^{-8})$. The order of the error converges to the finest solution fast with a smaller mesh size for space. The value of $\ln(\text{spatial grid points})$ against $\ln(\text{errors})$ can be plotted based on the data obtained in Table 5.3. The figure can be seen as below:

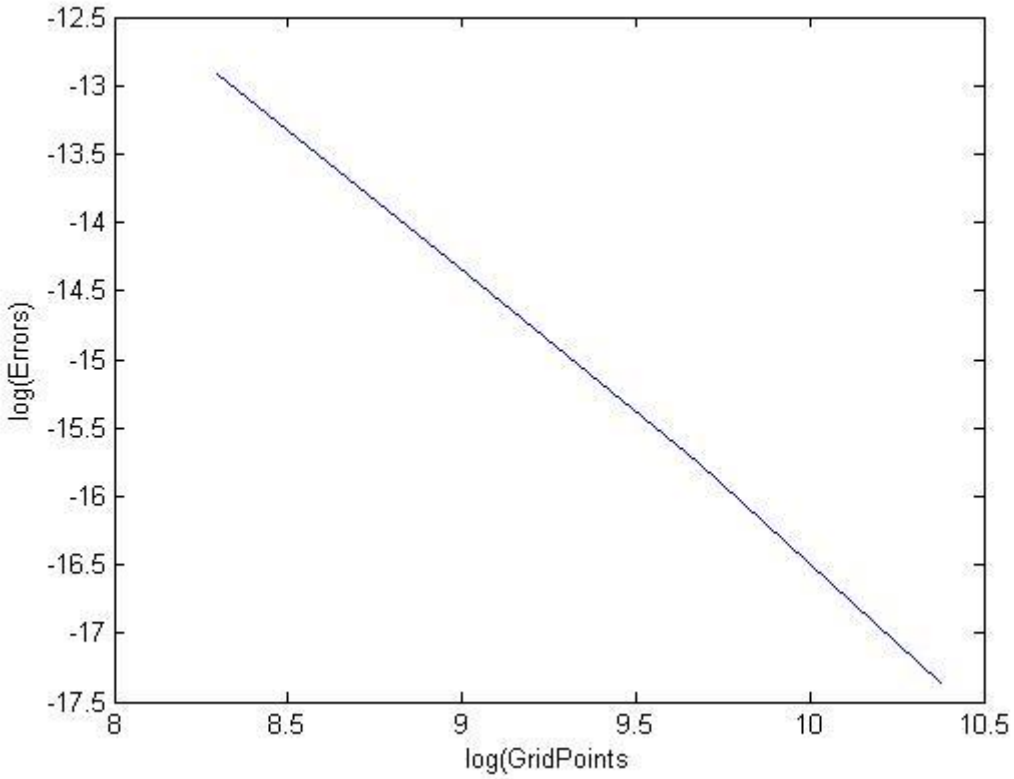

Figure 5.5 ln(spatial grid points) against ln(errors)

In Figure 5.5 the ln(errors) is almost linearly decrease against ln(spatial grid points), the absolute value of the slope is 2.13 based on the simulation data, which indicating the scheme has a second order convergence in space in this simulation test. The above test indicates that this finite difference method can converge to the finest mesh size for Δx and Δt with different tests of special and temporal mesh sizes. As the error is found to be very small in the above test, grid points are defined as $g_t = 2^2 * 10^3 + 1$ and $g_x = 41$.

To evaluate the convergence of the finite difference scheme, the simulation can be tested by changing both spatial and temporal mesh size. The temporal grid point number is defined as $g_t^i = 4^i * 10^4 + 1$ ($i = 1,2 \dots 6$) and the spatial grid point number is defined as $g_x^j = 2^j * 50 + 1$ ($j = 1,2 \dots 6$). Computational results at same location along x axis are taken ($x = 0$, $\frac{1}{4}L$, $\frac{1}{2}L, \frac{3}{4}, L$). The root-mean-square of the difference between the values on the coarser mesh and the values on the finer mesh is computed and can be defined as

$$E_h = \sqrt{\frac{1}{5}\sum_{n=1}^{5}(C_{TG}\left(\mathrm{x}=\mathrm{x_n}, \mathrm{g_t^{h+1}},\ \mathrm{g_x^{h+1}}\right) - C_{TG}\left(\mathrm{x}=\mathrm{x_n}, \mathrm{g_t^{h}},\ \mathrm{g_x^{h}}\right))^2}$$

where $\mathrm{x_n}$ indicates the same location in spatial axis ($x = 0,\ \frac{1}{4}L,\ \frac{1}{2}L, \frac{3}{4}, L$). The numerical result can be seen in the following table.

Coarse mesh	Fine mesh	E_h
$\mathrm{g_t^1} = 4^1 * 10^4 + 1$ $\mathrm{g_x^1} = 2^1 * 50 + 1$	$\mathrm{g_t^2} = 4^2 * 10^4 + 1$ $\mathrm{g_x^2} = 2^2 * 50 + 1$	$2.44 * 10^{-6}$
$\mathrm{g_t^2} = 4^2 * 10^4 + 1$ $\mathrm{g_x^2} = 2^2 * 50 + 1$	$\mathrm{g_t^3} = 4^\mathrm{i} * 10^4 + 1$ $\mathrm{g_x^3} = 2^\mathrm{j} * 50 + 1$	$0.62 * 10^{-6}$
$\mathrm{g_t^3} = 4^3 * 10^4 + 1$ $\mathrm{g_x^3} = 2^3 * 50 + 1$	$\mathrm{g_t^4} = 4^4 * 10^4 + 1$ $\mathrm{g_x^4} = 2^4 * 50 + 1$	$0.16 * 10^{-6}$
$\mathrm{g_t^4} = 4^4 * 10^4 + 1$ $\mathrm{g_x^4} = 2^4 * 50 + 1$	$\mathrm{g_t^5} = 4^5 * 10^4 + 1$ $\mathrm{g_x^5} = 2^5 * 50 + 1$	$0.04 * 10^{-6}$
$\mathrm{g_t^5} = 4^5 * 10^4 + 1$ $\mathrm{g_x^5} = 2^5 * 50 + 1$	$\mathrm{g_t^6} = 4^6 * 10^4 + 1$ $\mathrm{g_x^6} = 2^6 * 50 + 1$	$0.01 * 10^{-6}$

Table 5.4 The root-mean-square of the difference with different mesh size

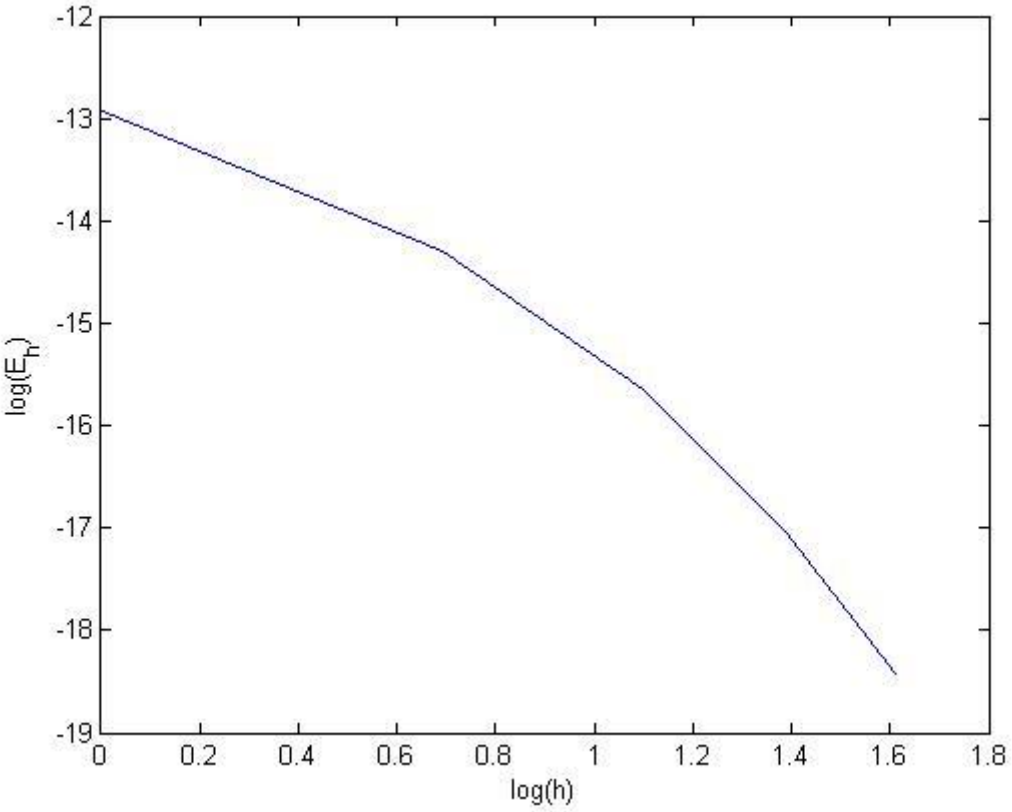

Figure 5.6 $ln(h)$ against $ln(E_h)$

It can be found from above table and figure that the root-mean-square has a smaller value with a finer mesh size for both g_x and g_t. The estimate of the error goes down by approximately a factor of 4 each time by computing $\ln(h)$ against $ln(E_h)$, indicating the finite difference scheme meets the demand for convergence in this non-linear problem.

5.5. A computational experiment

With the mathematical model and coefficients defined in Section 5.3, the computational simulation can be implemented with MATLAB. The absorption time T is defined as 10 minutes and the theoretical compartment number n is chosen from Chapter 3 and defined as $n = 2$. The substance concentrations at $t = 0$, 2.5 min , 5 min and 10 min are computed and shown as below:

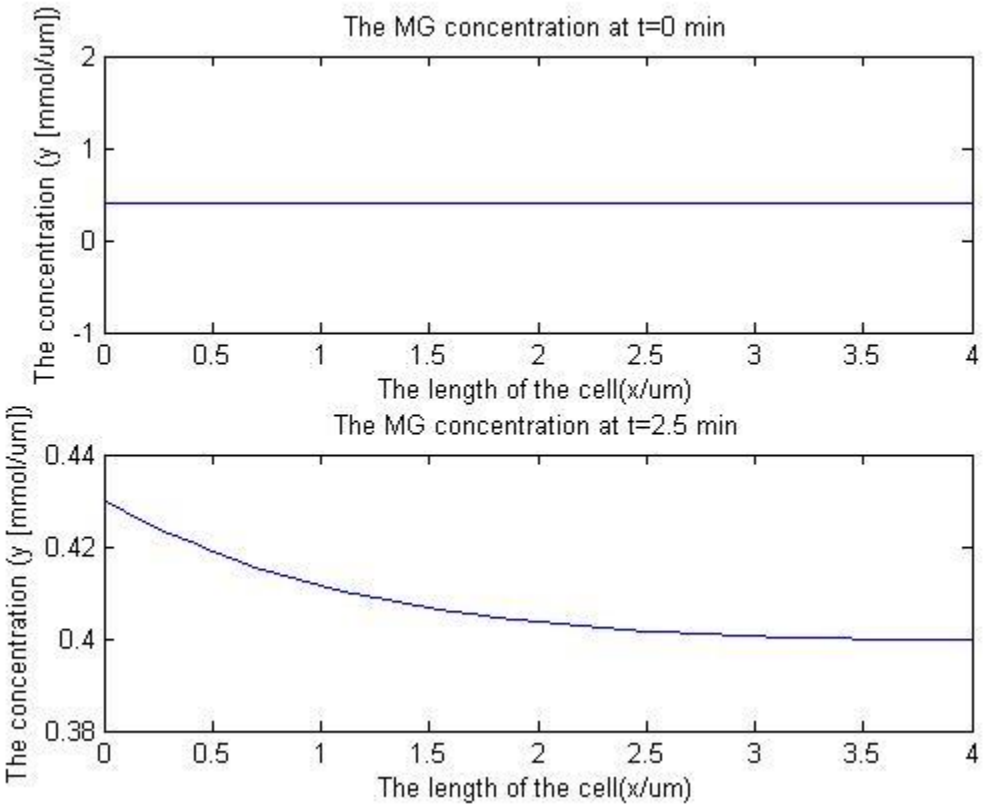

Figure 5.7 The concentration of MG at t=0 and 2.5 min

Figure 5.7 describes the concentration of MG inside the cell at t=0 and 2.5 min. The initial condition defines the MG concentration is a constant at $t = 0$. The Neumann boundary condition at $x = 0$ provides a flow of concentration into the cell, but it has delay feature from absorption process, therefore the concentration of MG near the apical membrane increases slowly initially.

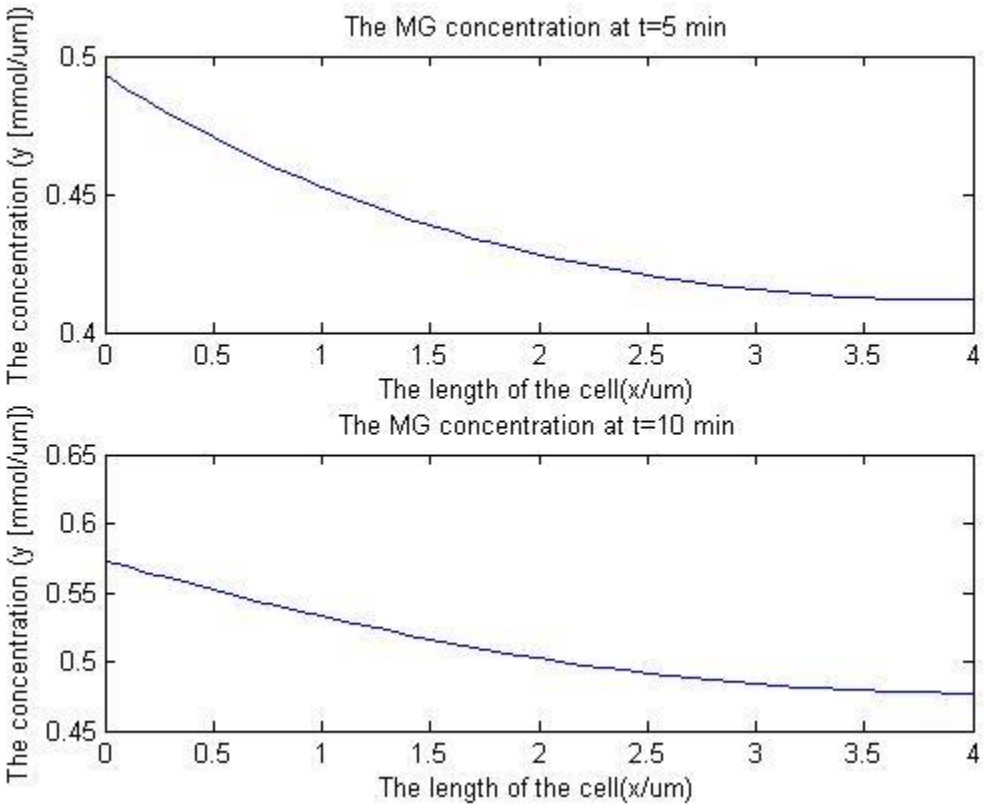

Figure 5.8 The concentration of MG at t=5 and 10 min

The concentration of MG increases monotonically inside the cell, but with a larger rate between t=5min and t=10 min. As the flow rate into the cell from apical membrane begins to have a strong inflow after the delay phenomenon, the concentration of MG increase dramatically after 2.5 mins of the absorption.

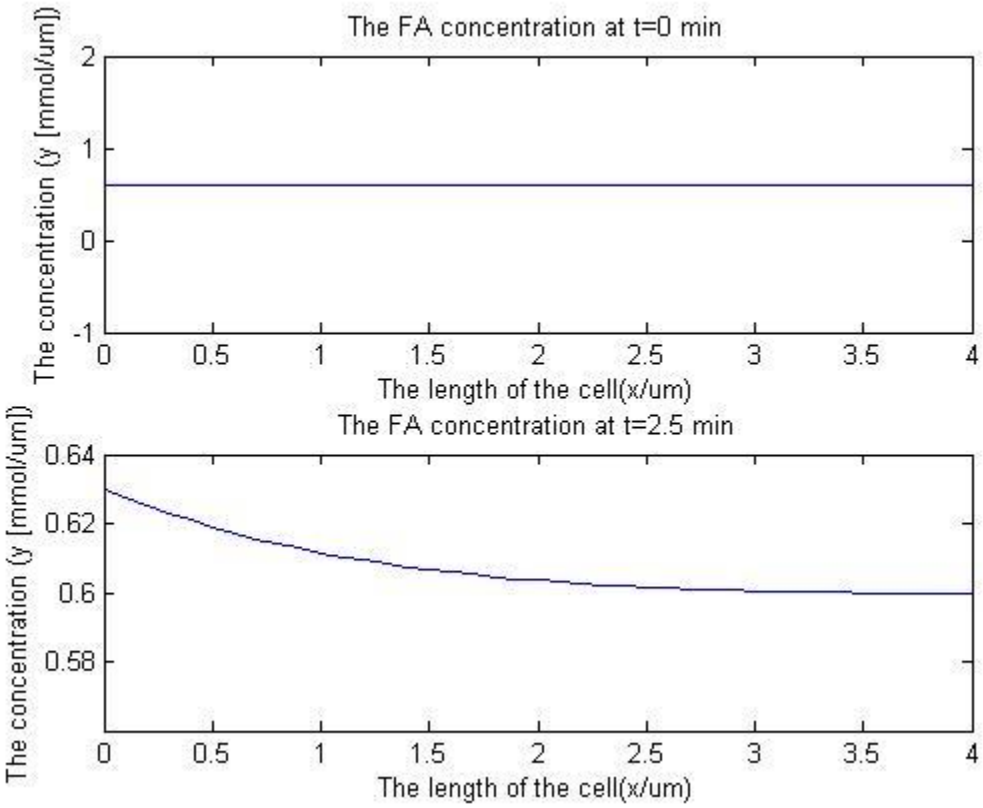

Figure 5.9 The concentration of fatty acids at t=0 and 2.5 min

In contrast to MG concentration, the fatty acids concentration has a larger transport rate from the apical membrane. The concentration in such boundary increases faster from t=0 to t= 2.5 minutes compared to the MG concentration.

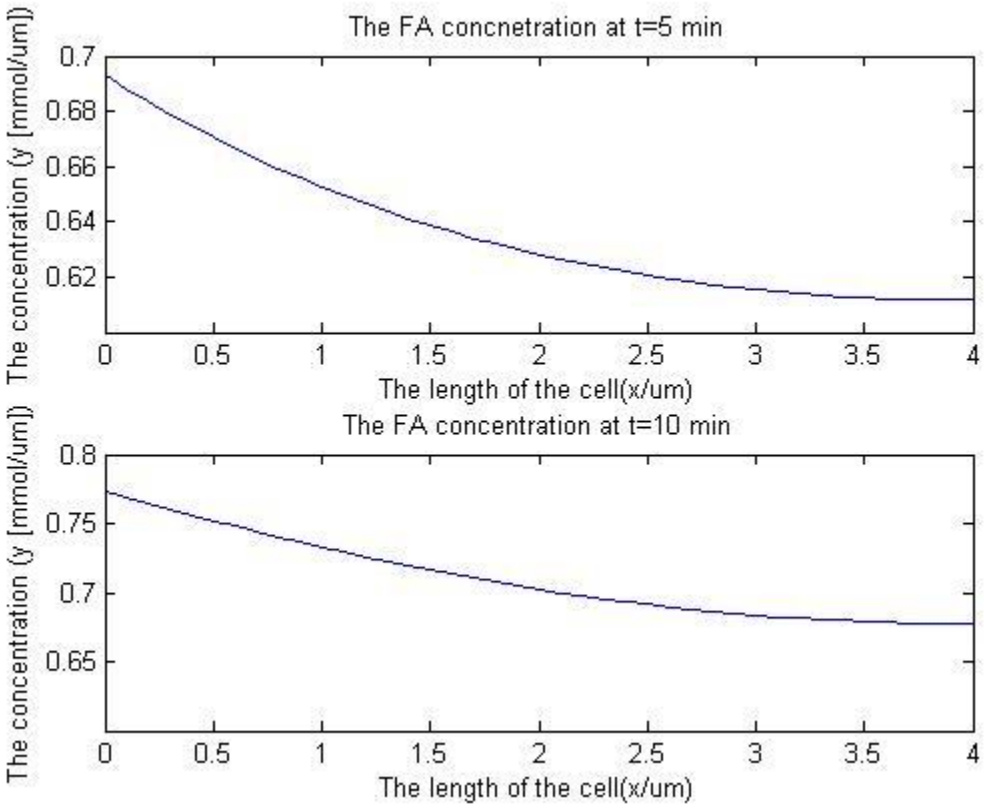

Figure 5.10 The concentration of fatty acids at t=5 and 10 min

From t=5 min to t=10 min, the fatty acids concentration on the boundary increase from about 0.69 $mmol/um$ to about 0.77 $mmol/um$. The larger diffusion coefficient and faster inflow rate into the cell leads to a larger concentration difference inside the epithelial cell for FA than the MG profile.

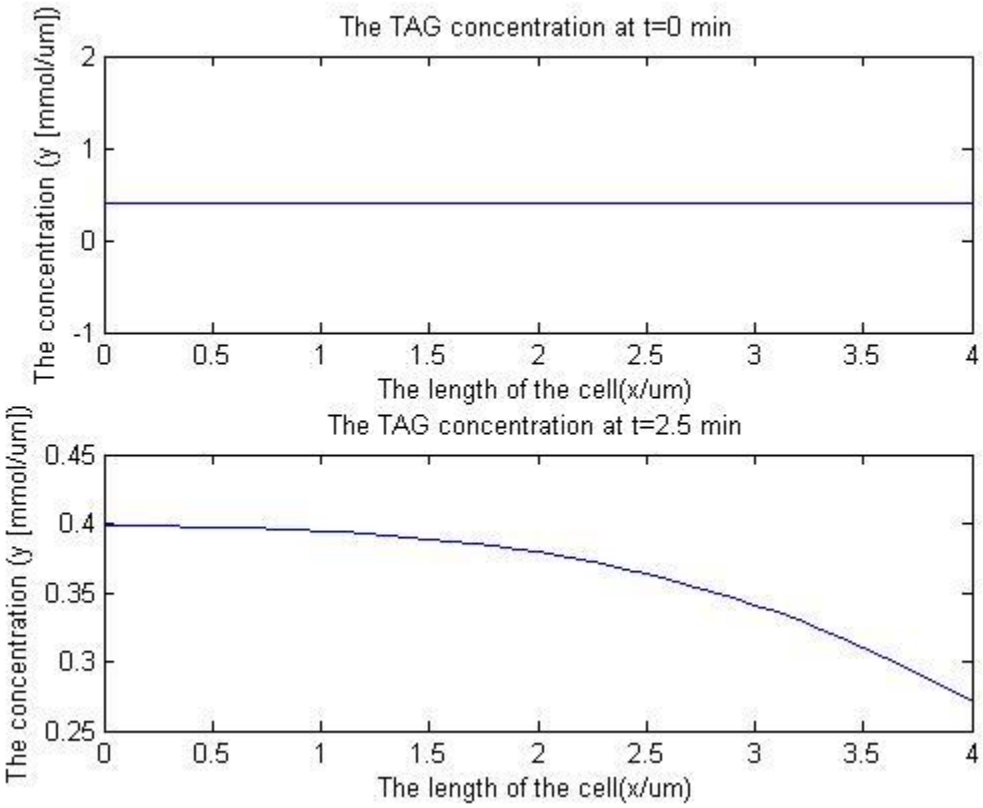

Figure 5.11 The concentration of TAG at t=0 and 2.5 min

In contrast to MG and fatty acids, the TAG has a zero flux boundary condition along $x = 0$. The TAG concentration has a flow out of the cell at $x = \mathrm{L}$. The concentration of the boundary decrease from $0.4\ mmol/um$ at $t = 0$ to about $0.27 mmol/um$ at $t = 2.5\ min$.

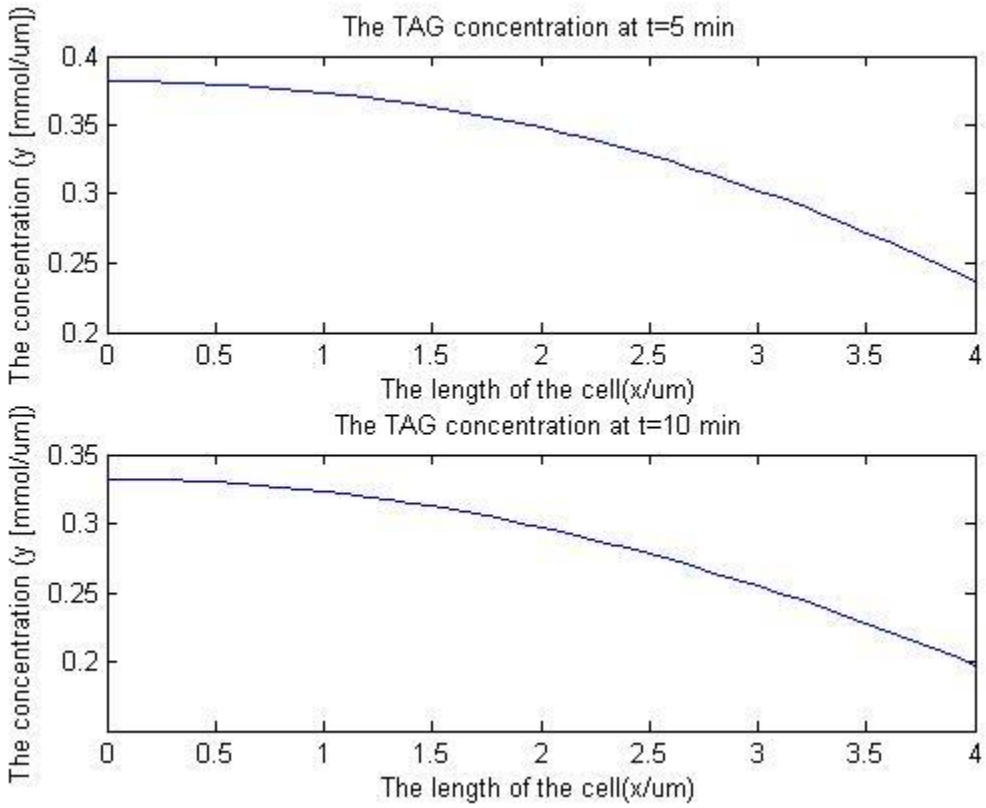

Figure 5.12 The concentration of TAG at t=5 and 10 min

Figure 5.12 indicates the TAG concentration inside the cell from t=5 to t= 10 min. It can be seen from the Figure 5.12 that the concentration along $x = 0$ has a slight decrease during this period from about $0.4\,mmol/um$ to $0.32\,mmol/um$ mmol. The concentration of TAG inside is affected by the transport and esterification reaction inside the cell during this period.

5.6. The fatty acids concentration with uncertainty in boundary condition

As is shown is Figure 5.1, the basolateral membrane of epithelial cell contains a small, finger-like structures known as intestinal villi. The villi link the lumen of small intestine and the inner enviroment of epithelial cells. The MG and fatty acid need to pass through the villi structure and then enter the intestinal cell. The intestinal villi consist of some brush border membrane. It can

increase the surface area of the intestinal walls, which can highly extend the surface for absorption and provide a higher force for substance to enter the epithelial cell [77]. There are many nutrients and enzymes lying on the surface of villi [171]. The activity of enzymes attached to the villi are various in terms of individuals [122]. Due to these complexity and missing information from physiological knowledge, the gradient for substances passing through the membrane into the cell, which is the boundary condition in the model, exhibits uncertainties.

As described in Chapter 2 that the uncertainty can be represented by assuming unknown random terms in the boundary condtion. The coefficients in the boundary condition as defined in Equation (5.15) to (5.17) thus take the form

$$k_4 = 0.32 \tag{5.29}$$

$$k_2 = 0.2 + \sigma_3 \tag{5.30}$$

$$k_3 = 0.4 + \sigma_4 \tag{5.31}$$

The constant part in the coefficients is defined in Section 5.3.2. The unknown random terms σ_3 and σ_4 are introduced into the model to represent uncertainties of coefficients.

5.6.1. The Monte Carlo simulation with normal distribution in uncertainty at t=10 min

In this section, the random uncertainty term is assumed to have a normal distribution which is described in Chapter 2. The normal (or Gaussian) distribution is a common continuous probability distribution and often used in the natural and social sciences to represent real-valued random variables whose distribution are not known [7, 137]. The probability density of the normal distribution is:

$$f(x|\mu_n, \sigma_n) = \frac{1}{\sigma_n\sqrt{2\pi}} e^{-\frac{(x-\mu_n)^2}{2\sigma_n^2}} \tag{5.32}$$

Here μ_n is the mean of distribution and σ_n^2 is the variance. The notation of normal distribution is written as $\mathcal{N}(\mu_n, \sigma_n^2)$. In this section one example is defined to have a normal distribution with mean value equal to 0 and variance equal to 0.01 for randomness, which indicate

$$\sigma_3 = \sigma_4 = \mathcal{N}(0, 0.01) \tag{5.33}$$

The uncertainty in boundary condition is studied by means of Monte Carlo method. The Monte Carlo method provides a repeated sampling with normal distribution in uncertainty. In this section, the PDE model in Equation (5.6) to (5.8) is computed when $N = 512$ times with the uncertain parameters in boundary condition defined in Equation (5.29) to (5.31). Other values of N were also tested in the next section. The concentration of MG and fatty acids at t=10 minutes along the cell is shown in the following figures.

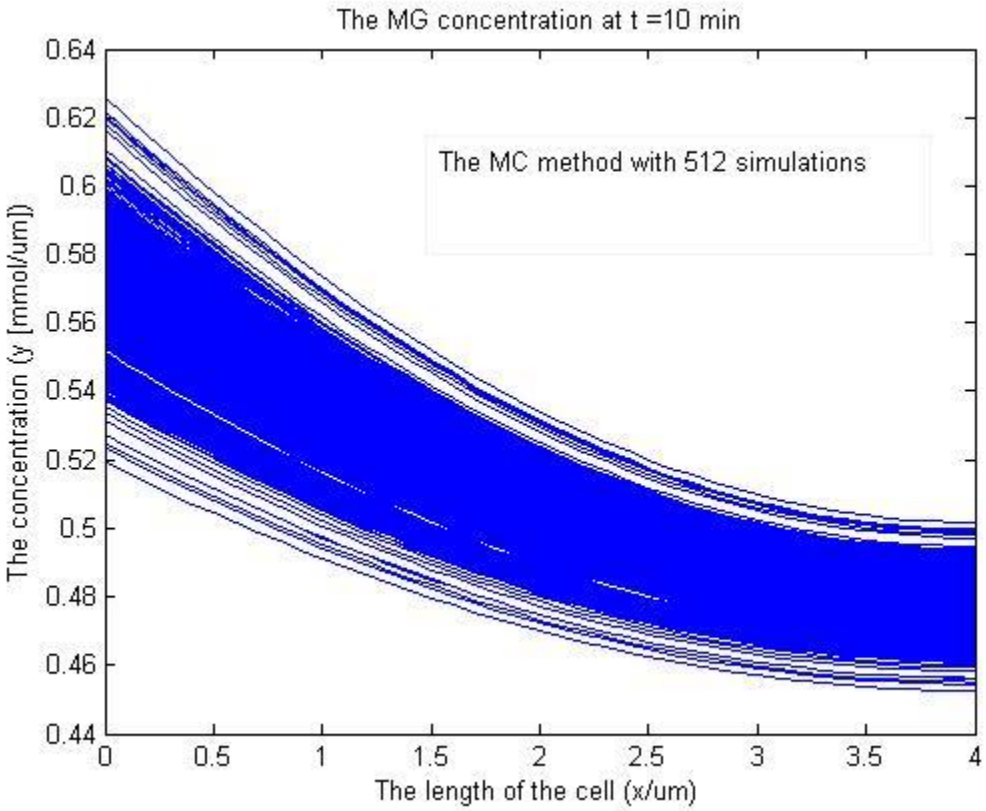

Figure 5.13 The concentration of MG at t=10 min

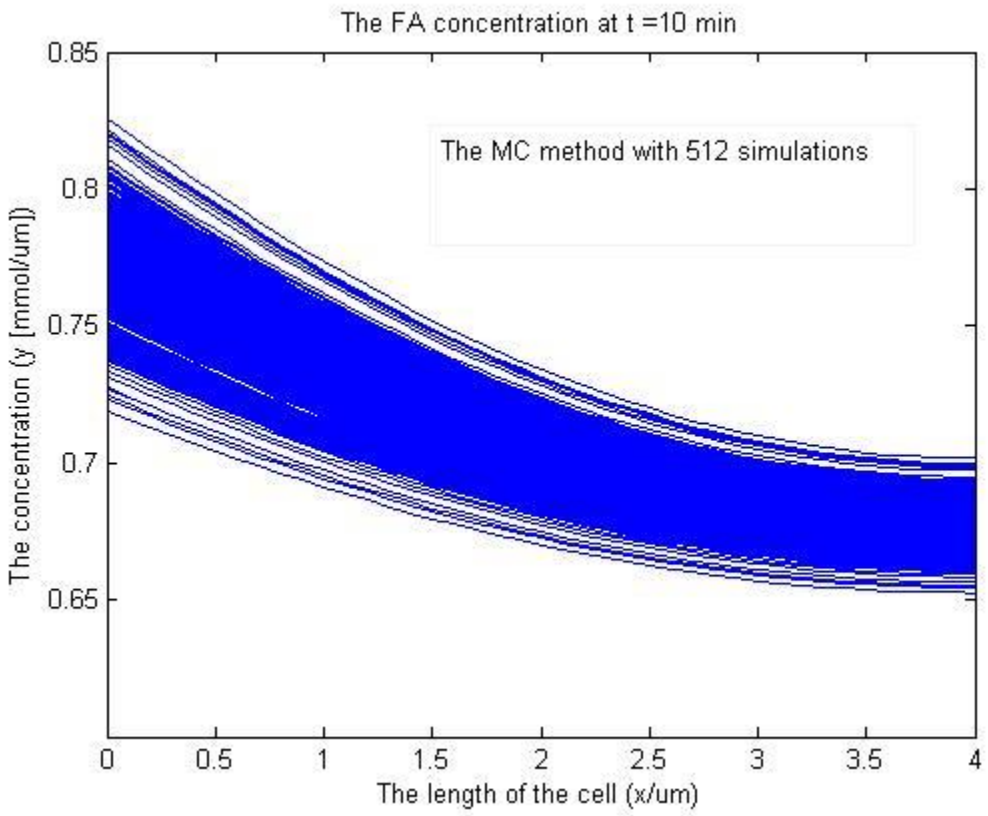

Figure 5.14 The concentration of FA at t=10 min

Figure 5.14 indicates the concentration of MG and FA along the cell. There are 512 simulations in this Monte Carlo simulation. It can be seen that the concentration of the FA and MG has a big difference near the apical membrane ($x = 0$). It means that the randomness in the parameter can provide various gradients for MG and FA inflow into the cell. Even though the TAG has zero-flux boundary condition near the apical membrane, the uncertainty for MG and FA concentration can also affect the interactive system and leads to the differences for TAG concentration. This can be seen in the following figure.

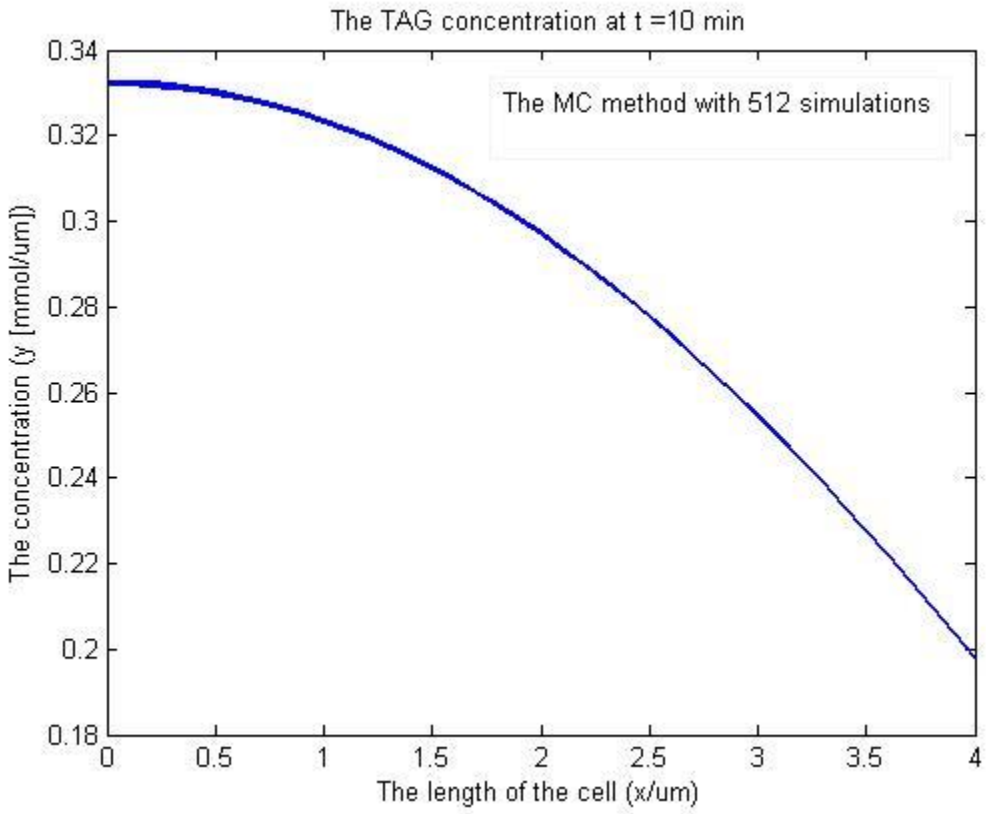

Figure 5.15 The concentration of TAG at t=10 min

From above figure it can be seen that the TAG concentration inside the cell is also affected by the randomness of the inflow gradient from MG and FA, especially near the apical membrane. As the normal distribution provides a large range for the possible concentration in this absorption system, an estimated interval is needed to predict the TAG concentration with uncertainty MG and FA inflow gradient.

5.6.2. The confidence interval for triglyceride

The concept of confidence interval was introduced by a paper of Jerzy [128]. The confidence interval is a type of interval estimate for a sample. The definition of confidence interval defined as below:

Let $0 < \beta < 1, \chi$ be a set of samples. The random interval ($a(\chi)$, $b\ (\chi)$) is called a $100(1-\beta)\%$ confidence interval for θ if

$$P(a(\chi) < \theta < b(\chi)) = 1 - \beta$$

Note: $a(\chi)$ and $b(\chi)$ are not allowed to depend on θ.

The random interval ((χ) , $b(\chi)$) is an estimator. The corresponding interval estimate is ($a(\chi)$, $b(\chi)$) . Usually $\beta = 0.05,$ or 0.01,giving a 95% or 99% confidence interval. In statistics, a confidence interval is a kind of interval estimation for samples, but it does not represent any single sample and is expressed by a percentage. For example, a 95% confidence interval means the statistician is 95% confident that the values in the samples are in this interval. There are many factors which can affect the confidence interval including sample size, population variability and level of interval.

In this study, the confidence interval of substance concentration can represent the influence of uncertainty in the boundary condition. As the boundary condition has a normal distribution perturbation, the confidence interval for concentration is calculated with the formula for normal distribution which is based on central limit theory.

The process for computing confidence intervals is quite simple if the sample is obtained. Assume there is a normal distribution $\mathcal{N}(\mu, \sigma^2)$ has mean value μ and variance σ^2, and $X_1, X_2, \ldots X_n$ has this $\mathcal{N}(\mu, \sigma^2)$ distribution.

$$(\bar{X} - z_{\beta/2}\frac{\sigma}{\sqrt{n}}, \bar{X} + z_{\beta/2}\frac{\sigma}{\sqrt{n}})$$

is a $1-\beta$ confidence interval for μ and n is the number of samples which is the repeated simulations in Monte Carlo method. The $\bar{X}$ is the mean value of sample and z_β is obtained from the equation $\Phi(z_\beta) = 1 - \beta$, where Φ is the value of the cumulative distribution function of the

normal distribution [154]. As the 95% confidence interval for concentration is considered in this study and $\Phi(1.96) = 1 - \frac{5\%}{2} = 97.5\%$, the value of $z_{\beta/2}$ is equal to 1.96 for this analysis. And the $\bar{X}$, σ and n is from the samples from Monte Carlo simulations.

For this uncertainty defined in Equation (5.33), the confidence interval provides estimations for the concentration of fatty acids and the monoglycerides inside the cell, and the confidence interval for triglyceride can evaluate the influence of uncertain inflow into the epithelial cell.

5.6.3. The length of confidence interval for triglyceride concentration

As the FA and MG have uncertainty on the apical membrane, the effect of this uncertain inflow on the TAG concentration inside the cell is the key factor in the absorption process. The brush border structure on the apical membrane provide the randomness in the boundary condition at $x = 0$. The concentration of TAG near the basolateral membrane can be measured by the confidence interval on the boundary at $x = L$. By assuming same simulation number ($N = 512$), the length of confidence interval for TAG in different locations of the cell at $t = 10$ min can be seen as below:

Location	Length of confidence interval
$x = 0$	$3.29 * 10^{-5}$
$x = \frac{1}{4}L$	$2.96 * 10^{-5}$
$x = \frac{1}{2}L$	$2.35 * 10^{-5}$
$x = \frac{3}{4}L$	$1.79 * 10^{-5}$
$x = L$	$1.33 * 10^{-5}$

Table 5.5 The length of confidence interval at different location of the cell

From above table the confidence interval for TAG at some specific locations in the cell is presented. The length of the confidence interval indicates a higher uncertainty near the apical membrane. The length of the confidence interval inside the cell at different location along x axis can be plotted and shown in the following figure.

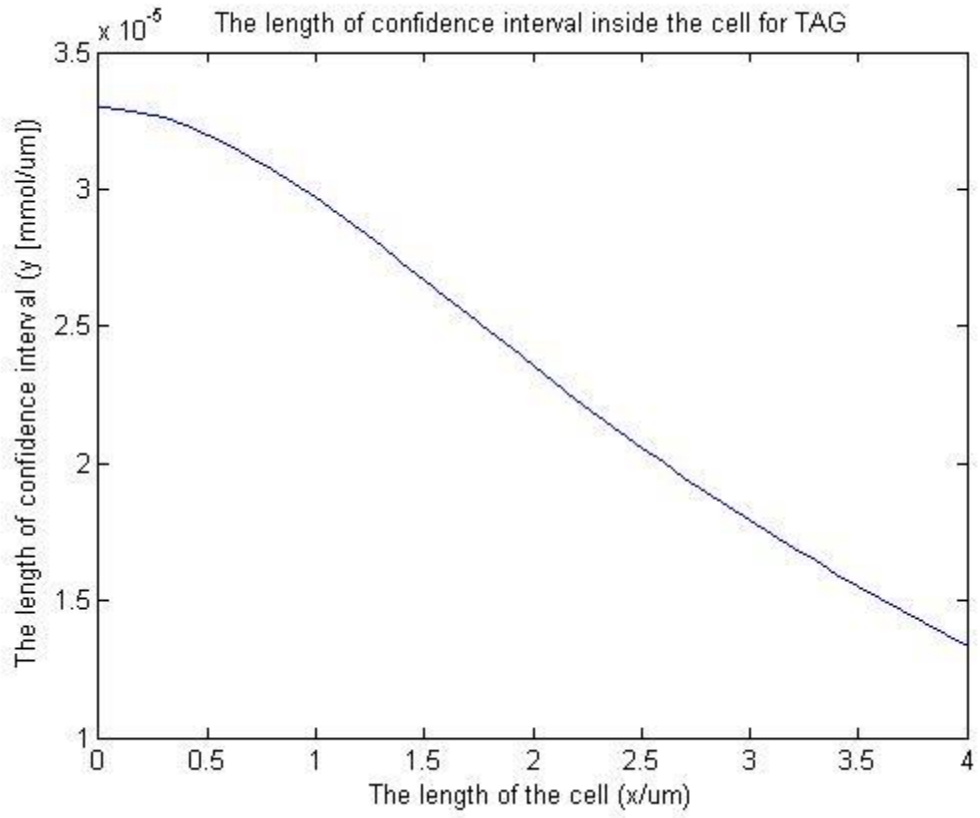

Figure 5.16 The length of confidence interval for TAG inside the cell

It can be seen from the figure that the length of confidence interval has a maximum value at $x = 0$, which indicates a large uncertainty near the apical membrane. This is due to the random parameters in the boundary conditions for MG and FA, and these uncertainties indirectly affect the concentration of TAG as the esterification process leads to the production of TAG inside the cell. As the TAG has a flow out of the basolateral membrane, the confidence interval at $x = L$ for TAG provides the effect of brush border effect in the cellular transport. A good estimation for TAG can be obtained with a small length of confidence interval for biologists.

The length of confidence interval is closely related to the sample size which is the number of simulations in Monte Carlo method in this study. The sample size study is significant to consider the reliability of sample and the confidence interval. In 2012, Cock investigated how to obtain the sample size information from the confidence interval [87] and Robert and Casella reviewed the computation methods and found that the classic Monte Carlo integration is inadequate for sample size determination due to the computational requirement. [88] In this thesis, different sample sizes in Monte Carlo simulation are used to compute the confidence interval. In the computational experiment, the increase of simulation number can obviously decrease the length of the confidence interval and it can be seen in the following figure.

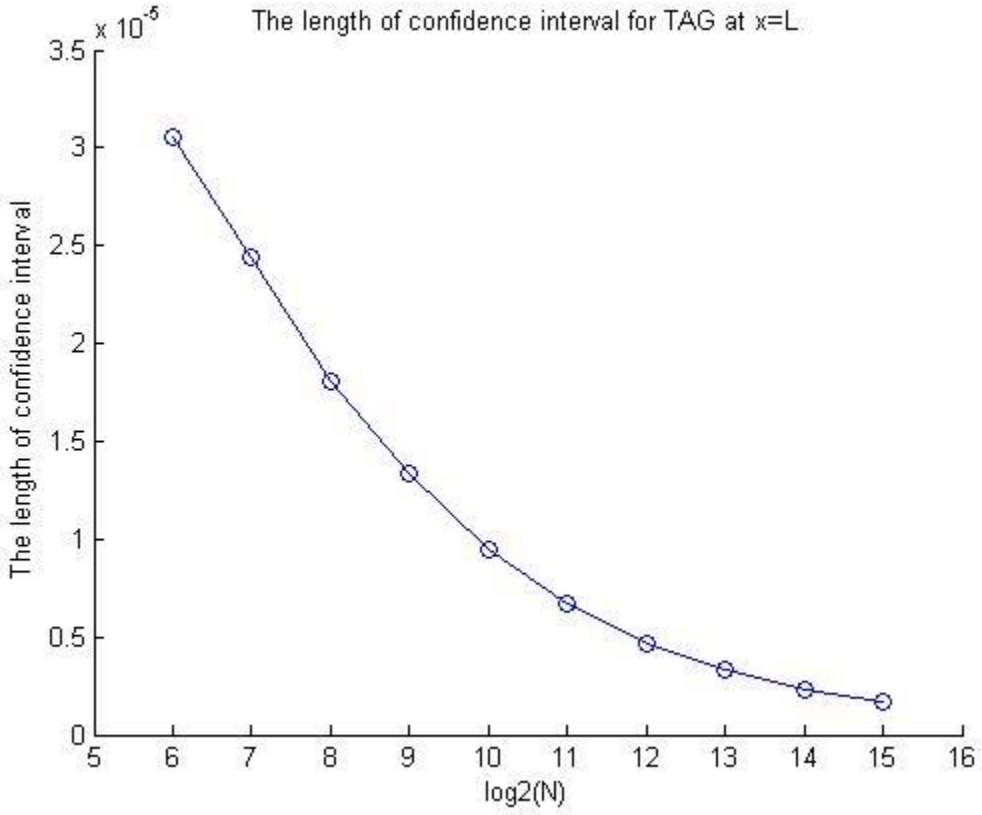

Figure 5.17 The confidence interval for fatty acids with difference sample sizes

In Figure 5.17 the x axis is the logarithm of the sample size to base 2 (i.e. with 512 simulations the $\log_2 N = 9$) and the y axis is the length of confidence interval. The length exhibits a dramatic decrease from 128 simulations to 32768 simulations. This conclusion can also apply to confidence interval of other substances such as MG and FA.

5.6.4. The accumulated flux for triglyceride concentration

In the definition of the cellular model in Equation 5.2 to 5.4, the triglyceride can pass through the basolateral membrane which is described at $x = L$. The uncertainty is defined for the parameters at $x = 0$ and handles the inflow into the epithelial cell. The influence for outflow on the other side of the boundary can be considered in this study. In this section the accumulated flux for TAG concentration on $x = L$ is computed to evaluate the uncertainty of inflow into the cell.

In the transport for a substance inside the cell, the flux is defined as a rate of flow of a substrate per unit area. The dimension for flux is $[\text{quantity}][\text{time}]^{-1}[area]^{-1}$. In this study, the particle flux [51] is considered and the rate of transfer of TAG particles through the basolateral membrane. The problem is defined in one-dimension and the unit of flux at $x = L$ (f_{TG}) can be defined as $[number\ of\ particles\ ][um]^{-1}[min]^{-1}$.

Therefore the accumulated flux in this study can focus on the how many TAG molecules pass through the membrane in a unit area. The accumulated flux per unit area can be defined as :

$$q = \int f_{TG}\, dt \tag{5.34}$$

q integrates flux over time and can be described as an accumulated flux per unit area for triglyceride concentration.

For the state of the basolateral membrane, it is assumed that the concentration of TAG has a flow out of the cell from $x = L$. It can be considered that the flux goes from regions of high concentration to regions of low concentration. In the finite difference method in Section 5.4, the spatial grid point defines the concentration for TAG at $x = L$ as C_M ($M = 41$ in this example).

The difference across the membrane needs to be considered by using a fictitious point C_{M+1}, then the flux per unit area is related to the concentration gradient in membrane and in a finite difference form it can be assumed as

$$f_{TG} = \frac{C_{M+1} - C_{M-1}}{2\Delta x} \tag{5.35}$$

$\mathrm{C_{M-1}}$ indicates a close neighbour point for the membrane and the fictitious point $\mathrm{C_{M+1}}$ represents the concentration of TAG outside the domain. The length between these two points is 2Δx in the finite difference method in this case. According to the definition for boundary condition and Equation (5.23) the flux per unit area can be defined as

$$f_{TG} = k_4 C_M \tag{5.36}$$

This is the flux. For the accumulated flux in Equation (5.23) , the time interval can be divided as $(0, \Delta t, 2\Delta t, \ldots n\Delta t)$ in the discretisation process and the integral for Equation (5.23) can be approximated as

$$q = \int f_{TG}\, dt = \sum_{i=1}^{n} \Delta t k_4 C_M(t_i) \tag{5.37}$$

The Equation (5.37) can be used to measure the level of accumulated flux for TAG passing the basolateral membrane for unit area in this study and the uncertainty for the outflow from the cell. In Equation (5.30) and (5.31), the randomness is added to the parameter for the inflow rate into the cell and the random number is assumed to have a normal distribution with mean value equal to 0. The accumulated flux can be computed without randomness for parameters k_2 and k_3. As in Section 5.5, the grid points in the finite difference method are defined as $\mathrm{n} = 4001$ and $\mathrm{M} = 41$. The accumulated flux with constant $\mathrm{k_2}$ and $\mathrm{k_3}$ is

$$q_c = 0.04129 \tag{5.38}$$

By considering the parameters with randomness in the parameters in the inflow gradient for MG and FA, the accumulated flux for TAG can be accumulated. Considering the simulation time $N = 8192$ in the Monte-Carlo method and that the maximum time is 10 minutes, there are samples of accumulated flux can be obtained and the sample size is 8192. The frequency of values in the sample can be computed by dividing intervals into different sections. For example, divide the x-axis with different parts with 0.001 interval size ($[0 \quad 0.001]$, $[0.001 \quad 0.002]$ $[0.002 \quad 0.003]$ ... $[q_{max} - 0.001 \quad q_{max}]$). The standard deviation of the sample is $2.7 * 10^{-6}$ and the frequency of the value of q in each interval can be computed and considered as a likelihood of distribution. The similar application can be found in [2].

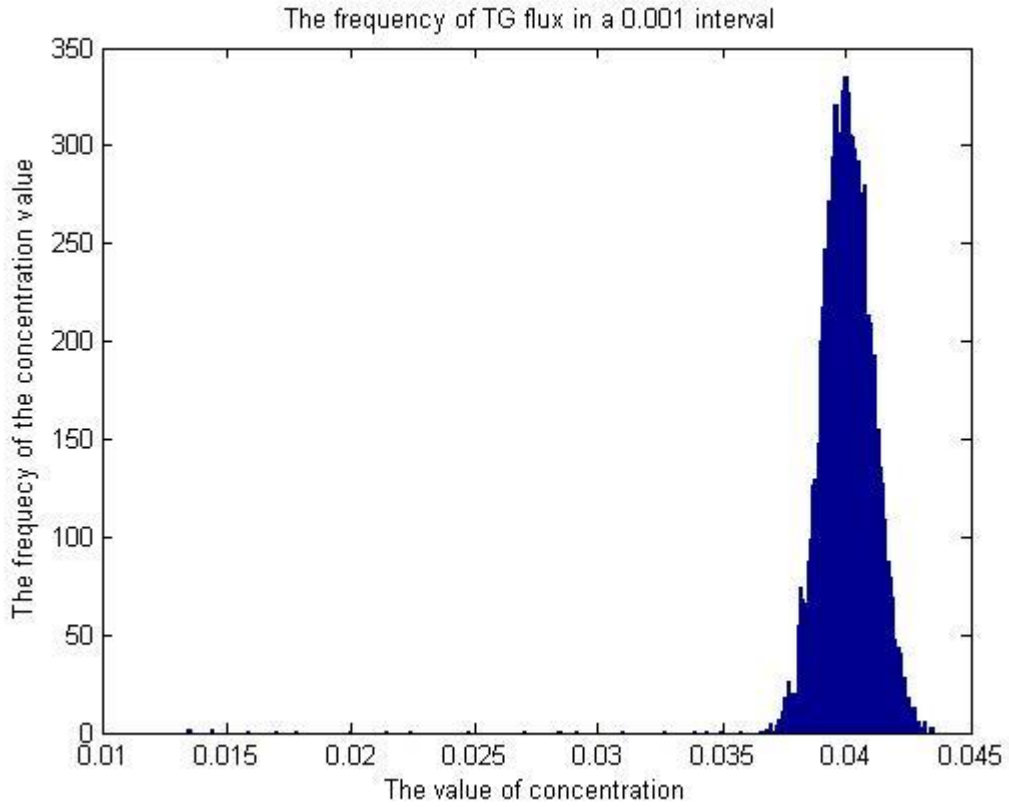

Figure 5.18 The frequency of the accumulated flux for TAG

The expect value for the accumulated flux per unit area in the Monte-Carlo method is 0.0413 mmol. The expect value is close to the result with constant parameters in Equation (5.38). As the

randomness in the parameter follows a normal distribution, if the output for uncertainty is reasonable, the probability distribution for output and input should have similar characteristics [2]. It is found from Figure 5.18 that the expect value for accumulated flux does not make a big difference for parameters without randomness. Also the likelihood distribution for accumulated flux is almost symmetric from the above figure. All these results indicate a good simulation for the output uncertainty for the mathematical model.

5.7. Summary

In this chapter, the lipid and fatty acids transport at the cellular level is described by using a reaction-diffusion system. The source term in the PDEs is introduced to encapsulate the esterification reaction inside the epithelial cell of the small intestine. This model is solved by finite difference method in the computational simulation to model the concentration inside the cell changing along with time. In Section 5.5 the missing information in the model and biological experiment is represented as uncertainty in the boundary condition. The Monte Carlo method is applied to obtain the samples of fatty acids concentration.

This reaction-diffusion model is used for substance transport inside the absorptive intestinal cell. This PDE system considers the effect of exterior influence of the blood vessel in the boundary condition. The uncertainty study provides a first attempt to describe the missing information in the cellular model.

Chapter 6 Conclusion

This chapter contains a summary of the research work of this thesis, along with some suggestions for future work.

6.1. Summary of the Work

This study focuses on the absorption and metabolism of triglyceride. Three models were built to represent the lipid digestion. The first model considers the absorption delay phenomenon in human digestive system. The transit compartments before the plasma compartment were assumed to handle the delay for transport of fatty acids. The inverse approach can provide the optimal parameter that indicates the transfer rate from delay compartment to plasma. This absorption delay can be coupled with the metabolism of fatty acids in the blood vessel. A modified model is built by considering the absorption and metabolism process for fatty acids. The parameters in the model are taken from literature or inverse approach.

This novel model extends a macroscopic compartment model to include the effect of metabolism and absorption for fatty acids kinetics. The modified system provides a description of fatty acids dynamics in the blood vessel, and has a better data fitting performance compared to the linear absorption model in the inverse problem. The absorption rate inside the body is accurately approximated in the model. The outcome of the parameter estimation provides a novel way of measuring the absorption rate for fatty acids.

The second model looks at the hydrolysis process of triglyceride in the absorption process. The hydrolysis is the reaction that the triglyceride releases fatty acid molecules before it is involved in metabolism in humans. Based on the chemical reaction among TAG, DG, MG and fatty acids, an ODE system was built for the dynamics of substances in this reaction. A set of in vitro data was used as the measurements in the inverse problem. With QPSO method in the inverse approach, the optimal parameters in the model were obtained and the different weights in the multi-objective optimisation were investigated in the computational analysis. With the parameters obtained in the inverse approach, the prediction from the numerical estimation indicates that the substances can remain in a stable state with a longer reaction time.

The contribution of the hydrolysis model includes a first attempt to propose a general form of compartment model describing the stepwise hydrolysis and esterification process for triglyceride. This novel compartment model contains all significant reactions amongst TAG, DG, MG and fatty acids, and a regulator term is defined in the ODE system handling the complex enzymatic reactions or model error. In a numerical exercise with a set of in vitro data, the modified model from general form is used in the inverse problem. The multi-objective optimisation problem is addressed by a constructive way of considering both the error function in inverse approach and the physiological understanding in the data.

The third model gives diffusion reaction system for the triglyceride transport at the cellular level. In the PDE system, the domain size, initial condition and boundary condition are defined based on the features of epithelial cells, and the 1-D problem is solved by the finite difference method. To illustrate the missing information in the model, the uncertainty was assumed in the boundary condition. The confidence interval of the substance concentration was computed with samples

obtained by Monte Carlo method. The computational work about the uncertainty can provide an estimated interval of substance concentration for biologists.

This model provides a first attempt to develop a microscopic system for fatty acids transport inside the epithelial cells of the small intestine. The concentrations of TAG, MG and fatty acids are studied and PDEs are used in the model. For the diffusion model at cellular level, a source term is defined in the PDE system as regulation in the model. The details of reaction inside the cell are described in the model by means of regulator in PDEs. In the numerical example, the missing information in the model and data is expressed as uncertainty in the boundary conditions. This uncertainty is based on full consideration of the cell structure, enzymatic reaction, pH value and so on. This novel idea of uncertainty is mathematically represented by randomness in the parameters of the model. The Monte Carlo method is used to calculate the possible substance concentration in the cell. These stochastic outcomes provide a prediction for lipids transport inside the cell.

6.2. The contribution of the work

The contributions of the work are listed below:

- A macroscopic metabolism compartment model for fatty acids concentration in the blood vessel was supplemented with absorption knowledge. The resulting ODE system combines the absorption and metabolism processes.

- A general form of compartment model for triglyceride hydrolysis and esterification was built. The concept of a regulator in the model is developed to include and describe the enzymatic reaction and missing information in the model.

- A reaction-diffusion model for the fatty acids transport at the cellular level was developed. The source term was used in the model as a regulation to any missing processes in physics.

- Numerical techniques of handling in vivo and in vitro data for the inverse problem were refined. The multi-objective optimisation problem was discussed in terms of the physiological knowledge in the chemical reaction.

- The missing information of cellular model was examined by using uncertainty in the boundary condition. “Stochastic outcome” of the model in terms of these uncertainty input was studied.

6.3. Suggestions for future work

There are some suggestions for the research in this thesis. For the compartment model in Chapter 3, the idea of considering absorption and metabolism process can be used for modelling other substances such as glucose or carbohydrate. More numerical techniques can be applied in the inverse problem along with absorption data. The general form of hydrolysis model in Chapter 4 provides a fundamental system for hydrolysis and esterification processes. Future work can be done to use the general form in different experimental data and reaction. The regulator in the model can be modified accordingly. Chapter 5 includes a concept to use reaction-diffusion system to model the substances transport in the absorptive cell. This concept can be extended for absorption of other nutrients in food at cellular level. The idea of defining uncertain coefficients in the model can be used to represent effects or noise due to missing information in the physical model. The uncertainty study for the epithelial cell can be developed to consider more factors that are not included in the model.

The above mentioned model can ultimately be coupled together to provide a coherent numerical model for absorption and metabolism through various organs into the cellular scale absorption model and eventually into the blood stream. The absorption and metabolism computational system can be built in this way and it would be an important in silico tool generating appropriate data to supplement and complement experimental data. It would also be possible to provide information on the design of laboratory experiments and the estimation of substance’s concentration in different organs in human body.

References

1. Ader, M., Bergman, R. N. (1990). Peripheral effects of insulin dominate suppression of fasting hepatic glucose production. *American Journal of Physiology-Endocrinology And Metabolism*, *258*(**6**), E1020-E1032.
2. Aguilar, Q., Allmaras, M., Bangerth, W., Tenorio, L., (2015) Statistics of parameters estimates: A concrete example, *SIAM Review,* 57(**1**), 131-149.
3. Ali, S., Leonard, S. A., Kukoly, C. A., James Metzger, W., Wooles, W. R., Mcginty J. F., Nyce, J. W. (2001). Absorption, distribution, metabolism, and excretion of a respirable antisense oligonucleotide for asthma. *American journal of respiratory and critical care medicine*, *163*(**4**), 989-993.
4. Auchmuty, J. F. G., Nicolis, G. (1976). Bifurcation analysis of reaction-diffusion equations—III. Chemical oscillations. *Bulletin of Mathematical Biology*, *38*(**4**), 325-350.
5. Avdeef, A. (2012). *Absorption and drug development: solubility, permeability, and charge state*. John Wiley Sons.
6. Avdeef, A., Bendels, S., Tsinman, O., Tsinman, K., Kansy, M. (2007). Solubility-excipient classification gradient maps. *Pharmaceutical research*,*24*(**3**), 530-545.
7. Azzalini, A., Capitanio, A. (1999). Statistical applications of the multivariate skew normal distribution. *Journal of the Royal Statistical Society: Series B (Statistical Methodology)*, *61*(**3**), 579-602.
8. Baier, L. J., Bogardus, C., Sacchettini, J. C. (1996). A polymorphism in the human intestinal fatty acid binding protein alters fatty acid transport across Caco-2 cells. *Journal of Biological Chemistry*, *271*(**18**), 10892-10896.

9. Baier, L. J., Bogardus, C., Sacchettini, J. C. (1996). A polymorphism in the human intestinal fatty acid binding protein alters fatty acid transport across Caco-2 cells. *Journal of Biological Chemistry*, *271*(**18**), 10892-10896.
10. Basu, R., Di Camillo, B., Toffolo, G., Basu, A., Shah, P., Vella, A., Cobelli, C. (2003). Use of a novel triple-tracer approach to assess postprandial glucose metabolism. *American Journal of Physiology-Endocrinology And Metabolism*, *284*(**1**), E55-E69.
11. Beers, R. F., & Sizer, I. W. (1952). A spectrophotometric method for measuring the breakdown of hydrogen peroxide by catalase. *Journal of biological chemistry*, *195*(**1**), 133-140.
12. Belfiore, F., Iannello, S., Volpicelli, G. (1998). Insulin sensitivity indices calculated from basal and OGTT-induced insulin, glucose, and FFA levels.*Molecular genetics and metabolism*, *63*(**2**), 134-141.
13. Benet, L. Z., Kroetz, D. L., Sheiner, L. B. (1996). Pharmacokinetics: the dynamics of drug absorption, distribution, metabolism, and elimination. *Goodman and Gilman's the pharmacological basis of therapeutics*, 3-27.
14. Berezovsky, F., Karev, G., Song, B., Castillo-Chavez, C. (2005). A simple epidemic model with surprising dynamics. *Mathematical biosciences and engineering*, *2*(**1**), 133-152.
15. Berger, A. H., Knudson, A. G., Pandolfi, P. P. (2011). A continuum model for tumour suppression. *Nature*, *476*(**7359**), 163-169.
16. Bergman, R. N., Phillips, L. S., & Cobelli, C. (1981). Physiologic evaluation of factors controlling glucose tolerance in man: measurement of insulin sensitivity and beta-cell glucose sensitivity from the response to intravenous glucose.*Journal of Clinical Investigation*, *68*(**6**), 1456.
17. Bergström, C. A., Luthman, K., Artursson, P. (2004). Accuracy of calculated pH-dependent aqueous drug solubility. *European journal of pharmaceutical sciences*, *22*(**5**), 387-398.
18. Berk, A., Zipursky, S. L. (2000). *Molecular cell biology* (**4**). New York: WH Freeman..
19. Bezerra, R. M., Dias, A. A. (2004). Discrimination among eight modified Michaelis-Menten kinetics models of cellulose hydrolysis with a large range of substrate/enzyme ratios. *Applied biochemistry and biotechnology*, *112*(**3**), 173-184.
20. Bhatia, R. B., Brinker, C. J., Gupta, A. K., Singh, A. K. (2000). Aqueous sol-gel process for protein encapsulation. *Chemistry of Materials*, *12*(**8**), 2434-2441.
21. Binnerts, A., Swart, G. R., Wilson, J. H., Hoogerbrugge, N., Pois, H. A., Birkenhager, J. C., Lamberts, S. W. (1992). The effect of growth hormone administration in growth hormone deficient adults on bone, protein, carbohydrate and lipid homeostasis, as well as on body composition. *Clinical endocrinology*, *37*(**1**), 79-87.
22. Boender, C. G. E., Kan, A. R., Timmer, G. T., Stougie, L. (1982). A stochastic method for global optimization. *Mathematical programming*, *22*(**1**), 125-140..
23. Boden, G., Chen, X. I. N. H. U. A., Ruiz, J., White, J. V., Rossetti, L. (1994). Mechanisms of fatty acid-induced inhibition of glucose uptake. *Journal of Clinical Investigation*, *93*(**6**), 2438.

24. Boston, R. C., Moate, P. J. (2008). NEFA minimal model parameters estimated from the oral glucose tolerance test and the meal tolerance test.*American Journal of Physiology-Regulatory, Integrative and Comparative Physiology*, *295*(**2**), R395-R403.
25. Boston, R. C., Roche, J. R., Ward, G. M., Moate, P. J. (2008). A novel minimal model to describe non-esterified fatty acid kinetics in Holstein dairy cows. *Journal of Dairy research*, *75*(**01**), 13-18.
26. Braseamble, D. L. (2007). The perilipin family of structural lípid droplet proteins: stabilization of lípid droplets and control of lipolysis. *Journal of Lipid Research*, ***48***, 2574-2559.
27. Brown, G. W., Cohen, P. P. (1959). Comparative biochemistry of urea synthesis I. Methods for the quantitative assay of urea cycle enzymes in liver.*Journal of Biological Chemistry*, *234*(**7**), 1769-1774.
28. Brown, N. A., Bron, A. J. (1987). An estimate of the human lens epithelial cell size in vivo. *Experimental eye research*, *44*(**6**), 899-906.
29. Bryan, K. (1969). A numerical method for the study of the circulation of the world ocean. *Journal of Computational Physics*, *4*(**3**), 347-376.
30. Bryant, N. J., Govers, R., James, D. E. (2002). Regulated transport of the glucose transporter GLUT4. *Nature reviews Molecular cell biology*, *3*(**4**), 267-277.
31. Butcher, J. C. (1987). *The numerical analysis of ordinary differential equations: Runge-Kutta and general linear methods*. Wiley-Interscience.
32. Carey, M. C., Small, D. M., & Bliss, C. M. (1983). Lipid digestion and absorption. *Annual Review of Physiology*, *45*(**1**), 651-677.
33. Chahinian, H., Nini, L., Boitard, E., Dubès, J. P., Comeau, L. C., Sarda, L. (2002). Distinction between esterases and lipases: a kinetic study with vinyl esters and TAG. *Lipids*, *37*(**7**), 653-662.
34. Charney, J. G., Fjörtoft, R., Von Neumann, J. (1950). Numerical integration of the barotropic vorticity equation. *Tellus*, *2*(**4**).
35. Chen, C. L., Tsai, H. W., Wong, S. S. (2010). Modeling the physiological glucose–insulin dynamic system on diabetics. *Journal of Theoretical Biology*, *265*(**3**), 314-322.
36. Chen, X., Guo, J. S. (2005). Existence and uniqueness of entire solutions for a reaction–diffusion equation. *Journal of Differential Equations*, *212*(**1**), 62-84.
37. Cheng, H., Leblond, C. P. (1974). Origin, differentiation and renewal of the four main epithelial cell types in the mouse small intestine V. Unitarian theory of the origin of the four epithelial cell types. *American Journal of Anatomy*, *141*(**4**), 537-561.
38. Chew, Y. H., Chua, L. S., Cheng, K. K., Sarmidi, M. R., Aziz, R. A., Lee, C. T. (2008). Kinetic study on the hydrolysis of palm olein using immobilized lipase. *Biochemical Engineering Journal*, *39*(**3**), 516-520.
39. Clapper, J. R., Duranti, A., Tontini, A., Mor, M., Tarzia, G., Piomelli, D. (2006). The fatty-acid amide hydrolase inhibitor URB597 does not affect triacylglycerol hydrolysis in rat tissues. *Pharmacological research*, *54*(**5**), 341-344.

40. Clerc, M., Kennedy, J. (2002). The particle swarm-explosion, stability, and convergence in a multidimensional complex space. *Evolutionary Computation, IEEE Transactions on*, *6*(**1**), 58-73.
41. Clifford, M. N. (2000). Chlorogenic acids and other cinnamates–nature, occurrence, dietary burden, absorption and metabolism. *Journal of the Science of Food and Agriculture*, *80*(**7**), 1033-1043.
42. Compeau, D. R., Higgins, C. A. (1995). Computer self-efficacy: Development of a measure and initial test. *MIS quarterly*, 189-211.
43. Cook, S. I., Sellin, J. H. (1998). Review article: short chain fatty acids in health and disease. *Alimentary Pharmacology and Therapeutics*, *12*(**6**), 499-507.
44. Cox, P. J., Ryan, D. A., Hollis, F. J., Harris, A. M., Miller, A. K., Vousden, M., Cowley, H. (2000). Absorption, disposition, and metabolism of rosiglitazone, a potent thiazolidinedione insulin sensitizer, in humans. *Drug Metabolism and Disposition*, *28*(**7**), 772-780.
45. Culler, D. E., Singh, J. P., Gupta, A. (1999). *Parallel computer architecture: a hardware/software approach*. Gulf Professional Publishing.
46. Dai, H. B., Liang, Y., Ma, L. P., Wang, P. (2008). New insights into catalytic hydrolysis kinetics of sodium borohydride from Michaelis− Menten model. *The Journal of Physical Chemistry C*, *112*(**40**), 15886-15892.
47. Dalla Man, C., Raimondo, D. M., Rizza, R. A., Cobelli, C. (2007). GIM, simulation software of meal glucose—insulin model. *Journal of diabetes science and technology*, *1*(**3**), 323-330.
48. Dalton, A. J., Kahler, H., Lloyd, B. J. (1951). The structure of the free surface of a series of epithelial cell types in the mouse as revealed by the electron microscope. *The Anatomical Record*, *111*(**1**), 67-77.
49. Davenport, H. W. (1982). *Physiology of the digestive tract*. Year book medical publishers.
50. Dette, H., Biedermann, S. (2003). Robust and efficient designs for the Michaelis–Menten model. *Journal of the American Statistical Association*, *98*(**463**), 679-686.
51. Deventer. J. M., Held . A., Madany. S. T., Klemm. O., (2015). Sized-resolved eddy covariance fluxes of nucleation ot accumulation mode aerosol particles over a coniferous forest. *Agricultural and Forest Meteorology*. 214-215, 328-340.
52. Dokoumetzidis, A., Papadopoulou, V., Macheras, P. (2006). Analysis of dissolution data using modified versions of Noyes–Whitney equation and the Weibull function. *Pharmaceutical research*, *23*(**2**), 256-261.
53. Dybkov, V. I. (2010). *Reaction diffusion and solid state chemical kinetics*. Trans Tech Publ.
54. Dyer, J., Merediz, E., Salmon, K. S. H., Proudman, C. J., Edwards, G. B., Shirazi-Beechey, S. P. (2002). Molecular characterisation of carbohydrate digestion and absorption in equine small intestine. *Equine veterinary journal*, *34*(**4**), 349-358.
55. Eberhart, R. C., Kennedy, J. (1995). A new optimizer using particle swarm theory, Proceedings of the Sixth International Symposium on Micro Machine and Human Science.

56. Engl, H. W., Hanke, M., Neubauer, A. (1996). *Regularization of inverse problems*, 375. Springer Science and Business Media.
57. Esau, C., Davis, S., Murray, S. F., Yu, X. X., Pandey, S. K., Pear, M., Monia, B. P. (2006). miR-122 regulation of lipid metabolism revealed by in vivo antisense targeting. *Cell metabolism*, *3*(**2**), 87-98.
58. Eurell, J. A., Frappier, B. L. (2013). *Dellmann's textbook of veterinary histology*. John Wiley and Sons.
59. Ewens, W. J., Grant, G. R. (2006). *Statistical methods in bioinformatics: an introduction*. Springer Science and Business Media.
60. Filbet, F., Laurençot, P., Perthame, B. (2005). Derivation of hyperbolic models for chemosensitive movement. *Journal of Mathematical Biology*, *50*(**2**), 189-207.
61. Feher, G., Kip, A. F. (1955). Electron spin resonance absorption in metals. I. Experimental. *Physical Review*, *98*(**2**), 337.
62. Ferrannini, E., Camastra, S., Coppack, S. W., Fliser, D., Golay, A., Mitrakou, A. (1997). Insulin action and non-esterified fatty acids. *Proceedings of the Nutrition Society*, *56*(**02**), 753-761.
63. Ferreira Jr, S. C., Martins, M. L., Vilela, M. J. (2002). Reaction-diffusion model for the growth of avascular tumor. *Physical Review*, *65*(**2**).
64. Fisher, R. A. (1937). The wave of advance of advantageous genes. *Annals of Eugenics*, *7*(**4**), 355-369.
65. Floege, J., Alpers, C. E., Burns, M. W., Pritzl, P., Gordon, K., Couser, W. G., Johnson, R. J. (1992). Glomerular cells, extracellular matrix accumulation, and the development of glomerulosclerosis in the remnant kidney model.*Laboratory investigation; a journal of technical methods and pathology*, *66*(**4**), 485-497.
66. Flyvbjerg, H., Jobs, E., Leibler, S. (1996). Kinetics of self-assembling microtubules: an" inverse problem" in biochemistry. *Proceedings of the National Academy of Sciences*, *93*(**12**), 5975-5979.
67. Frayn, K. N. (1998). Non-esterified fatty acid metabolism and postprandial lipaemia. *Atherosclerosis*, ***141***, S41-S46.
68. Frayn, K. N. (1998). Regulation of fatty acid delivery in vivo. In *Skeletal Muscle Metabolism in Exercise and Diabetes* (171-179). Springer US.
69. Ganong, W. F., Barrett, K. E. (2005). *Review of medical physiology* (**21**). New York New York: McGraw-Hill Medical.
70. Garland, M., Le Grand, S., Nickolls, J., Anderson, J., Hardwick, J., Morton, S, Volkov, V. (2008). Parallel computing experiences with CUDA. *IEEE micro*, (**4**), 13-27.
71. Gatenby, R. A., Gawlinski, E. T. (1996). A reaction-diffusion model of cancer invasion. *Cancer research*, *56*(**24**), 5745-5753.

72. Gelman, A., Bios, F., Jiang, J. (1996). Physiological pharmacokinetic analysis using polulation modelling and informative prior distributions. *Journal of the American Statistical Association*, 91(**436**), 1400-1412.
73. Gentleman, R. C., Carey, V. J., Bates, D. M., Bolstad, B., Dettling, M., Dudoit, S., Zhang, J. (2004). Bioconductor: open software development for computational biology and bioinformatics. *Genome biology*, *5*(**10**), R80.
74. Gerlowski , L. E ., Jain, R. K., (2010) Physiologically based pharmacokinetic modelling : Princiles and applications, 72(**10**), 1103-1127.
75. Goldbeter, A. (2013). Oscillatory enzyme reactions and Michaelis-Menten kinetics. *Federation of European Biochemical Societies letter*, 587(**17**) , 2778-2784.
76. Graham, R. (1996). Systematic derivation of a rotationally covariant extension of the two-dimensional newell-whitehead-segel equation. *Physical review letters*, *76*(**12**), 2185.
77. Guo, P., Weinstein, A. M., Weinbaum, S. (2000). A hydrodynamic mechanosensory hypothesis for brush border microvilli. *American Journal of Physiology-Renal Physiology*, *279*(**4**), 698-712.
78. Gupta, A. R., Venkataramani, B. (1988). Sorption of uranyl ions on hydrous oxides. A new surface hydrolysis model. *Bulletin of the Chemical Society of Japan*, *61*(**4**), 1357-1362.
79. Gusfield, D. (1997). *Algorithms on strings, trees and sequences: computer science and computational biology*. Cambridge university press.
80. Hall, M., Frank, E., Holmes, G., Pfahringer, B., Reutemann, P., Witten, I. H. (2009). The WEKA data mining software: an update. ACM SIGKDD Explor Newslett; **11**: 10–8.
81. Hauser, H., Dyer, J. H., Nandy, A., Vega, M. A., Werder, M., Bieliauskaite, E, Phillips, M. C. (1998). Identification of a receptor mediating absorption of dietary cholesterol in the intestine. *Biochemistry*, *37*(**51**), 17843-17850.
82. Hay, E. D. (Ed.). (2013). *Cell biology of extracellular matrix*. Springer Science and Business Media.
83. Hennessy, J. L., Patterson, D. A. (2011). *Computer architecture: a quantitative approach*. Elsevier.
84. Holland, J. H. (1962). Outline for a logical theory of adaptive systems. *Journal of the ACM (JACM)*, *9*(**3**), 297-314.
85. Hopfer, U., Nelson, K., Perrotto, J., Isselbacher, K. J. (1973). Glucose transport in isolated brush border membrane from rat small intestine. *Journal of Biological Chemistry*, *248*(**1**), 25-32.
86. Howard, B. V., Klimes, I., Vasquez, B., Brady, D., Nagulesparan, M., Unger, R. H. (1984). The Antilipolytic Action of Insulin in Obese Subjects with Resistance to Its Glucoregulatory Action. *The Journal of Clinical Endocrinology and Metabolism*, *58*(**3**), 544-548.
87. Huang, Y., Wang, S. (2008). Multilevel thresholding methods for image segmentation with Otsu based on QPSO. In *Image and Signal Processing, 2008. CISP'08. Congress on* (**3**.701-705).
88. Hubbard, M. E., Byrne, H. M. (2013). Multiphase modelling of vascular tumour growth in two spatial dimensions. *Journal of theoretical biology*, ***316***, 70-89.

89. James, A. T. (1960). Qualitative and quantitative determination of the fatty acids by gas-Liquid Chromatography. *Methods of Biochemical Analysis, **8***, 1-59.
90. Jenkins, D. J., Kendall, C. W., Axelsen, M., Augustin, L. S., Vuksan, V. (2000). Viscous and nonviscous fibres, nonabsorbable and low glycaemic index carbohydrates, blood lipids and coronary heart disease. *Current opinion in lipidology*, *11*(**1**), 49-56.
91. Jenkins, T. C. (1993). Lipid metabolism in the rumen. *Journal of dairy science*,*76*(**12**), 3851-3863.
92. Jurs, P. C., Bakken, G. A., McClelland, H. E. (2000). Computational methods for the analysis of chemical sensor array data from volatile analytes.*Chemical Reviews*, *100*(**7**), 2649-2678.
93. Koga, K., Osuga, Y., Yano, T., Momoeda, M., Yoshino, O., Hirota, Y., Taketani, Y. (2003). Characteristic images of deeply infiltrating rectosigmoid endometriosis on transvaginal and transrectal ultrasonography. *Human Reproduction*, *18*(**6**), 1328-1333.
94. Kawano, Y., Kiyoyama, S., Shiomori, K., Baba, Y., Hano, T. (1994). Hydrolysis of olive oil with lipase in a “VibroMixer”. *Journal of fermentation and bioengineering*, *78*(**4**), 293-297.
95. Keating, K. A., Quinn, J. F. (1998). Estimating species richness: the Michaelis-Menten model revisited. Oikos, 411-416.
96. Kibangou, Ida B., Saïd Bouhallab, Gwénaële Henry, François Bureau, Stéphane Allouche, Anne Blais, Patricia Guérin, Pierre Arhan, and Dominique L. Bouglé. (2005). Milk proteins and iron absorption: contrasting effects of different caseinophosphopeptides. *Pediatric research* 58(**4**), 731-734.
97. Kleywegt, A. J., Shapiro, A., & Homem-de-Mello, T. (2002). The sample average approximation method for stochastic discrete optimization. S*IAM Journal on Optimization*, 12(**2**), 479-502.
98. Klopman, G., Stefan, L. R., Saiakhov, R. D. (2002). ADME evaluation: 2. A computer model for the prediction of intestinal absorption in humans. *European journal of pharmaceutical sciences*, 17(**4**), 253-263.
99. Klotz, I. M. (1946). The application of the law of mass action to binding by proteins; interactions with calcium. *Archives of biochemistry*, **9**, 109-117.
100. Kolodny, R., Guibas, L., Levitt, M., Koehl, P. (2005). Inverse kinematics in biology: the protein loop closure problem. *The International Journal of Robotics Research*, **24**, 151-163.
101. Krebs, M., Stingl, H., Nowotny, P., Weghuber, D., Bischof, M., Waldhäusl, W., Roden, M. (2000). Prevention of in vitro lipolysis by tetrahydrolipstatin. *Clinical Chemistry*, 46(**7**), 950-954.
102. Kuczera, G., Parent, E. (1998). Monte Carlo assessment of parameter uncertainty in conceptual catchment models: the Metropolis algorithm. *Journal of Hydrology*, 211(**1**), 69-85.
103. Kumar, D., Murthy, G. S. (2013). Stochastic molecular model of enzymatic hydrolysis of cellulose for ethanol production. *Biotechnology for biofuels*, 6(**1**), 1-20.
104. Lanczos, C. (1950). An iteration method for the solution of the eigenvalue problem of linear differential and integral operators. United States Governm. Press Office.

105. Lehmann, E. D., Deutsch, T. (1992). A physiological model of glucose-insulin interaction in type 1 diabetes mellitus. *Journal of Biomedical Engineering*, 14(**3**), 235-242.
106. Lenne, P. F., Wawrezinieck, L., Conchonaud, F., Wurtz, O., Boned, A., Guo, X. J., Marguet, D. (2006). Dynamic molecular confinement in the plasma membrane by microdomains and the cytoskeleton meshwork. *The EMBO journal*, 25(**14**), 3245-3256.
107. Li, J., Kuang, Y. (2007). Analysis of a model of the glucose-insulin regulatory system with two delays. *SIAM Journal on Applied Mathematics*, 67(**3**), 757-776.
108. Lindblom, G., Johansson, L. B., Arvidson, G. (1981). Effect of cholesterol in membranes. Pulsed nuclear magnetic resonance measurements of lipid lateral diffusion. *Biochemistry*, 20(**8**), 2204-2207.
109. Lipinski, B., Herzog, H., Kops, E. R., Oberschelp, W., Müller-Gärtner, H. W. (1997). Expectation maximization reconstruction of positron emission tomography images using anatomical magnetic resonance information. Medical Imaging, *IEEE Transactions on*, 16(**2**), 129-136.
110. Liu, L., Sun, J., Zhang, D., Du, G., Chen, J., Xu, W. (2009). Culture conditions optimization of hyaluronic acid production by Streptococcus zooepidemicus based on radial basis function neural network and quantum-behaved particle swarm optimization algorithm. *Enzyme and Microbial Technology*, 44(**1**), 24-32.
111. Longuet-Higgins, M. S., Cokelet, E. D. (1976). The deformation of steep surface waves on water. I. A numerical method of computation. In Proceedings of the Royal Society of London A: Mathematical, *Physical and Engineering Sciences* **, 350**. The Royal Society.
112. Lowe, M. E. (1997). Structure and function of pancreatic lipase and colipase. *Annual Review of Nutrition*, 17(**1**), 141-158.
113. Lu, H. P., Xun, L., Xie, X. S. (1998). Single-molecule enzymatic dynamics. *Science*, 282(**5395**), 1877-1882.
114. Luquet, S., Gaudel, C., Holst, D., Lopez-Soriano, J., Jehl-Pietri, C., Fredenrich, A., Grimaldi, P. A. (2005). Roles of PPAR delta in lipid absorption and metabolism: a new target for the treatment of type 2 diabetes. *Biochimica et Biophysica Acta (BBA)-Molecular Basis of Disease*, 1740(**2**), 313-317.
115. Makroglou, A., Li, J., Kuang, Y. (2006). Mathematical models and software tools for the glucose-insulin regulatory system and diabetes: an overview. *Applied Numerical Mathematics*, 56(**3**), 559-573.
116. Malmberg, K., Rydén, L., Efendic, S., Herlitz, J., Nicol, P., Waldenstrom, A., Welin, L. (1995). Randomized trial of insulin-glucose infusion followed by subcutaneous insulin treatment in diabetic patients with acute myocardial infarction (DIGAMI study): effects on mortality at 1 year. *Journal of the American College of Cardiology*, 26(**1**), 57-65.

117. Man, C. D., Rizza, R., Cobelli, C. (2007). Meal simulation model of the glucose-insulin system. Biomedical Engineering, *IEEE Transactions on*, 54(**10**), 1740-1749.
118. Manitz, R., Lucht, W., Strehmel, K., Weiner, R., Neubert, R. (1998). On mathematical modeling of dermal and transdermal drug delivery. *Journal of Pharmaceutical Sciences*, 87(**7**), 873-879.
119. Marchesini, G., Brizi, M., Bianchi, G., Tomassetti, S., Bugianesi, E., Lenzi, M., Melchionda, N. (2001). Nonalcoholic fatty liver disease a feature of the metabolic syndrome. *Diabetes*, 50(**8**), 1844-1850.
120. McArthur, M. J., Atshaves, B. P., Frolov, A., Foxworth, W. D., Kier, A. B., Schroeder, F. (1999). Cellular uptake and intracellular trafficking of long chain fatty acids. *Journal of lipid research*, 40(**8**), 1371-1383.
121. Michaelis, L., Menten, M. L. (1913). Die kinetik der invertinwirkung. *Biochem*, **49**, 352.
122. Miki, T., Lehmann, T., Cai, H., Stolz, D. B., Strom, S. C. (2005). Stem cell characteristics of amniotic epithelial cells. *Stem Cells*, 23(**10**), 1549-1559.
123. Minami, E., Saka, S. (2006). Kinetics of hydrolysis and methyl esterification for biodiesel production in two-step supercritical methanol process. *Fuel*, 85(**17**), 2479-2483.
124. Morbiducci, U., Di Benedetto, G., Kautzky-Willer, A., Deriu, M. A., Pacini, G., Tura, A. (2011). Identification of a model of non-esterified fatty acids dynamics through genetic algorithms: The case of women with a history of gestational diabetes. *Computers in Biology and Medicine*, 41(**3**), 146-153.
125. Morton, N. M., Emilsson, V., Liu, Y. L., Cawthorne, M. A. (1998). Leptin action in intestinal cells. *Journal of Biological Chemistry,* 273(**40**), 26194-26201.
126. Murota, K., Terao, J. (2003). Antioxidative flavonoid quercetin: implication of its intestinal absorption and metabolism. *Archives of Biochemistry and Biophysics*, 417(**1**), 12-17.
127. Mythili, A., Srinivasan, S., Sujatha, C. M., Kavitha, G., Ramakrishnan, S. (2014). Analysis of restrictive pulmonary function abnormality using spirometric investigations and QPSO feature selection. *International Journal of Biomedical Engineering and Technology*, 16(**3**), 195-208.
128. Neyman, J. (1937). Outline of a theory of statistical estimation based on the classical theory of probability. Philosophical Transactions of the Royal Society of London. Series A, *Mathematical and Physical Sciences*, 236(**767**), 333-380.
129. Nguyen, V. K., Hernandez-Vargas, E. A. (2015). Identifiability challenges in mathematical models of viral infectious diseases. *Ifac Papersonline*, 48(**28**), 257-262.
130. Nilsson-Ehle, P., Egelrud, T., Belfrage, P., Olivecrona, T., Borgström, B. (1973). Positional specificity of purified milk lipoprotein lipase. *Journal of Biological Chemistry*, 248(**19**), 6734-6737.

131. Omkar, S. N., Khandelwal, R., Ananth, T. V. S., Naik, G. N., Gopalakrishnan, S. (2009). Quantum behaved Particle Swarm Optimization (QPSO) for multi-objective design optimization of composite structures. *Expert Systems with Applications*, 36(**8**), 11312-11322.
132. Orhon, D., Çokgör, E. U., Sözen, S. (1999). Experimental basis for the hydrolysis of slowly biodegradable substrate in different wastewaters. *Water science and technology*, 39(**1**), 87-95.
133. Othmer, H. G., Dunbar, S. R., Alt, W. (1988). Models of dispersal in biological systems. *Journal of Mathematical Biology*, 26(**3**), 263-298.
134. Pace, C. N., Vajdos, F., Fee, L., Grimsley, G., Gray, T. (1995). How to measure and predict the molar absorption coefficient of a protein. *Protein science: a publication of the Protein Society*, 4(**11**), 2411.
135. Paolisso, G., Tataranni, P. A., Foley, J. E., Bogardus, C., Howard, B. V., Ravussin, E. (1995). A high concentration of fasting plasma non-esterified fatty acids is a risk factor for the development of NIDDM. *Diabetologia*, 38(**10**), 1213-1217.
136. Parker, R. S., Doyle, F. J., Ward, J. H., Peppas, N. A. (2000). Robust H~ Glucose Control in Diabetes Using a Physiological Model. *AICHE Journal*,46(**12**), 2537-2549..
137. Patel, J. K., Read, C. B. (1996). Handbook of the normal distribution (**150**). CRC Press.
138. Pavan, A., Thomaseth, K., Valerio, A. (2003). Modeling population kinetics of free fatty acids in isolated rat hepatocytes using Markov Chain Monte Carlo. *Annals of Biomedical Engineering*, 31(**7**), 854-866.
139. Pedersen, S. (1981). Delay in the absorption rate of theophylline from a sustained release theophylline preparation caused by food. *British Journal of Clinical Pharmacology*, 12(**6**), 904.
140. Pittler, M. H., Ernst, E. (2004). Dietary supplements for body-weight reduction: a systematic review. *The American Journal of Clinical Nutrition*, 79(**4**), 529-536.
141. Polidori, D., Sha, S., Mudaliar, S., Ciaraldi, T. P., Ghosh, A., Vaccaro, N., Henry, R. R. (2013). Canagliflozin lowers postprandial glucose and insulin by delaying intestinal glucose absorption in addition to increasing urinary glucose excretion results of a randomized, placebo-controlled study. *Diabetes Care*,36(**8**), 2154-2161.
142. Powell, M. J. (1977). Restart procedures for the conjugate gradient method. *Mathematical Programming*, 12(**1**), 241-254.
143. Pratt, A. C., Wattis, A. D., Salter, A.M. (2015). Mathematical modelling of hepatic lipid metabolism, *Mathematical Bioscienecs*, 262, 167-181.
144. Pritchard, J. K., Stephens, M., Donnelly, P. (2000). Inference of population structure using multilocus genotype data. *Genetics*, 155(**2**), 945-959.

145. Quaglino Jr, D., Nanney, L. B., Ditesheim, J. A., Davidson, J. M. (1991). Transforming growth factor-beta stimulates wound healing and modulates extracellular matrix gene expression in pig skin: incisional wound model. *The Journal of Investigative Dermatology*, 97(**1**), 34-42.

146. Quettier, A. L., Eastmond, P. J. (2009). Storage oil hydrolysis during early seedling growth. *Plant Physiology and Biochemistry*, 47(**6**), 485-490.

147. Raben, A., Agerholm-Larsen, L., Flint, A., Holst, J. J., Astrup, A. (2003). Meals with similar energy densities but rich in protein, fat, carbohydrate, or alcohol have different effects on energy expenditure and substrate metabolism but not on appetite and energy intake. *The American Journal of Clinical Nutrition*,77(**1**), 91-100.

148. *Ramachandran, M*., *Tsokos, C. (2015). Mathematical statistics with application in R.*

149. Randle, P., Newsholme, E. A., Garland, P. B. (1964). Regulation of glucose uptake by muscle. 8. Effects of fatty acids, ketone bodies and pyruvate, and of alloxan-diabetes and starvation, on the uptake and metabolic fate of glucose in rat heart and diaphragm muscles. *Biochemical Journal*, 93(**3**), 652.

150. Randle, P. J., Garland, P. B., Hales, C. N., Newsholme, E. A. (1963). The glucose fatty-acid cycle its role in insulin sensitivity and the metabolic disturbances of diabetes mellitus. *The Lancet*, 281(**7285**), 785-789.

151. Renardy, M., Rogers, R. C. (2006). An introduction to partial differential equations (**13**). Springer Science and Business Media.

152. Reya, T., Morrison, S. J., Clarke, M. F., Weissman, I. L. (2001). Stem cells, cancer, and cancer stem cells. *Nature*, 414(**6859**), 105-111.

153. Rice, J. R. (2014). Numerical Methods in Software and Analysis. Elsevier.

154. Rice, W. R. (1989). Analyzing tables of statistical tests. *Evolution*, 223-225.

155. Roussel, C. J., Roussel, M. R. (2004). Reaction–diffusion models of development with state-dependent chemical diffusion coefficients. *Progress in Biophysics and Molecular Biology*, *86*(**1**), 113-160.

156. Rowland, M., Tozer, T. N. (1995). Concepts and applications. *Clinical Pharmacokinetics*, 3.

157. Roy, A. (2008). Dynamic modeling of free fatty acid, glucose, and insulin during rest and exercise in insulin dependent diabetes mellitus patients. *ProQuest*.

158. Roy, A., Parker, R. S. (2006). Dynamic modeling of free fatty acid, glucose, and insulin: An extended" minimal model. *Diabetes Technology and Therapeutics*, 8(**6**), 617-626.

159. Saaty, T. L. (2004). Mathematical methods of operations research. Courier Corporation.

160. Sarcina, M., Murata, N., Tobin, M. J., Mullineaux, C. W. (2003). Lipid diffusion in the thylakoid membranes of the cyanobacterium Synechococcus sp.: effect of fatty acid desaturation. *FEBS Letters*, 553(**3**), 295-298.
161. Savic, R. M., Jonker, D. M., Kerbusch, T., Karlsson, M. O. (2007). Implementation of a transit compartment model for describing drug absorption in pharmacokinetic studies. *Journal of Pharmacokinetics and Pharmacodynamics*, 34(**5**), 711-726.
162. Scalbert, A., Morand, C., Manach, C., Rémésy, C. (2002). Absorption and metabolism of polyphenols in the gut and impact on health. *Biomedicine and Pharmacotherapy*, 56(**6**), 276-282.
163. Schlenk, H., Gellerman, J. L. (1960). Esterification of fatty acids with diazomethane on a small scale. *Analytical Chemistry*, 32(**11**), 1412-1414.
164. Schuchardt, U., Sercheli, R., Vargas, R. M. (1998). Transesterification of vegetable oils: a review. *Journal of the Brazilian Chemical Society*, 9(**3**), 199-210.
165. Scow, R. O., Hamosh, M., Blanchette-Mackie, E. J., Evans, A. J. (1972). Uptake of blood triglyceride by various tissues. *Lipids*, 7(**8**), 497-505.
166. Seppälä-Lindroos, A., Vehkavaara, S., Häkkinen, A. M., Goto, T., Westerbacka, J., Sovijärvi, A., Yki-Järvinen, H. (2002). Fat accumulation in the liver is associated with defects in insulin suppression of glucose production and serum free fatty acids independent of obesity in normal men. *The Journal of Clinical Endocrinology and Metabolism*, 87(**7**), 3023-3028.
167. Sethi, T., Rintoul, R. C., Moore, S. M., MacKinnon, A. C., Salter, D., Choo, C, Haslett, C. (1999). Extracellular matrix proteins protect small cell lung cancer cells against apoptosis: a mechanism for small cell lung cancer growth and drug resistance in vivo. *Nature medicine*, 5(**6**), 662-668.
168. Shahidi, F., Kamil, Y. J. (2001). Enzymes from fish and aquatic invertebrates and their application in the food industry. *Trends in Food Science and Technology*, 12(**12**), 435-464.
169. Sheiner, L. B., Beal, S. L. (1980). Evaluation of methods for estimating population pharmacokinetic parameters. I. Michaelis-Menten model: routine clinical pharmacokinetic data. *Journal of Pharmacokinetics and Biopharmaceutics*, 8(**6**), 553-571.
170. Shiomori, K., Hayashi, T., Baba, Y., Kawano, Y., Hano, T. (1995). Hydrolysis rates of olive oil by lipase in a monodispersed OW emulsion system using membrane emulsification. *Journal of fermentation and bioengineering*, 80(**6**), 552-558.
171. Simoni, G., Brambati, B., Danesino, C., Rossella, F., Terzoli, G. L., Ferrari, M., Fraccaro, M. (1983). Efficient direct chromosome analyses and enzyme determinations from chorionic villi samples in the first trimester of pregnancy. *Human Genetics*, 63(**4**), 349-357.
172. Skrzypek, T., Piedra, J. V., Skrzypek, H., Kazimierczak, W., Szymańczyk, S., Pawłowska, M., Zabielski, R. (2007). Intestinal villi structure during the development of pig and wild boar crossbreed neonates. *Livestock Science*,109(**1**), 38-41.

173. Sopher, A. B., Thornton, J. C., Wang, J., Pierson, R. N., Heymsfield, S. B., Horlick, M. (2004). Measurement of percentage of body fat in 411 children and adolescents: a comparison of dual-energy X-ray absorptiometry with a four-compartment model. *Pediatrics*, 113(**5**), 1285-1290.
174. Srinivasan, R., Kadish, A. H., Sridhar, R. (1970). A mathematical model for the control mechanism of free fatty acid-glucose metabolism in normal humans. *Computers and Biomedical Research*, 3(**2**), 146-165.
175. Stein, G. (2012). Molecular and cellular approaches to the control of proliferation and differentiation. Academic Press.
176. Steinke, J. M., Shepherd, A. P. (1988). Diffusion model of the optical absorbance of whole blood. *JOSA A*, 5(**6**), 813-822.
177. Staden, R. (1982). Automation of the computer handling of gel reading data produced by the shotgun method of DNA sequencing. *Nucleic Acids Research*,10(**15**), 4731-4751.
178. Su, Y., Wei, J., Shi, J. (2009). Hopf bifurcations in a reaction–diffusion population model with delay effect. *Journal of Differential Equations*, 247(**4**), 1156-1184.
179. Summers, L. K., Fielding, B. A., Herd, S. L., Ilic, V., Clark, M. L., Quinlan, P. T., Frayn, K. N. (1999). Use of structured triacylglycerols containing predominantly stearic and oleic acids to probe early events in metabolic processing of dietary fat. *Journal of Lipid Research*, 40(**10**), 1890-1898.
180. Sun, J., Lai, C. H., Xu, W., Chai, Z. (2007). A novel and more efficient search strategy of quantum-behaved particle swarm optimization. In Adaptive and natural computing algorithms , 394-403. Springer Berlin Heidelberg.
181. Sun, J., Xu, W., Fang, W. (2006). Solving multi-period financial planning problem via quantum-behaved particle swarm algorithm. *Computational Intelligence***,**1158-1169. Springer Berlin Heidelberg.
182. Sweadner, K. J., Goldin, S. M. (1980). Active transport of sodium and potassium ions. Mechanism, function and regulation. *New England Journal of Medicine*, 302(**14**), 777-783.
183. Tanigaki, M., Sakata, M., Takaya, H., Mimura, K. (1995). Hydrolysis of palm stearin oil by a thermostable lipase in a draft tube-type reactor. *Journal of Fermentation and Bioengineering*, 80(**4**), 340-345.
184. Tarantola, A. (2005). Inverse problem theory and methods for model parameter estimation. SIAM
185. Taylor, V., Welcher, A. A., Suter, U. (1995). Epithelial membrane protein-1, peripheral myelin protein 22, and lens membrane protein 20 define a novel gene family. *Journal of Biological Chemistry*, 270(**48**), 28824-28833.

186. Teusink, B., Diderich, J. A., Westerhoff, H. V., Van Dam, K., Walsh, M. C. (1998). Intracellular glucose concentration in derepressed yeast cells consuming glucose is high enough to reduce the glucose transport rate by 50%. *Journal of Bacteriology*, 180(**3**), 556-562.

187. Thiébaud, D., DeFronzo, R. A., Jacot, E., Golay, A., Acheson, K., Maeder, E., Felber, J. P. (1982). Effect of long chain triglyceride infusion on glucose metabolism in man. *Metabolism*, 31(**11**), 1128-1136.

188. Tian, N., Lai, C. H. (2014). Parallel quantum-behaved particle swarm optimization. *International Journal of Machine Learning and Cybernetics*, 5(**2**), 309-318.

189. Tian, N., Sun, J., Xu, W., Lai, C. H. (2011). Estimation of unknown heat source function in inverse heat conduction problems using quantum-behaved particle swarm optimization. *International Journal of Heat and Mass Transfer*, 54(**17**), 4110-4116.

190. Tojo, K., Chiang, C. C., Chien, Y. W. (1987). Drug permeation across the skin: effect of penetrant hydrophilicity. *Journal of Pharmaceutical Sciences*, 76(**2**), 123-126.

191. Tolić, I. M., Mosekilde, E., Sturis, J. (2000). Modeling the insulin–glucose feedback system: the significance of pulsatile insulin secretion. *Journal of Theoretical Biology*, 207(**3**), 361-375.

192. Tsai, S. W., Wu, G. H., Chiang, C. L. (1991). Kinetics of enzymatic hydrolysis of olive oil in biphasic organic‐aqueous systems. *Biotechnology and Bioengineering*, 38(**7**), 761-766.

193. Tsoukias, N. M., George, S. C. (1998). A two-compartment model of pulmonary nitric oxide exchange dynamics. Journal of Applied Physiology,85(**2**), 653-666.

194. Usansky, H. H., Sinko, P. J. (2005). Estimating human drug oral absorption kinetics from Caco-2 permeability using an absorption-disposition model: model development and evaluation and derivation of analytical solutions for ka and Fa. *Journal of Pharmacology and Experimental therapeutics*, 314(**1**), 391-399.

195. Van den Bergh, F. (2001) An analysis of particle swarm optimizer, Ph.D thesis, University of Pretoria, South Africa,.

196. Van De Waterbeemd, H., Smith, D. A., Beaumont, K., Walker, D. K. (2001). Property-based design: optimization of drug absorption and pharmacokinetics. *Journal of medicinal Vhemistry*, 44(**9**), 1313-1333.

197. Van Haastert, P. J., Devreotes, P. N. (2004). Chemotaxis: signalling the way forward. *Nature Reviews Molecular cell biology*, 5(**8**), 626-634.

198. Vereb, G., Szöllősi, J., Matko, J., Nagy, P., Farkas, T., Vigh, L. M. L. W. T. A., Damjanovich, S. (2003). Dynamic, yet structured: the cell membrane three decades after the Singer–Nicolson model. *Proceedings of the National Academy of Sciences*, 100(**14**), 8053-8058.

199. Virkamäki, A., Korsheninnikova, E., Seppälä-Lindroos, A., Vehkavaara, S., Goto, T., Halavaara, J., Yki-Järvinen, H. (2001). Intramyocellular lipid is associated with resistance to in vivo insulin

actions on glucose uptake, antilipolysis, and early insulin signaling pathways in human skeletal muscle. *Diabetes*, 50(**10**), 2337-2343.

200. Wang, W. C., Natelson, R. H., Stikeleather, L. F., Roberts, W. L. (2013). Product sampling during transient continuous countercurrent hydrolysis of canola oil and development of a kinetic model. *Computers and Chemical Engineering*, **58**, 144-155.
201. Waterman, M. S. (1995). Introduction to computational biology: maps, sequences and genomes. CRC Press.
202. Wessel, M. D., Jurs, P. C., Tolan, J. W., Muskal, S. M. (1998). Prediction of human intestinal absorption of drug compounds from molecular structure.Journal of chemical information and computer sciences, 38(**4**), 726-735.
203. Wilkinson, J. H. (1965). The algebraic eigenvalue problem , **87**. Oxford: Clarendon Press.
204. Wu, X., Cao, G., Prior, R. L. (2002). Absorption and metabolism of anthocyanins in elderly women after consumption of elderberry or blueberry. *The Journal of nutrition*, 132(**7**), 1865-1871.
205. Xia, X., Xie, Z. (2001). DAMBE: software package for data analysis in molecular biology and evolution. *Journal of heredity*, 92(**4**), 371-373.
206. Yong, P. Y., Baird, D. T., Thong, K. J., McNeilly, A. S., Anderson, R. A. (2003). Prospective analysis of the relationships between the ovarian follicle cohort and basal FSH concentration, the inhibin response to exogenous FSH and ovarian follicle number at different stages of the normal menstrual cycle and after pituitary down regulation. *Human Reproduction,* 18(**1**), 35-44.